ON THE THEORY OF AMORPHOUS SOLIDS

AND OF EXCITONS.

Rafael Angel Barrio Paredes

Department of Theoretical Physics

University of Oxford

A thesis submitted for the degree of

Doctor of Philosophy

at Oxford University

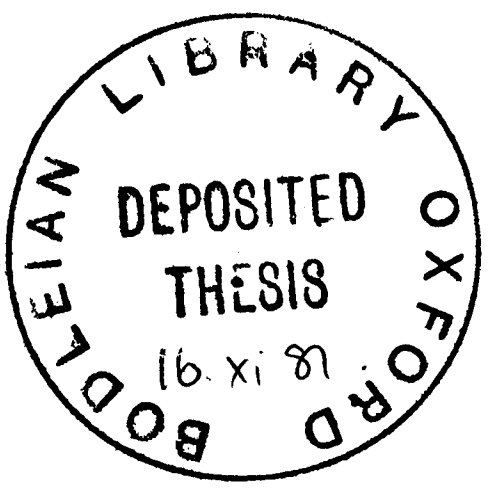

Wolfson College 1981

A MIS PADRES

Acknowledgements

I am deeply indebted to my supervisor Prof. R. J. Elliott not only for his continuous support and guidance, common characteristic of all supervisors, but for his strange ability for finding the correct answers to scientific matters and his tremendous personal concern.

It is my pleasure to acknowledge the Instituto de Investigaciones en Materiales (UNAM) for the support during all the time I spent in Oxford.

I would like to thank my colleagues and friends, in Mexico, Julia Tagüeña and Eugenio Cetina, and in Oxford, Kimmo Kaski and Alison Walker for the stimulating discussions and continuous encouragement.

I am indebt to Prof. M. F. Thorpe for the enjoyable visit to Michigan State University, where a substantial part of this work was done. Also, I should like to thank Dr. F. L. Galeener for suggesting the study of defects in silica.

Many thanks to Dr. Delano Saldin and Dr. Alison Walker for their careful reading of the manuscript.

Finally, to Guðmundur Haraldsson thanks for loaning his typewriter and his friendship.

ABSTRACT.

This thesis consists of two completely separate parts: In part I some problems related to phonons in amorphous solids are considered, whilst Part II is devoted to the study of excitons in Cuprous Oxide (Cu_2O).

Part I.- A theoretical model, suitable to treat vibrations in tetrahedrally coordinated amorphous systems is developed and permits the study of a number of situations of current interest. Three of these situations are studied in detail:

1) The local response of hydrogen in amorphous silicon when a single silicon is attached to one, two or three hydrogens. The differences between these three configurations are discussed and a direct connection with experimental results is suggested.

2) The interesting case of an amorphous alloy, where both, topological and substitutional disorder are present. This is treated within the spirit of the Coherent Potential Approximation. The particular alloy chosen (Si-Ge) is readily tractable because of the similar bond characteristics of both components, which allows the neglect of force constant changes.

3) The Raman spectrum of AX_2 glasses. The model adopted permits the investigation of the local response at the defect sites for a number of defects. In order to explain the defect lines observed in the experiments, four plausible defect configurations are considered: a missing A-X bond, a X-A double bond, an A-A bond, and a square ring (two tetrahedra sharing an edge).

A simple model to calculate the Raman response in amorphous solids is also outlined.

Part II.- The valence band of Cu_2O is studied in detail to account for the deviations from the hydrogenic law of the exciton spectrum. The appearance of the two series of excitons is explained in terms of a spin-orbit splitting of the valence band in the centre of the Brillouin Zone,

using a Tight-Binding Approximation. The deviations of the lowest exciton levels from their expected values are seen to arise from an admixture of the two components of the split -off valence band due to direct Coulomb and exchange interactions. The Hamiltonian used corresponds to the so called "Spherical Approximation" and the results obtained are in remarkable agreement with the experiments.

Table of Contents

PART I: ON AMORPHOUS SOLIDS

PART I

ON AMORPHOUS SOLIDS

INTRODUCTION.

Amorphous materials have attracted an enormous amount of attention in the recent years (Ziman (1979). This is mainly because of their potential and actual applications in the technology of many useful devices. Their properties differ considerably from their crystalline counterparts and the physics involved is not very well understood.

The difficulties in the understanding of these systems arise from the lack of translational symmetry, that prevents the use of fundamental simplifications that make crystalline solids readily tractable. Thus, one has to deal with a very complex many-body system.

Among the interesting features that one can study in topologically disordered solids are the lattice vibrations, which are related to very important physical properties, such as the specific heat, superconductivity, melting and ferroelectricity.

It is clear from the theoretical point of view, when dealing with phonons, that the starting point is to investigate the spatial configuration at equilibrium. The continuous random network of Zachariasen(1932) provides a useful model to describe a wide range of glasses, and in particular, the tetrahedrally coordinated ones, such as Si, Ge, SiO_2, GeO_2, $ZnCl_2$, etc.

The Born Model-Hamiltonian (Born(1914)) has proved to be an excellent approximation to the interatomic potential in these glasses. Taking these two models for the configuration and coupling of the atoms, a direct way of solving the problem is to consider a random cluster of atoms, as large as possible, and to diagonalize numerically the Heisenberg equations of motion. A review of these numerical techniques is found in Dean(1972). A random clus-

ter of about 330 atoms in SiO_2 is solved in Bell et al. (1968) and the remarkably successful results could be found in Bell & Dean (1970).

Although these numerical methods are of great value, they do not provide an insight into the fundamental physics of the systems. In order to avoid losing the thread in cumbersome calculations, one has to imagine very simplified models that could be handled analytically, although, because of their very nature, a direct comparison with experiment is severely restricted.

Attemps to take advantage of the good knowledge about phonons in crystals and then, to use perturbation theory to describe them in amorphous solids are unsuccessful, because it is not clear how an amorphous material may be regarded as a highly disordered crystal. Therefore, new approaches that do not rely upon translational symmetry are needed.

Among these, the Bethe lattice (Domb(1960)), based on the Bethe-Peierls Approximation (Bethe(1935); Peierls (1936)), provides a useful model to simulate systems without translational symmetry. The Bethe lattice is a regularly coordinated network without closed loops (a tree), which allows decoupling of the equations of motion and their exact solution (see for instance Thorpe & Weaire (1971)). The mathematical simplicity obtained with a Bethe lattice model compensates its numerous non-physical features, provided one selects properly the physically significant results from the others.

This model is adopted in this thesis to study several interesting problems related with the vibrations in tetrahedrally coordinated amorphous solids. The quantity of interest will be the density of vibrational states (DOS), because it is closely related to many physical properties of the solids. However, it must be pointed out that in some situations, namely a typical scattering problem, a

knowledge of the phonon eigenvectors is also required.

In Chapter I the model is discussed in general. The conveniences and drawbacks of the use of a Bethe lattice are pointed out, and various ways of obtaining the displacement-displacement Green's function in closed form are also explained.

With the Green's functions formalism it is possible to investigate not only the DOS, but most of the experimental quantities which are related to correlation functions. In the last section of Chapter I is included a simple model to investigate the Raman response of a tetrahedrally coordinated amorphous material. The simplicity of the mathematics involved in the use of a Bethe lattice yields results that would otherwise be unattainable.

Hydrogenated amorphous silicon (a-Si:H) is a material that has created a great deal of interest at the present time, mainly in experimental research. It also provides fertile soil for theoretical research. In Chapter II the local DOS in the neighbourhood of a hydrogen site is investigated for different configurations, i.e. when one, two or three hydrogens are attached to a single Si atom. The characteristics of the spectra are examined for each configuration, and a direct comparison with inelastic neutron scattering experiments is shown to be possible.

The model adopted here is particularly suitable for studying the DOS of an amorphous alloy. In Chapter III a Si-Ge amorphous alloy is treated using the Coherent Potential Approximation (CPA). The results are compared with other calculations and with experimental data.

Raman scattering measurements in SiO_2 and GeO_2 glasses (Galeener & Lucovsky(1976)) show sharp peaks that are attributed to defects. The Bethe lattice model is generalized to AX_2 glasses in Chapter IV in order to study local DOS for a number of possible defects. The problem of calculating the Raman response in AX_2 glasses is dis-

cussed, and a model similar to the one used for simple tetrahedral networks is developed. The results allow one to make some important remarks about the possible existence of a given defect in the material.

C H A P T E R I

THE MODEL

1.- BASIC CONCEPTS

The harmonic Hamiltonian, within the adiabatic approximation, can be written as:

$$H = \frac{1}{2} \sum_{\alpha,\ell} \frac{P_\alpha(\ell)}{M_\alpha(\ell)} + \frac{1}{2} \sum_{\alpha,\alpha'} \sum_{\ell,\ell'} \bar{\Phi}_{\alpha\alpha'}(\ell,\ell')\, u_\alpha(\ell)\, u_{\alpha'}(\ell') \qquad \text{(I.1)}$$

where $P_\alpha(\ell)$ and $u_\alpha(\ell)$ are the cartesian components (α) of the momentum and displacement operators respectively, of an atom at site (ℓ). $M_\alpha(\ell)$ is the mass of atom ℓ, and Φ is the harmonic force constant.

The problem of evaluating the tensor that couples atoms at sites ℓ and ℓ' from first principles is enormous and therefore, some simplifications are needed. Born(1914) suggested that, in a solid, the atoms interact only with their nearest neighbours through a central force α (along the line joining them) and a non-central force β. The potential between two adjacent atoms i and j is then

$$V_{ij} = \frac{(\alpha-\beta)}{2} \left\{ [\bar{u}(i) - \bar{u}(j)] \cdot \hat{r}_{ij} \right\}^2 + \frac{\beta}{2} [\bar{u}(i) - \bar{u}(j)]^2 \qquad \text{(I.2)}$$

$\hat{r}_{ij}$ is a unit vector along the line joining the atoms.

Once (I.2) is introduced into (I.1) the solution requires a knowledge of the topological structure of the system. In the case of a diamond lattice, the solution is well known (Cochran (1966); Thorpe(1974a)), but when there is no crystallinity, the infinite set of equations of motion derived from (I.1) and (I.2) has to be truncated. Numerical calculations for finite clusters, using a potential like (I.2), have been performed (Dean (1972)), but the problem with clusters is that, in three dimensions, there is a substantial fraction of surface atoms, and it is difficult to distinguish their role. Periodic boundary conditions will give spurious standing waves arising from

the artificially constructed periodicity, whilst free ends boundary conditions will produce an unnaturally large amplitude of vibration at the surface sites. Attemps to solve the equations of motion for a finite cluster, imposing reasonable boundary conditions, have been made. On the one hand, Thorpe (1973) developed the so called "Structural Potential Approximation", in which a potential imposed on the surface atoms of a cluster is self-consistently determined by demanding the mean square amplitude be the same for all atoms (surface and bulk), at each frequency. For a five atom tetrahedron the result is exactly the same as for a Bethe lattice.

On the other hand, Yndurain & Sen (1976) have applied to the lattice dynamics the "Cluster-Bethe Lattice" theory, developed for the electronic problem by Joannopoulos & Yndurain (1974), in which a cluster could be studied exactly and the surface atoms are connected to Bethe lattices. They solve the pure Bethe lattice equations of motion by the transfer matrix method, and the result agrees entirely with the five atom cluster in the structural potential approximation, as expected.

2.- THE BETHE LATTICE

In this work the Bethe lattice is used almost exclusively to simulate an amorphous material. Some objections concerning the physical significance of such a system could arise, therefore a word must be said about its properties.

A Bethe lattice is an artifact constructed mathematically and for which some theoretical models give exact solutions (Domb (1960)). It can be regarded as a first approximation for any given lattice, in which all connected diagrams without closed loops are summed exactly. Because of its unphysical nature, some problems arise when compared

with other lattices. First of all, its dimensionality is not well defined. For a coordination Z>2, every branch emerging from a given site needs a further dimension, in order to preserve the geometrical homogeneity of the lattice. This leads to the fact that such a structure is physically unrealizable and that the coordinates of the sites are not defined. However, a Bethe lattice of any Z retains "one-dimensional" characteristics, in the sense that it is simply connected and there is only one path between any given pair of sites. Therefore, it seems impossible to simulate genuine topological disorder, because a "glassy tree" is like a "linear glass" and cannot be equated with the irregular connectivity of the actual amorphous material (for a study of a topological defect see Thorpe et al. (1973)). Also, the question of electron mobility in a Bethe lattice is not clear because of this one-dimensional nature of the network.

Perhaps the most unwanted features of the Bethe lattice are: i) the unnaturally large surface and ii) the pathological band edges.

In any finite tree of coordination Z, the ratio of the number of sites on the surface to the total number of sites is

$$\frac{S}{N} = Z(Z-1)^{\ell-1} \Big/ \left(\frac{Z(Z-1)^{\ell}-2}{Z-2} \right) \qquad \text{(I.3)}$$

where ℓ is the number of steps from the centre to the surface. As $\ell \to \infty$ the ratio tends to the constant $(Z-2)/(Z-1)$, which is not negligible. Thus, the "bulk solution" must be supplemented with a discrete spectrum of surface states. This matter is discussed in detail by Nagle et al. (1972). However, one can get rid of unpleasant surface effects by considering an infinite Bethe lattice, which is an homogeneous system, and whose solution is the bulk solution of the tree.

When comparing the DOS for a Bethe lattice with, for instance, the diamond lattice Fig.(I.1), one notices that the band edges are not attained by the Bethe lattice.

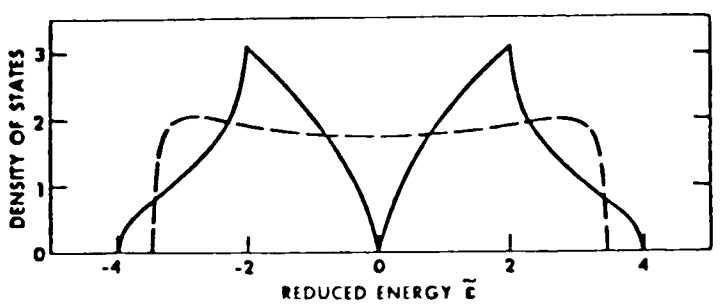

Fig. (I.1) Density of states for a diamond(——) and Bethe lattices (---), for a s-type tight binding Hamiltonian ($H=\sum_i |i><i'|$)

This is a general feature that could be understood in terms of the moments of the spectral density: For a tight -binding Hamiltonian of the type (I.1), the moments μ_ℓ are proportional to the number of paths that start and end at the same site. For a given number of steps 2ℓ, there are only $Z(Z-1)^{\ell-1}$ paths of that sort in a Bethe lattice (which correspond to the ones retracing the path), but in a diamond lattice there is a further contribution to a given moment ($\ell \geq 6$) arising from the rings present in the latter structure. Hence, it is seen that the states on the band edges are cut off in a Bethe lattice. However, there is always a state on the true band edge, but its weight is 1/N and it is negligible in the limit of large N.

For a better discussion on this subject see Thorpe et al. (1973). This effect on the band edges could give rise to spurious peaks there, which have to be carefully considered (Joannopoulos & Yndurain (1974)).

After this long exposition of the inconveniences of a Bethe lattice, one could conclude that it is such an inadequate model as to be of no use in practice. Nevertheless none of the drawbacks mentioned before is really inextricable and the difficulties could be overcome, as will become clear in the course of this dissertation.

There are three important reasons that compelled us to choose the Bethe lattice as a reasonable approximation for an amorphous system, and these are:

i) The systems may be solved exactly. The mathematics involved are so simple as to permit the study of more complicated situations than amenable by other models.

ii) The local environment of the atoms and the short range properties are well preserved throughout the system.

iii) No long range order is assumed and the the DOS is rather featureless,as is found in the real amorphous materials. Therefore, any structure detected arises from changes in the local environment of the atoms.

But the real justification will be found in this thesis, when the results produced are analysed and the unphysical features are discovered and their causes identified.

3.-DISPLACEMENT-DISPLACEMENT GREEN'S FUNCTION

Here we develop an alternative way of solving the pure Bethe lattice with the Born Hamiltonian (I.2). This derivation leads to expresions particularly suitable for handling the problems studied.

Consider a perfectly tetrahedrally coordinated net-

work of atoms of mass M, coupled by the potential (I.2), and concentrate on a particular bond:

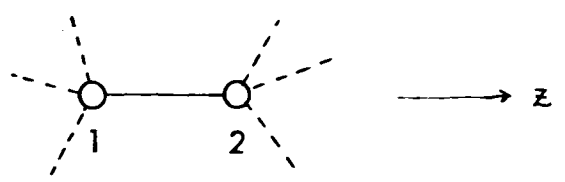

Fig.(I.2)

The equation of motion for the x-component of the displacement of particle 1 is

$$M\omega^2 u_x(1) = \beta [u_x(1) - u_x(2)] + V_\perp u_x(1) \,, \qquad \text{(I.4a)}$$

a similar equation holds for $u_y(1)$. For the z-component

$$M\omega^2 u_z(1) = \alpha [u_z(1) - u_z(2)] + V_{\parallel} u_z(1) \,, \qquad \text{(I.4b)}$$

$V_{\parallel}$ and $V_\perp$ represent the effective potentials from the bonds shown by dashed lines in Fig.(I.2). On the other side of the bond

$$M\omega^2 u_x(2) = \beta [u_x(2) - u_x(1)] + etc. \,, \qquad \text{(I.5)}$$

etc represents whatever is on the right of site 2. In the case of having a regular lattice this term is $V_\perp u_x(2)$. Solving for $u_x(1)$ in (I.4a) and inserting into (I.5)

$$\left(M\omega^2 - \beta - \frac{\beta^2}{M\omega^2 - \beta - V_\perp} \right) u_x(2) = etc. \qquad \text{(I.6)}$$

An analogous equation holds for the z-component. It is convenient to define effective force parameters

$$\alpha_{eff} = \alpha + \frac{\alpha^2}{M\omega^2 - \alpha - V_{\parallel}} \quad , \tag{I.7a}$$

$$\beta_{eff} = \beta + \frac{\beta^2}{M\omega^2 - \beta - V_{\perp}} \quad . \tag{I.7b}$$

It is possible to find self-consistency conditions for the effective potentials if they are written in terms of the quantities (I.7). The effective potential due to the three dashed bonds in Fig.(I.2) is then

$$\sum_{j=1}^{3} \{\beta_{eff} r^2 + (\alpha_{eff} - \beta_{eff}) r_j^2\} = 3\beta_{eff} r^2 + (\alpha_{eff} - \beta_{eff})(\tfrac{4}{3} r^2 - z^2) \quad , \tag{I.8}$$

the last step follows because in a tetrahedron

$$\sum_{j=1}^{4} r_j^2 = \frac{4}{3} r^2 \quad ; \qquad \bar{r}_4 = (0,0,z) \tag{I.9}$$

Therefore, from (I.5)

$$V_{\perp} = \frac{4\alpha_{eff} + 5\beta_{eff}}{3} \quad , \tag{I.10a}$$

$$V_{\parallel} = \frac{\alpha_{eff} + 8\beta_{eff}}{3} \quad . \tag{I.10b}$$

Equations (I.10) are self-consistent coupled equations for $V_{\perp}$ and $V_{\parallel}$. At this point it is desirable to introduce the displacement-displacement Green's function. We define it in the same way as Zubarev (1960). The equation of motion for the Fourier transform of the double-time thermodynamic Green's function (Elliott & Leath(1975)), using the Hamiltonian (I.1) is

$$M_{\alpha}(\ell)\omega^2 G_{\alpha\alpha'}(\ell,\ell';\omega) = \delta_{\alpha\alpha'}\delta(\ell,\ell') + \sum_{\alpha''\ell''} \Phi_{\alpha\alpha''}(\ell,\ell'') G_{\alpha''\alpha'}(\ell'',\ell') \quad , \tag{I.11}$$

or, in a condensed matrix notation

$$[M\omega^2 - \Phi] G(\omega) = 1 \quad . \tag{I.12}$$

The transformation to normal modes also diagonalizes

this matrix. Substituting (I.10) into (I.6) to find the normal modes gives

$$G_{xx} = \frac{1}{M\omega^2 - \frac{4}{3}(\alpha_{eff} + 2\beta_{eff})} = \frac{1}{M\omega^2 - \frac{4}{9}(V_{11} + 2V_{\perp})} \quad . \tag{I.13}$$

This Green's function do not depend on the site because all sites are equivalent in a Bethe lattice. It is also isotropic, that is

$$G_{xx} = G_{yy} = G_{zz} = g \quad . \tag{I.14}$$

Now, a self-consistent equation could be found for g. From (I.10) and (I.13) one can solve for β:

$$\left[V_{\perp} - \left(M\omega^2 - \frac{1}{g} - \beta\right)\right]\left[V_{\perp} - \left(M\omega^2 - \beta\right)\right] = \beta^2 \, , \tag{I.15}$$

therefore

$$V_{\perp} = M\omega^2 - \beta - \frac{1}{2g} \pm \sqrt{\frac{1}{4g^2} + \beta^2} \quad ; \tag{I.16a}$$

a similar procedure results in

$$V_{11} = M\omega^2 - \alpha - \frac{1}{2g} \pm \sqrt{\frac{1}{4g^2} + \alpha^2} \quad . \tag{I.16b}$$

Care must be taken with the signs of the square roots in (I.16); they must be chosen in order to satisfy (I.13) identically. Combining (I.16) and(I.13) a self consistent equation for g is obtained

$$1 + g\left[M\omega^2 - \frac{4}{3}(\alpha + 2\beta)\right] = \mp\frac{2}{3}\sqrt{1 + (2\alpha g)^2} \mp \frac{4}{3}\sqrt{1 + (2\beta g)^2} \, . \tag{I.17}$$

This equation is exactly equation (14) in Thorpe (1973). The best way to solve it is by squaring the roots and by finding the zeros of the resultant quartic equation

$$[C^4-2C^2(D+E)+(D-E)^2]g^4+4[C^3-C(D+E)]g^3+[\tfrac{14}{9}C^2-2(D+E)-\tfrac{8}{3}(D-E)]g^2+$$

$$+[\tfrac{-44}{9}C]g-\tfrac{5}{3}=0 \quad , \tag{I.18}$$

where

$$C = M\omega^2-\tfrac{4}{3}(\alpha+2\beta) \quad ,$$

$$D = \tfrac{16}{9}\alpha^2 \quad , \tag{I.19}$$

$$E = \tfrac{64}{9}\beta^2 \quad .$$

The values of the parameters, appropriate for Si are

$$\begin{aligned} M &= 28 \\ \alpha &= 1.774 \\ \beta &= 0.323 \ , \end{aligned} \tag{I.20}$$

the units of α and β are such that if M is in atomic units, ω is in $10^{-3}\,cm^{-1}$.

When ω is real, (I.18) has only real roots, except when ω is inside the band, where a single pair of complex roots appears. The correct root is then the one that gives the positive DOS. In the actual calculation, a small imaginary part ($10\ cm^{-1}$) was added to ω. In that case the physical root is the one with the biggest imaginary part (this also holds outside the band).

The DOS is

$$\rho(\omega)=\frac{-2M\omega}{\pi}\ \underset{\varepsilon\to 0^+}{Im}\ g(\omega+i\varepsilon) \quad , \tag{I.21}$$

because the equivalence of all sites and Tr(g)=Ng. This is plotted in Fig.(I.3c).

It is interesting to investigate the limit when only central forces are present (β=0). Equation (I.17) gives

$$g^2\left[9\left(M\omega^2-\tfrac{4}{3}\alpha\right)^2-16\alpha^2\right]-6g\left(M\omega^2-\tfrac{4}{3}\alpha\right)-3=0 \quad . \tag{I.22}$$

This equation is exactly the one which could be obtained using the mapping between the vibrational and the electronic problems (Weaire & Alben (1972)), by means of the Weaire and Alben Theorem (for details see Weaire & Thorpe (1971) and(1973)). They find that the normal modes are given by

$$M\omega^2 = \frac{4}{3}\alpha(1-\varepsilon) \qquad \text{(I.23)}$$

where ε is an eigenvalue of an s-like Hamiltonian (connectivity matrix). The eigenvalues ε could be found following the procedure in Thorpe & Weaire (1971). Equation (I.23) was also obtained by Thorpe & Galeener (1980) using a Lagrangian formulation. There are the normal modes without an s-component that are not included in the mapping (pure bonding and antibonding p-states). They produce δ-functions at the edges of the band (see for instance Straley (1972)). Actually equation (I.23) is completely general and it holds for any tetrahedrally coordinated structure with only central forces. Delta functions appear in the DOS of all such networks when only central forces are considered. In Fig. (I.3a) the DOS for this case is shown. The δ-functions appear at O and $\omega_{max}=\sqrt{8\alpha/3M}$.

Investigating the nature of these modes (Thorpe & Galeener (1980)), one realizes that the δ-functions at zero and ω_{max} correspond to transverse acoustic and transverse optic modes respectively. A glance at Fig.(I.3) reveals that the peaks in the spectrum for Si have their origin in those δ-functions. The weight of each one of them is one per atom.

Equations (I.17).(I.21) and (I.23) are the basic relations that provide the quantities of interest, that is, the displacement-displacement Green's function and the density of states. All of them have been derived elsewhere, but the present method allows an easy treatment of

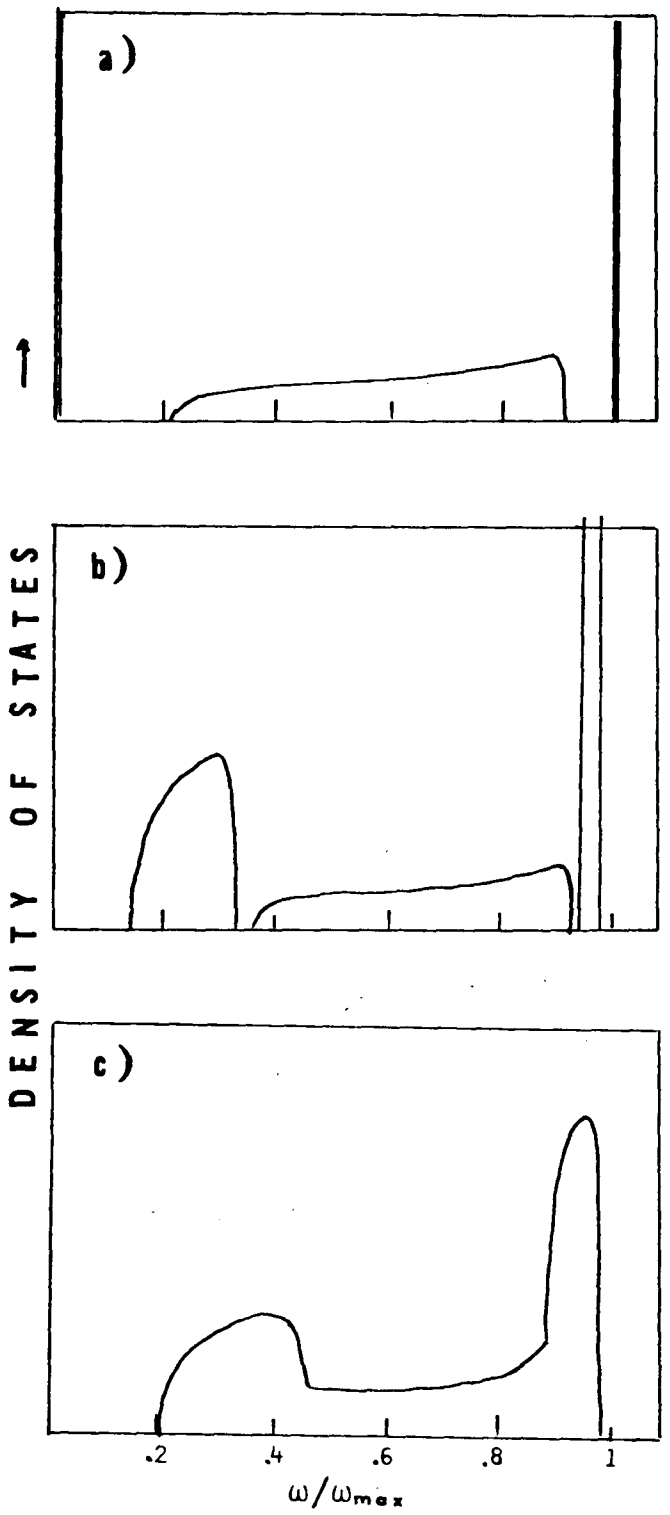

Fig.(I.3) Density of states for a Bethe lattice (eq. (I.21)) for a) $\beta/\alpha = 0$ (only central forces), b) $\beta/\alpha=.3$ and c) $\beta/\alpha=.6$ (value suitable for Si or Ge).

a number of problems, particularly those involving local defects. Its usefulness will be apparent in the course of this dissertation.

4.- RAMAN SCATTERING

The knowledge of only the DOS is not sufficient if one has to compare the theory with Raman scattering experiments, because of interference between the motion of different atoms.

This process is complicated and a detail model for the Raman scattering in amorphous systems is not available. We therefore present a very simple model that could help in the understanding of the process.

The reduced Raman cross section is related to the displacement-displacement Green's function by (Elliott et al. (1974)):

$$\frac{d\sigma}{d\Omega\, dE} \propto \sum_{\alpha\alpha' ll'} C_\alpha(l) C_{\alpha'}(l')\, \mathrm{Im} \langle\langle u_\alpha(l); u_{\alpha'}(l') \rangle\rangle_R \qquad \text{(I.24)}$$

where the retarded Green's function is defined as in Zubarev (1960). In general $C_\alpha(l)$ depends also on the direction of the photons and the polarization of the incident and scattered light. In this expresion the Raman polarizability is assumed to be proportional to the displacements. Let us assume that this tensor only couples displacements in such a way that it is different from zero when there is an effective change in the length of the bonds. This occurs when the displacement of a given site l is parallel to one of the four tetrahedral directions $z(l)$. Furthermore, we neglect the angular dependence of C. The cross section may be then written

$$\propto C^2 \frac{4}{3} \mathrm{Im} \sum_s g(0,s) \qquad \text{(I.25)}$$

where

$$g(0,s) = \sum_{\substack{l \text{ atoms} \\ \text{in shell } s}} \langle\langle u_{z(0)}(0); u_{z(0)}(0) \rangle\rangle_R \qquad \text{(I.26)}$$

These satisfy a recurrence relation

$$g(0,l) = -K\, g(0,l-1) \tag{I.27}$$

In fact the value of C(l) depends on the actual bond directions. In the amorphous material these will be variable. As a crude approximation to the orientational disorder we introduce an unknown factor (f) so that (I.24) becomes

$$C^2 \frac{4}{3} \mathrm{Im} \sum_s g(0,0)(-Kf)^s \propto \mathrm{Im}\left(\frac{g(0,0)}{1+Kf}\right) \tag{I.28}$$

The actual value of f is difficult to obtain. In a diamond lattice f=1 because the tetrahedra alternate in direction, in a Bethe lattice the coordinates of the atoms in a given shell are not defined (infinite dimension problem) and f could take any value from zero to one.

For a Bethe lattice with only central forces, it is easy to solve (I.27) using equations (I.22) and (I.23), one obtains

$$K = \frac{1}{6V}\left[\epsilon \pm \sqrt{\epsilon^2 - 12V^2}\right] \tag{I.29}$$

and

$$g(0,0) = \frac{1}{\epsilon - 4VK} \tag{I.30}$$

where

$$\epsilon = -3M\omega^2 + 4Va \tag{I.31}$$

The results for several values of f and parameters adequate for Si are shown in Fig(I.4). If f=0 the Raman intensity is exactly proportional to the DOS, but for any value of f$\neq$ 0 the DOS is modulated in such a way that the high frequency part of the spectrum is enhanced. This is observed in reality. The delta functions have been omitted from the plot, but their weight also changes with f. An additional spurious feature appears because there is a new pole where 1+kf=0. This occurs out of the band at $\epsilon = -fV(1+\frac{3}{f^2})$ which lies at higher frequencies. This unwanted feature is a drawback of the model and is due entirely to the Bethe lattice.

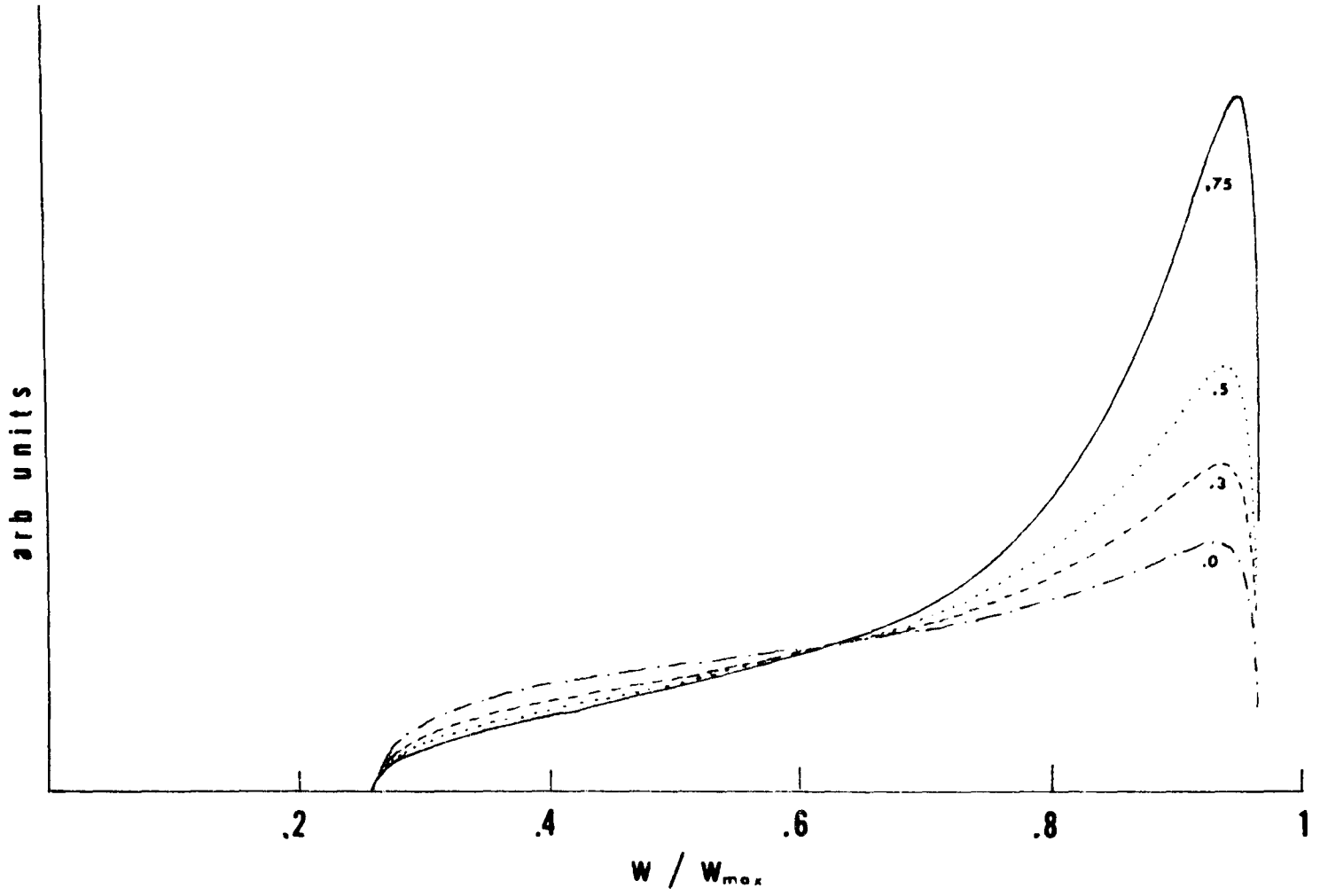

Fig.(I.4) Raman response for a Si Bethe lattice with central forces only. The values of f in equation (I.28) are shown in each curve.

The treatment is easily extended to the case of non-central forces. Using equation (I.13), one finds the new transfer matrix

$$K = \frac{-1}{\alpha}\left(\frac{1}{2g} \pm \sqrt{\frac{1}{4g^2} + \alpha^2}\right) \quad , \tag{I.32}$$

with g the solution of (I.18).

The plot of equation (I.28) using (I.32) and the proper factors is shown in Fig.(I.5). Notice that when f is approaching 3/4 the optical peak increases while the acoustic one decreases. Comparison of this figure with the real spectrum for Si (Fig.(III.1b)) is very encouraging

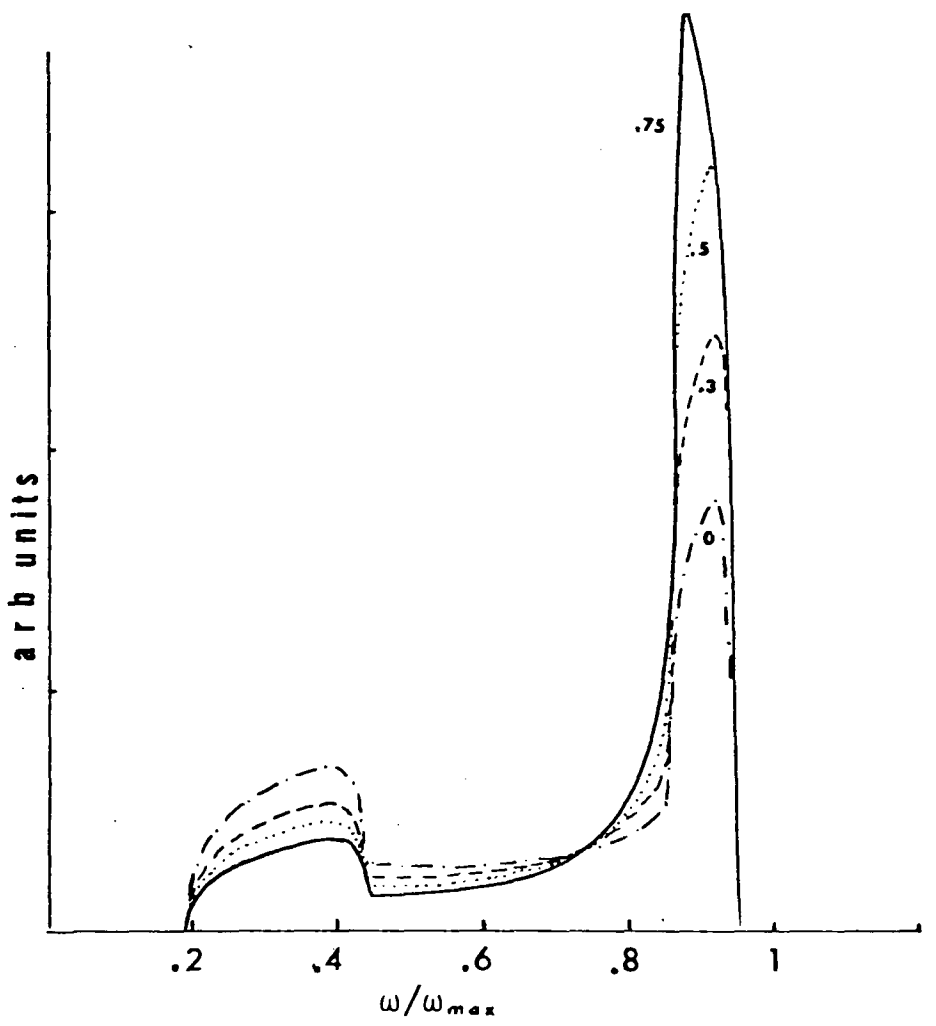

Fig.(I.5) As Fig.(I.4) but including non-central forces. $\beta/\alpha = 0.6$.

C H A P T E R I I

HYDROGENATED AMORPHOUS SILICON

1.- INTRODUCTION

During the past few years, an enormous amount of literature about a-Si:H has been produced. Very recently, a substantial number of experimental works have been devoted to the investigation of how the hydrogen atoms are distributed in the amorphous silicon matrix. Some observations using electron microscopy and nuclear magnetic resonance techniques (see for instance Bourret et al.(1981)) seem to suggest that the material is not homogeneous, but rather that the hydrogen tends to form clusters (presumably attached to the dangling bonds). Other authors suggest the formation of "domain walls" of hydrogen inside the material after some annealing (Knights (1979)), but up to the present time there is little agreement on this subject.

It is reasonable to expect that the local environment of the hydrogens will affect the vibrational properties of the material and, at present, there are good techniques for studying these properties. Inelastic neutron scattering seems to be an ideal tool for looking at the local vibrations of the hydrogen in a-Si, because the integrated intensity over the band is one order of magnitude stronger for H than for Si (Barrio & Thorpe (1981)). This is due to the very large incoherent scattering cross section for H. Hence, the experimentally determined incoherent scattering law $S(q,\omega)$ will reflect the form of the self correlation function on the hydrogen sites(Springer (1972)). These functions could be investigated using the formalism outlined in Chapter I.

Consider the three possible configurations of H in amorphous silicon:

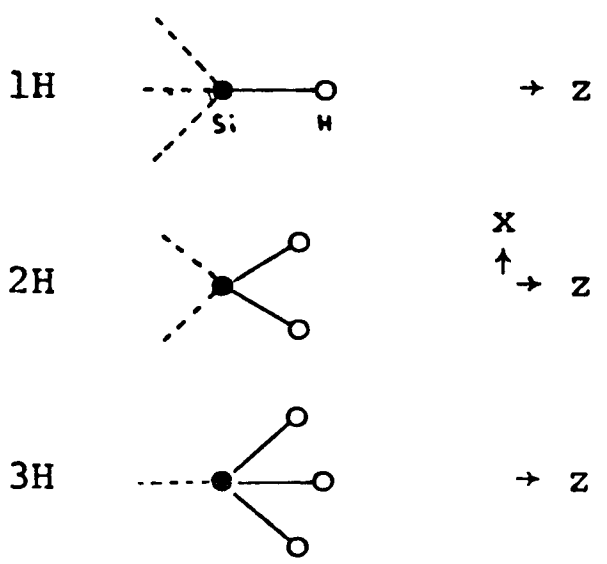

Fig.(II.1)

That is, one single hydrogen (o) attached to the Si network (1H), or two H attached to the same Si atom (2H), or three H on the same site (3H).

Our aim is to find the local response at the defect sites in each one of the three configurations and to investigate their distinctive features.

2.- LOCAL RESPONSE AT THE Si SITE AND NORMAL MODES.

The model is the following: We concentrate our attention on the defect site and attach Bethe lattices to the remaining bonds (shown by dashed lines in Fig,(II.1). The force constants in a Si-H bond are α' (central) and β' (non-central), and are taken as parameters to be adjusted with the observed frequencies of the bound states (Brodsky et al.(1977)).

The Green's function for the pure Si network (g) is the solution of (I.18) and could be found in the way described in Chapter I. All quantities of interest can be written in terms of g.

In the 1H case it is easy to find the Green's func-

tion at the surface Si atom by solving the equations of motion (I.6), putting α' and β' instead of α and β, and etc=0.

The displacement-displacement Green's function at the Si site (0) has two kinds of diagonal elements

$$g_{\parallel}^{①}(0,0) = \frac{1}{M\omega^2 - V_{\parallel} - \alpha' - \frac{\alpha'^2}{m\omega^2 - \alpha'}} , \qquad \text{(II.1a)}$$

$$g_{\perp}^{①}(0,0) = \frac{1}{M\omega^2 - V_{\perp} - \beta' - \frac{\beta'^2}{m\omega^2 - \beta'}} , \qquad \text{(II.1b)}$$

where m is the mass of the hydrogen; the superscript indicates that it is the 1H configuration and the z-axis($\parallel$) is denoted by the subscript. All other quantities have been defined before.

The poles of (II.1) provide equations to fit α' and β'. There is a stretching mode at $\omega_s \sim 2000$ cm^{-1} and a wagging mode at $\omega_w \sim 640$ cm^{-1} (Brodsky et al.(1977)). With equations (II.1) and (I.16) it is seen that

$$\alpha' = \left[\frac{1}{m\omega_s^2} + \frac{1}{\frac{1}{2g(\omega_s)} + \alpha + \sqrt{\frac{1}{4g^2(\omega_s)} + \alpha^2}} \right]^{-1} = 3.8603 , \qquad \text{(II.2a)}$$

$$\beta' = \left[\frac{1}{m\omega_w^2} + \frac{1}{\frac{1}{2g(\omega_w)} + \beta + \sqrt{\frac{1}{4g^2(\omega_w)} + \beta^2}} \right]^{-1} = 0.3897 , \qquad \text{(II.2b)}$$

where the units are the same as in (I.20).

If one does not consider any interaction between the hydrogens, it is straightforward to show that, in all cases, the normal modes equation is of the form

$$M\omega^2 = C_1 \alpha_{eff} + C_2 \beta_{eff} + C_3 \left(\frac{\alpha' m\omega^2}{m\omega^2 - \alpha'} \right) + C_4 \left(\frac{\beta' m\omega^2}{m\omega^2 - \beta'} \right) . \qquad \text{(II.3)}$$

The constants C_i are just geometrical factors for each configuration. In Table II.1 these values are shown and the normal mode frequencies are calculated using (II.3).

Table II.1

Normal modes without H-H interactions

conf.	dir.	C_1	C_2	C_3	C_4	$\omega_w(cm^{-1})$	$\omega_s(cm^{-1})$
1H	∥	1/3	8/3	1	0	---	2000
	⊥	4/3	5/3	0	1	640	---
2H	x	0	2	4/3	2/3	632	2011
	y	4/3	2/3	0	2	654	---
	z	2/3	4/3	2/3	4/3	641	1989
3H	∥	1	0	1/3	8/3	659	1977
	⊥	0	1	4/3	5/3	642	2011

From Table II.1 it is seen that the observed mode at 890 cm^{-1} (Brodsky et al.(1977)) is due to H-H interactions. We introduced a potential between hydrogens, following the model of Weber & Thorpe (1975):

$$\frac{\gamma}{2}\left\{\left[\hat{P}_1\cdot(\bar{u}_2-\bar{u}_0)+\hat{P}_2\cdot(\bar{u}_1-\bar{u}_0)\right]\right\}, \qquad \text{(II.4)}$$

where there are hydrogens at sites 1 and 2 and the surface Si atom is at site O. This is a potential of the Keating type (Keating (1966)), which has been proved useful in a number of systems*.

The equations of motion (I.1) are solved in the 2H case for a geometry in which the two hydrogens are in the x-z plane and the z-axis bisects the angle between them. It is found that the Green's functions at the Si site are:

$$g_{ii}^{(2)}(0,0)=\frac{1}{M\omega^2-\Sigma_i}\;; \qquad i=x,y,z \qquad \text{(II.5)}$$

*A central force between the hydrogens was also considered but this did not modify the results significantly.

where

$$\Sigma_x = 2m\omega^2\frac{[2(\alpha'-\beta')^2+(2\alpha'+\beta')(3m\omega^2-\alpha'-2\beta')]}{(3m\omega^2-\alpha'-2\beta')(3m\omega^2-2\alpha'-\beta')-2(\alpha'-\beta')^2} + 2\beta_{eff}\,, \qquad \text{(II.6a)}$$

$$\Sigma_y = \frac{2m\omega^2\beta'}{m\omega^2-\beta'^2} + \frac{4}{3}\alpha_{eff} + \frac{2}{3}\beta_{eff}\,, \qquad \text{(II.6b)}$$

$$\Sigma_z = 2m\omega^2\left[\frac{3m\omega^2(3m\omega^2-2\alpha'-\beta'-4\gamma)}{(3m\omega^2-\alpha'-2\beta'-2\gamma)(3m\omega^2-2\alpha'-\beta-4\gamma)-2(\alpha'-\beta'-2\gamma)^2}-1\right]+\frac{2}{3}\alpha_{eff}+\frac{4}{3}\beta_{eff}\,. \qquad \text{(II.6c)}$$

Equating Σ_z to $M\omega^2$ and putting ω=.890, the force constant was found to be

$$\gamma = 0.2069 \qquad \text{(in the same units)} \qquad \text{(II.7)}$$

Substituting this value in (II.6), the normal modes for the z-motion were found at 890 and 2000 cm^{-1}.

The motion of the atoms could be sketched thus:

2000 890

Fig.(II.2)

The mode at 890 cm^{-1} could be called "scissors" mode (ω_{sc}). All the other modes are those in Table II.1. Equations (II.6) reduce to the form (II.3) in the limit when $\gamma \to 0$.

For the 3H case, the equations of motion were solved at the Si site also, considering an interaction like(II.4) between all pairs of hydrogens and the z-axis opposite the bond which connects to the network. The Green's functions are

$$g_{\parallel}^{③}(0,0)=\frac{1}{M\omega^2-\alpha_{eff}-A}\quad , \tag{II.8a}$$

$$g_{\perp}^{③}(0,0)=\frac{1}{M\omega^2-\beta_{eff}-B}\quad , \tag{II.8b}$$

where

$$A=\frac{3m\omega^2\left[(\alpha'+8\beta'-4\gamma)(9m\omega^2-8\alpha'-\beta'-8\gamma)+8(\alpha'-\beta'-2\gamma)^2\right]}{(9m\omega^2-8\alpha'-\beta'-8\gamma)(9m\omega^2-\alpha'-8\beta'-4\gamma)-8(\alpha'-\beta'-2\gamma)^2}\quad , \tag{II.9a}$$

$$B=\frac{m\omega^2}{3(m\omega^2-\alpha-\frac{\gamma}{3})}\left\{\frac{(\alpha'-\beta'-2\gamma)}{\left(m\omega^2-\beta'-\frac{8}{3}\gamma-\frac{4\gamma}{9}\frac{(\alpha'-\beta'-2\gamma)}{(m\omega^2-\alpha'-\frac{\gamma}{3})}\right)}\left[\frac{4\gamma}{9(m\omega^2-\alpha'+\frac{\gamma}{3})}\left(4\alpha'+5\beta'+4\gamma-\frac{\beta'(\alpha'-\beta'-\gamma)}{m\omega^2-\beta'}\right)-\right.\right. \tag{II.9b}$$

$$\left.\left.-\frac{4}{3}\left(3\beta'+4\gamma-\frac{\beta'\gamma}{m\omega^2-\beta'}\right)\right]+4\alpha'+5\beta'+4\gamma-\beta'\frac{(\alpha'-\beta'+\gamma)}{m\omega^2-\beta'}\right\}\quad .$$

The position of the bound states were found by solving (II.8). All the results are shown on Table II.2

Table II.2

Normal modes with a Keating interaction

(frequencies in cm^{-1})

conf.	dir.	ω_w	ω_{sc}	ω_s
1H	∥	---	---	2000
	⊥	640	---	---
2H	x	632	---	2011
	y	654	---	---
	z	---	890	2000
3H	∥	---	793	1998
	⊥	630	936	2016

3.- RESPONSE AT THE H-SITES

The next step is to find the local response at the hydrogen sites. Therefore the equations of motion must be

solved for the hydrogen displacements. In the 1H case the solution is inmediate

$$g_{\parallel}^{(1)}(1,1) = \frac{1}{m\omega^2 - \alpha' - \frac{\alpha'^2}{M\omega^2 - \alpha' - V_{\parallel}}} \quad , \tag{II.10a}$$

$$g_{\perp}^{(1)}(1,1) = \frac{1}{m\omega^2 - \beta' - \frac{\beta'^2}{M\omega^2 - \beta' - V_{\perp}}} \quad . \tag{II.10b}$$

The local DOS at the hydrogen site is defined as

$$\rho_1^H(\omega) = \frac{-2m\omega}{\pi} Im\left(\frac{g_{\parallel}^{(1)}(1,1) + 2g_{\perp}^{(1)}(1,1)}{3}\right) \quad . \tag{II.11}$$

Finding the Green's function for the displacements along the coordinate axes is rather complicated for the 2H case. The equations of motion are simplified if linear combinations of the displacements are considered. It proved useful to define

$$g_{x\pm}^{(2)} = \frac{1}{2} \ll (u_x(2) \pm u_x(1)); (u_x(2) \pm u_x(1)) \gg \quad , \tag{II.12a}$$

$$g_y^{(2)} = \ll u_y(i); u_y(i) \gg \quad , \quad i = 1,2 \quad . \tag{II.12b}$$

$$g_{z\pm}^{(2)} = \frac{1}{2} \ll (u_z(2) \pm u_z(1)); (u_z(2) \pm u_z(1)) \gg \quad . \tag{II.12c}$$

It was found that

$$\begin{cases} g_{x+}^{(2)} = 1/\left[m\omega^2 - \frac{d(M\omega^2 - V_x)}{M\omega^2 - V_x - 2d}\right] \quad , \\ g_{x-}^{(2)} = 1/\left[m\omega^2 - h - \frac{f^2}{m\omega^2 - e} - \frac{2f^2p^2}{M\omega^2 - V_z - 2ep}\right] \quad , \end{cases} \tag{II.13a}$$

(II.13b)

$$g_y^{(2)} = 1/\left[m\omega^2 - \beta' - \frac{\beta'^2}{M\omega^2 - V_y - 2\beta' - \frac{\beta'^2}{m\omega^2 - \beta'}}\right] \quad ,$$

$$\begin{cases} g^{(2)}_{z+} = 1 \Big/ \left[m\omega^2 - \dfrac{k(M\omega^2 - V_z)}{M\omega^2 - V_z - 2k} \right] , \\ g^{(2)}_{z-} = 1 \Big/ \left[m\omega^2 - b - \dfrac{c^2}{m\omega^2 - a} - \dfrac{2c^2\ell^2}{M\omega^2 - V_x - 2a\ell} \right] , \end{cases} \qquad \text{(II.13c)}$$

where:

$$V_x = 2\beta_{eff}$$

$$V_y = \frac{2}{3}(2\alpha_{eff} + \beta_{eff})$$

$$V_z = \frac{2}{3}(\alpha_{eff} + 2\beta_{eff}) = \tfrac{1}{2}(M\omega^2 - 1/g)$$

$$a = \frac{1}{3}(2\alpha' + \beta') \qquad h = a + \frac{4}{3}\gamma$$

$$b = \frac{1}{3}(\alpha' + 2\beta) \qquad e = b + \frac{2}{3}\gamma \qquad \text{(II.14)}$$

$$c = \frac{\sqrt{2}}{3}(\alpha' - \beta') \qquad f + c - \frac{2\sqrt{2}}{3}\gamma$$

$$d = a + \frac{c^2}{m\omega^2 - b} \qquad k = e + \frac{f^2}{m\omega^2 - e}$$

$$\ell = \frac{m\omega^2}{m\omega^2 - a} \qquad p = \frac{m\omega^2}{m\omega^2 - e}$$

From the definitions (II.12) it is obvious that the sum of the functions (II.13) is exactly the same as the trace

$$\sum_{i,j} g_{ii}(j,j) \; ; \qquad i = x,y,z \; , \; j = 1,2 \qquad \text{(II.15)}$$

and therefore, the local DOS is

$$\rho_2^H(\omega) = \frac{-2m\omega}{\pi} Im \left(\frac{g^{(2)}_{x+} + g^{(2)}_{x-} + 2g^{(2)}_{y} + g^{(2)}_{z+} + g^{(2)}_{z-}}{6} \right) . \qquad \text{(II.16)}$$

The numbers produced by this equation were checked by solving the problem in the set of orthogonal axes (equation(II.5)) and also with an inverse-matrix method analogous to the one described below. The results for ρ_2^H were exactly the same for each frequency.

In the 3H case, the algebra involved in order to

close the equations of motion becomes very complicated. The eigenvectors are not found as easily as in the 2H case, therefore another method was developed to solve the problem. Once the full dynamical matrix is written down, one could divide it in such a way that the following relation holds

$$\begin{pmatrix} \underline{A} & \underline{B} \\ \underline{B}^T & \underline{C} \end{pmatrix} \begin{pmatrix} g_{ss} & g_{sH} \\ g_{Hs} & g_{HH} \end{pmatrix} = \begin{pmatrix} I_3 & 0 \\ 0 & I_9 \end{pmatrix} \tag{II.17}$$

where I_3 and I_9 are the identity matrices of dimension 3 and 9 respectively; g_{ss} is a 3×3 matrix that involves correlations at the Si site; g_{HH} is a 9×9 matrix containing all correlations between hydrogens; and g_{Hs} represents the H-Si correlations. It is clear that

$$g_{HH} = \{\underline{\underline{C}} - \underline{\underline{B}}^t \underline{\underline{A}}^{-1} \underline{\underline{B}}\}^{-1} \tag{II.18}$$

$\underline{\underline{A}}$ being a 3×3 diagonal matrix, is easily inverted and the expresion in {} is inverted numerically. All the matrices are written in terms of the parameters defined before and they are explicitly:

$$\underline{\underline{A}} = -\frac{1}{9} \begin{pmatrix} 12\alpha'+15\beta'+12\gamma+9\beta_{eff}-9M\omega^2 & 0 & 0 \\ 0 & 12\alpha'+15\beta'+12\gamma+9\beta_{eff}-9M\omega^2 & 0 \\ 0 & 0 & 3\alpha'-24\beta'+12\gamma+9\alpha_{eff}-9M\omega^2 \end{pmatrix} \tag{II.19}$$

$$\underline{\underline{B}} = -\frac{1}{9} \begin{pmatrix} k & o & 2\sqrt{2}\nu & \delta & \sqrt{12}\,\zeta & -\sqrt{2}\nu & \delta & -\sqrt{12}\,\zeta & -\sqrt{2}\nu \\ o & -\lambda & o & \sqrt{12}\,\zeta & \varepsilon & \sqrt{6}\nu & -\sqrt{12}\,\zeta & \varepsilon & -\sqrt{6}\nu \\ 2\sqrt{2}\nu & o & \mu & -\sqrt{2}\,\zeta & \sqrt{6}\,\zeta & \mu & -\sqrt{2}\,\zeta & -\sqrt{6}\,\zeta & \mu \end{pmatrix} \tag{II.20}$$

$$\underline{\underline{C}} = \frac{1}{9}\begin{pmatrix}
9m\omega^2-\Gamma & 0 & 2\sqrt{2}\sigma & 4\gamma & 0 & -\sqrt{2}\gamma & 4\gamma & 0 & -\sqrt{2}\gamma \\
0 & 9m\omega^2-\Lambda & 0 & -2\sqrt{2}\gamma & 0 & \sqrt{6}\gamma & 2\sqrt{2}\gamma & 0 & -\sqrt{6}\gamma \\
2\sqrt{2}\sigma & 0 & 9m\omega^2-\Upsilon & 2\sqrt{2}\gamma & 0 & -\gamma & 2\sqrt{2}\gamma & 0 & -\gamma \\
4\gamma & -2\sqrt{2}\gamma & 2\sqrt{2}\gamma & 9m\omega^2-\Delta & \sqrt{2}\sigma & -\sqrt{2}\gamma & -2\gamma & \sqrt{2}\gamma & -\sqrt{2}\gamma \\
0 & 0 & 0 & \sqrt{2}\sigma & 9m\omega^2-\Xi & \sqrt{6}\gamma & -\sqrt{2}\gamma & 6\gamma & -\sqrt{6}\gamma \\
-\sqrt{2}\gamma & \sqrt{6}\gamma & -\gamma & -\sqrt{2}\sigma & \sqrt{6}\sigma & 9m\omega^2-\Upsilon & -\sqrt{2}\gamma & \sqrt{6}\gamma & -\gamma \\
4\gamma & 2\sqrt{2}\gamma & 2\sqrt{2}\gamma & -2\gamma & -\sqrt{2}\gamma & -\sqrt{2}\gamma & 9m\omega^2-\Delta & -\sqrt{2}\gamma & -\sqrt{2}\sigma \\
0 & 0 & 0 & \sqrt{2}\gamma & 6\gamma & \sqrt{6}\gamma & -\sqrt{2}\sigma & 9m\omega^2-\Xi & -\sqrt{6}\sigma \\
-\sqrt{2}\gamma & -\sqrt{2}\gamma & -\gamma & -\sqrt{2}\gamma & -\sqrt{6}\gamma & -\gamma & -\sqrt{2}\sigma & -\sqrt{6}\sigma & 9m\omega^2-\Upsilon
\end{pmatrix} \qquad \text{(II.21)}$$

where

$$\begin{aligned}
\nu &= \alpha' - \beta' + \gamma \;;\; \sigma = \nu - 2\gamma \\
\tau &= \nu - 3\gamma \;;\; \Lambda = 9\beta' + 12\gamma \\
\kappa &= -8\alpha' - \beta' + 4\gamma \;;\; \Gamma = -\kappa + 8\gamma \\
\mu &= -\alpha' - 8\beta' - 4\gamma \;;\; \Upsilon = -\mu - 2\gamma \\
\varepsilon &= -6\alpha' - 3\beta' \;;\; \Delta = -\delta + 2\gamma \\
\delta &= -2\alpha' - 7\beta' - 8\gamma \;;\; \Xi = -\varepsilon + 6\gamma \;.
\end{aligned} \qquad \text{(II.22)}$$

The local DOS at the hydrogen site is defined as

$$\rho_3^H(\omega) = \frac{-2m\omega}{\pi} Im\left(\frac{Tr\, g_{HH}}{9}\right) \;. \qquad \text{(II.23)}$$

The local densities (II.11), (II.16) and (II.23) are shown in Fig.(II.3). The DOS for pure Si (eq.(I.21)) is also shown. The discussion of these results will be postponed until the end of the chapter.

The method used to find the local DOS for the 1H and the 2H cases permits the extraction of the partial densities for the components of the displacements. Those are defined by

$$\rho^H = \sum_j \rho_j^H \;, \qquad \text{(II.24)}$$

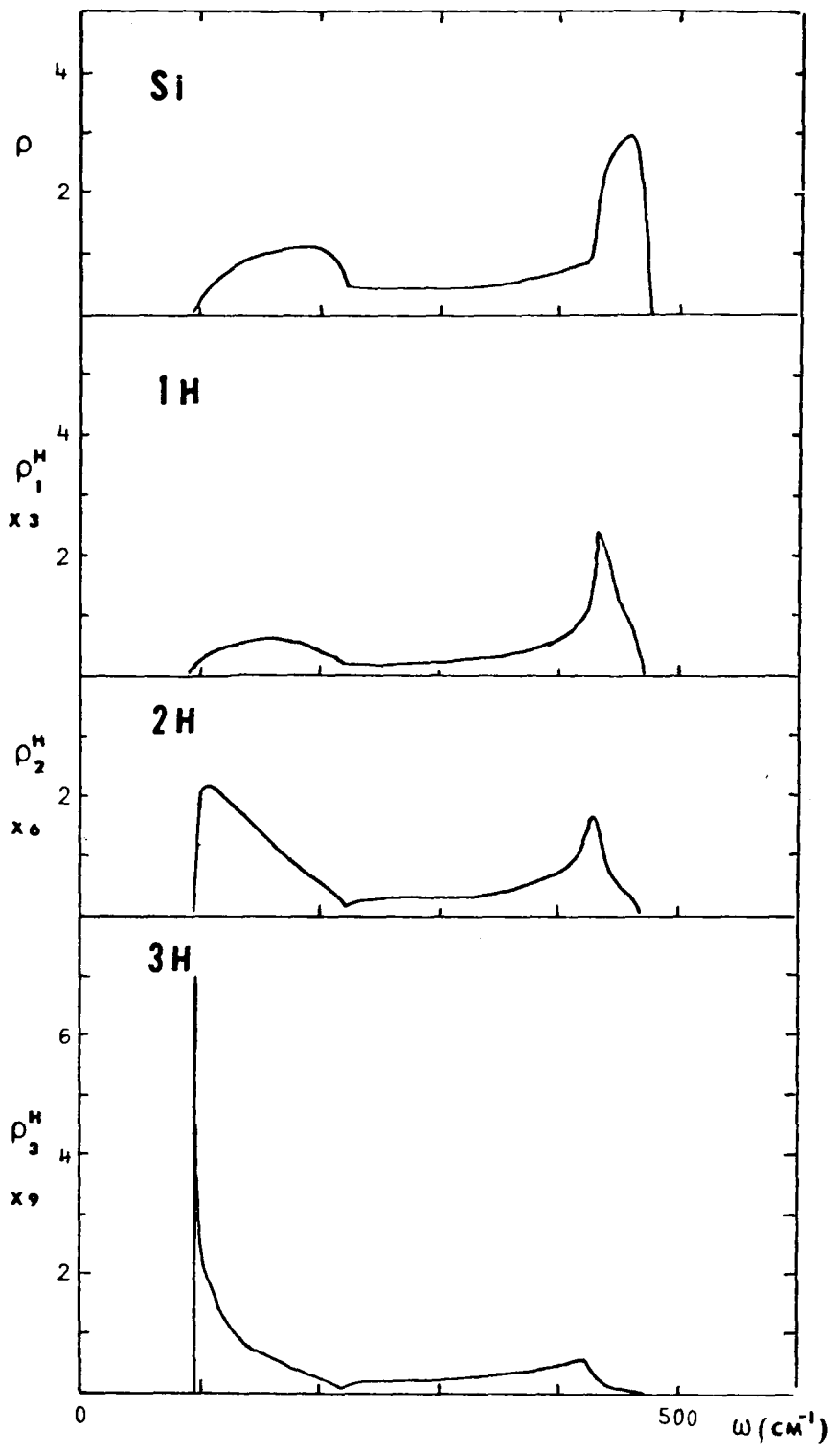

Fig.(II.3) Local response at the hydrogen sites for the configurations 1H, 2H and 3H. Compare with the pure Si density of states (ρ).

where j=x,y,z (or ($\parallel$,$\perp$)), and

$$\rho_j^H = \frac{-2m\omega}{\pi} Im\, g_{jj} \qquad (II.25)$$

These are shown in Fig.(II.4). Unfortunately, for the 3H case this separation was not possible, due to the numerical inversion involved.

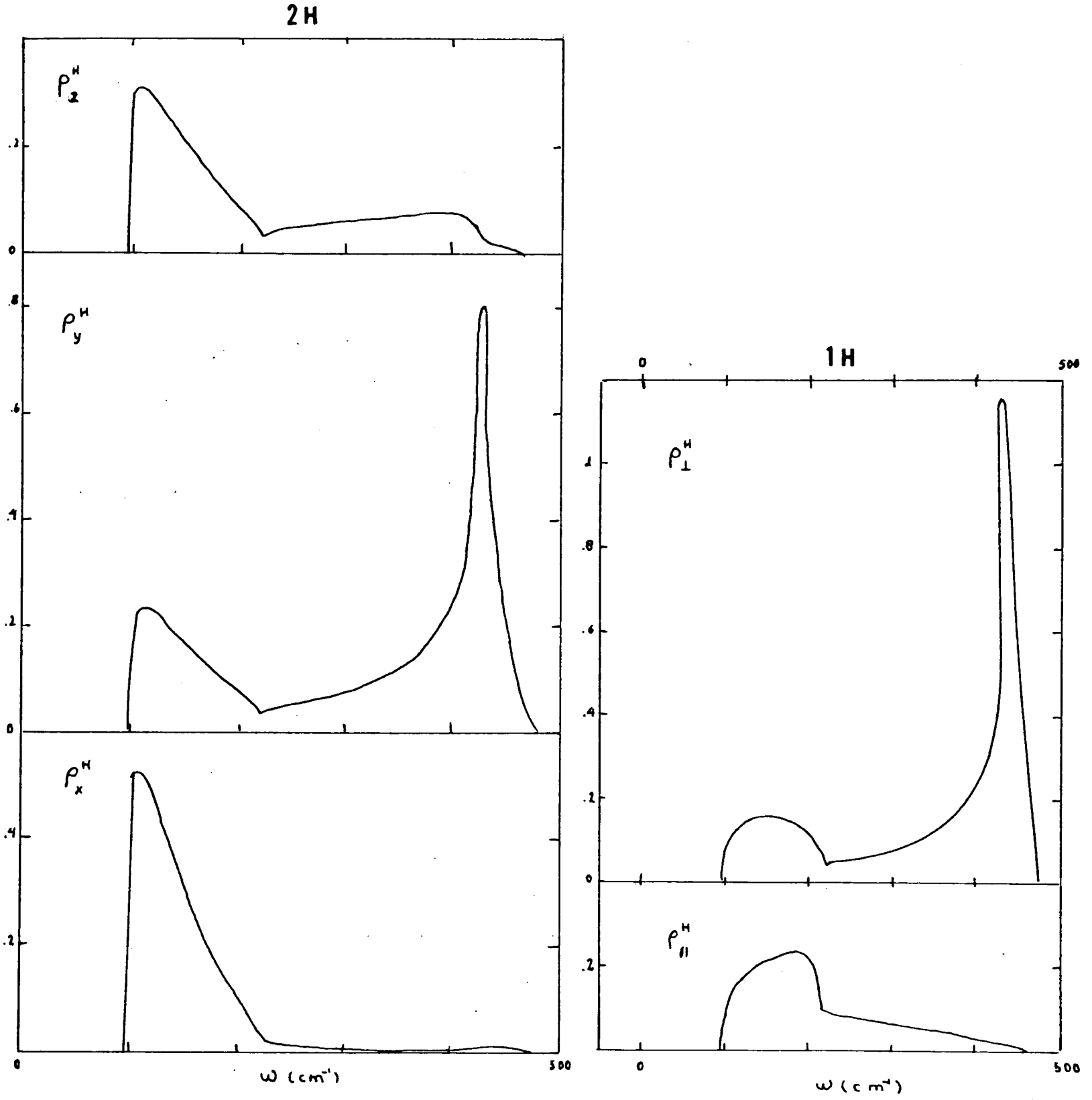

Fig.(II.4) Partial DOS at the hydrogen sites.

4.- FRACTION OF THE MODES ON THE DEFECT SITE

An interesting quantity that could give some information about the differences between the three configurations is the fraction (F) of the mode of frequency ω on the defect site (Dawber & Elliott (1963)). In the present case these quantities are

$$F_i = \frac{\rho_i^H}{\rho} \quad ; \quad i = 1, 2, 3 \qquad \text{(II.26)}$$

and are plotted in Fig.(II.5).

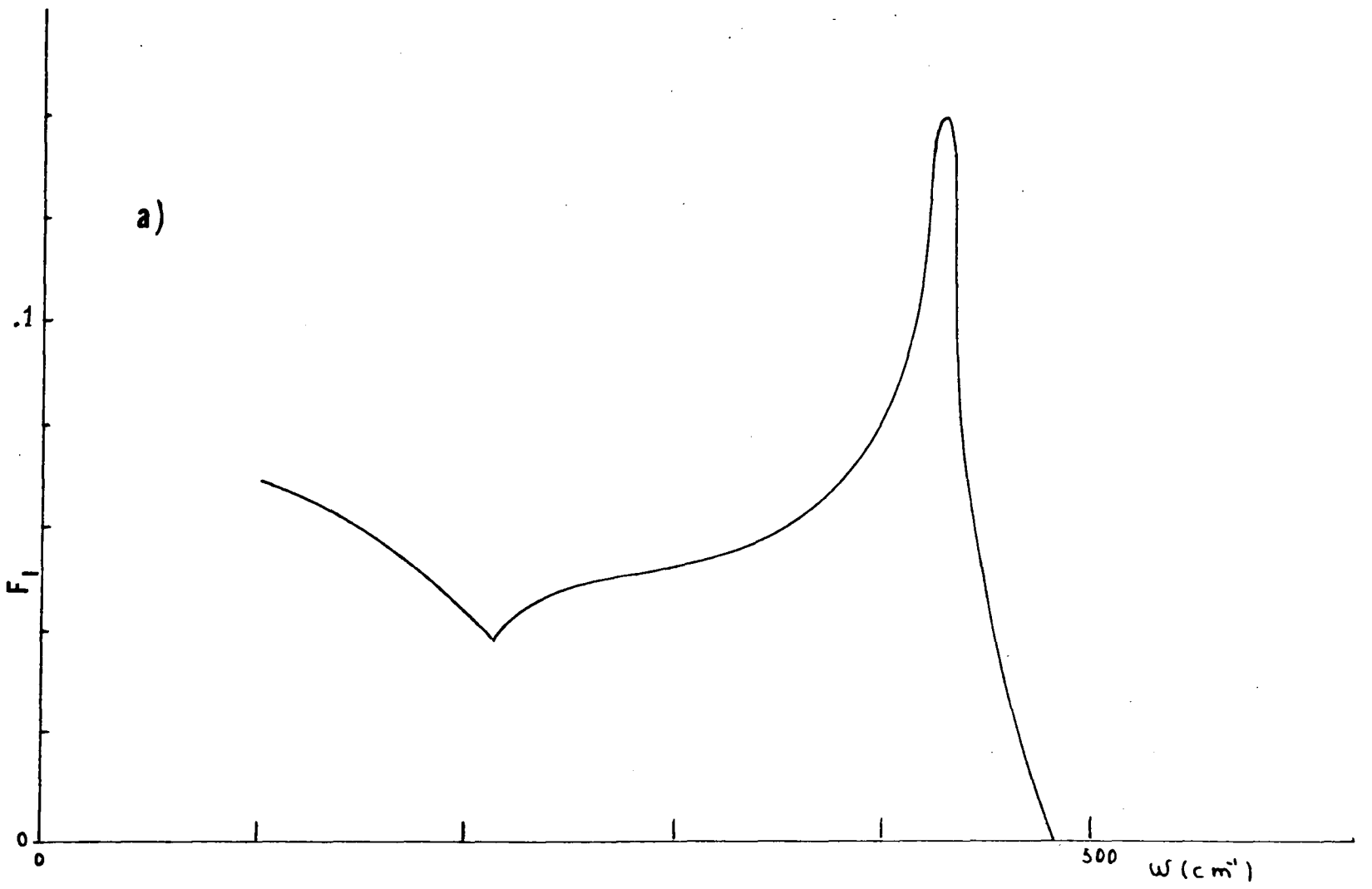

Fig.(II.5) Fraction of the band modes on the defect site. a) 1H, b) 2H, c) 3H.

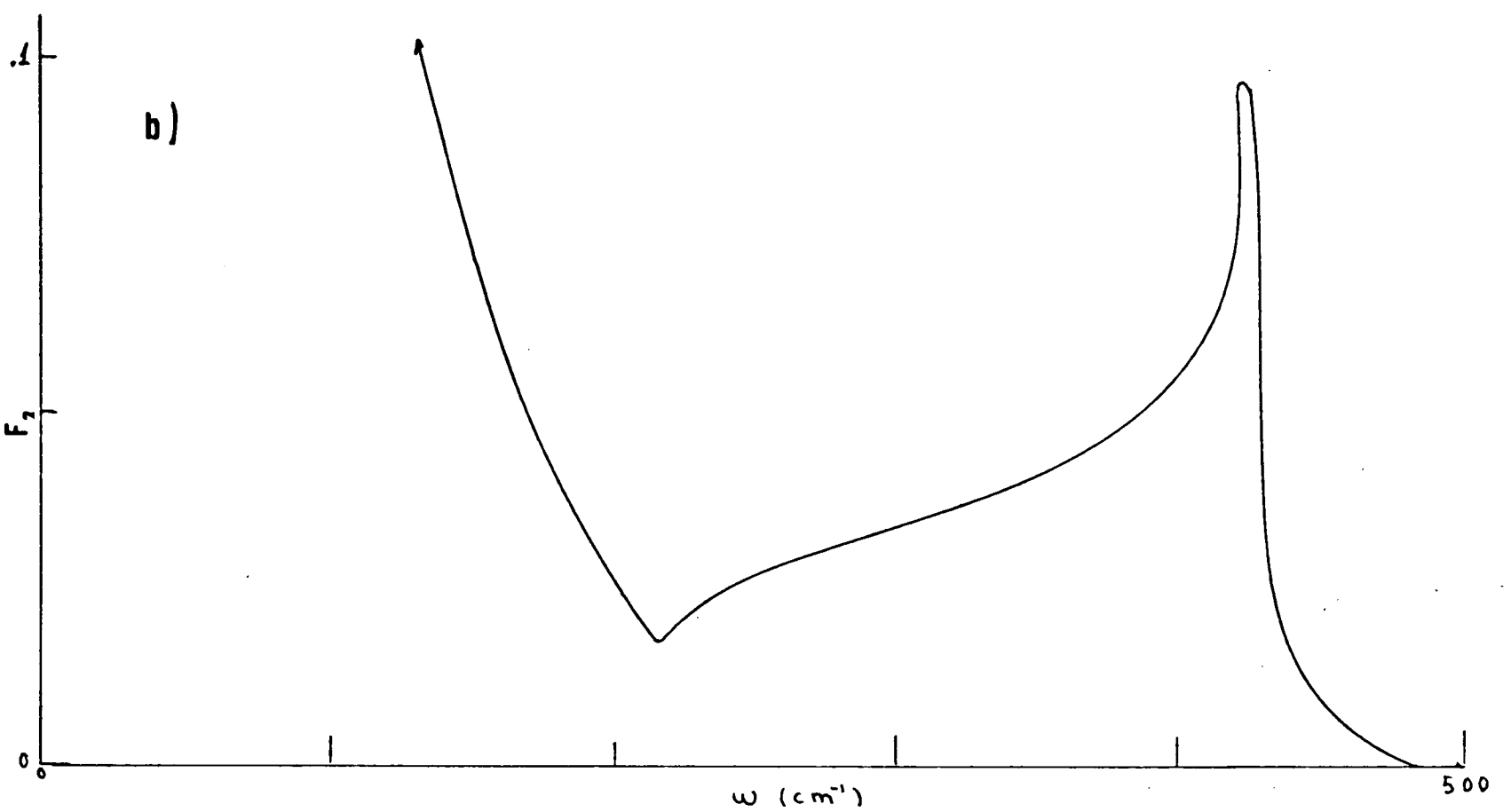
b)
.1
F_2
0
0
ω (cm⁻¹)
500

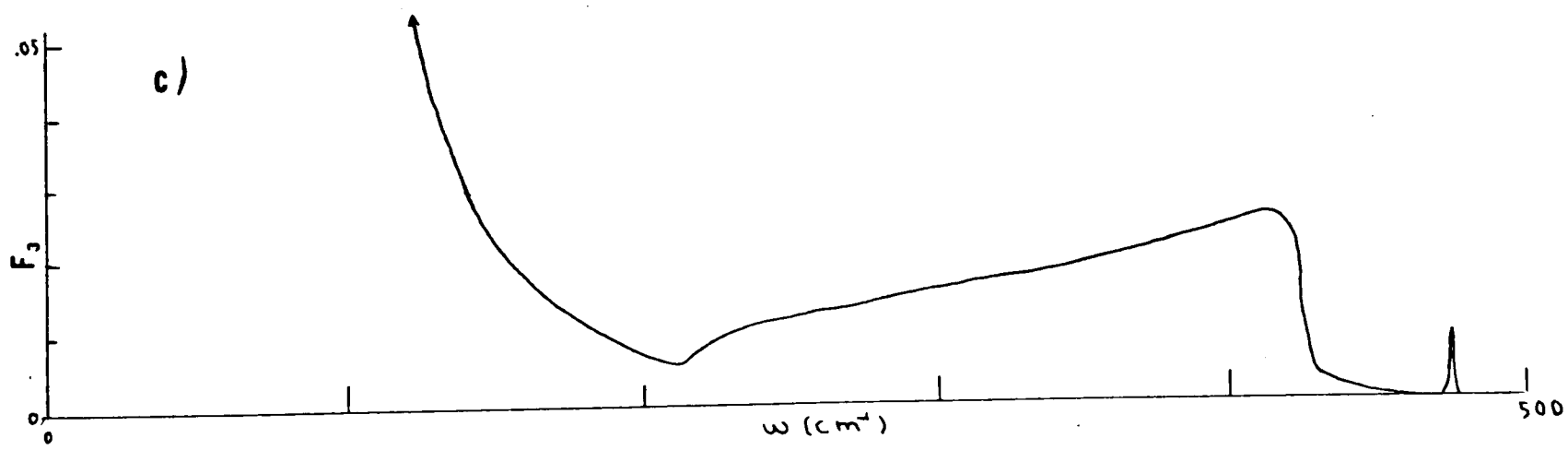
c)
.05
F_3
0
0
ω (cm⁻¹)
500

It is seen that there is a broad peak around 425 cm^{-1} whose height decreases with the perturbation (In the 3H case it is virtually nonexistent). It seems that it would be very difficult to distinguish these quantities experimentally, for the three configurations and therefore, alternative properties must be investigated. However, it is very useful to know that one should not expect dramatic changes in the shape of the $F_i(\omega)$ curves with the configuration.

It is worth noticing the pathological behaviour of $F_i(\omega)$ for small frequencies. Intuitively one should expect that this quantity may tend to the value m/M, because

$$\lim_{\omega \to 0}(F) = \frac{m}{M} \frac{\langle u_H^2 \rangle_0}{\langle u_{Si}^2 \rangle_0} = \frac{m}{M} \quad , \qquad \text{(II.27)}$$

that is, the mean square displacement of the H and Si atoms must be the same at low frequencies. In other words, the hydrogen must track the Si network exactly in this regime.

It is found that F_1 tends to the correct limit, but F_2 and F_3 get unreasonably large. We decided to investigate in detail this fact and learn if there is any physical reason to expect such a behaviour.

It is difficult to know what happens at very low frequencies, because the awkward behaviour of the Bethe lattice at the band edges, and also because there is an unphysical gap in the spectrum. However, the spectrum could be analytically continued by adding a small imaginary part to the frequency. Replacing ω^2 by $\omega^2+i\varepsilon$, where ε is a small positive number ($\sim 10^{-5}$) and calculating F_i we discovered that

$$\lim_{\omega \to 0}(F_1) = \frac{m}{M}\ (1.87) \qquad \text{(II.28a)}$$

$$\lim_{\omega \to 0} (F_2) = \frac{m}{M} (3.67) \quad , \tag{II.28b}$$

$$\lim_{\omega \to 0} (F_3) = \frac{m}{M} (14.56) \quad . \tag{II.28c}$$

These numbers are rather sensitive to the value of ε but the ones shown are a representative choice. The local DOS at the surface atom (ρ_s^i) (atom at site 0) were calculated using equations (II.1),(II.5) and (II.8), and the quantities F_i, ρ_s^i and ρ_i^H/ρ_s^i are shown in Fig.(II.6), Fig.(II.7) and Fig.(II.8) for the 1H, 2H and 3H respectively.

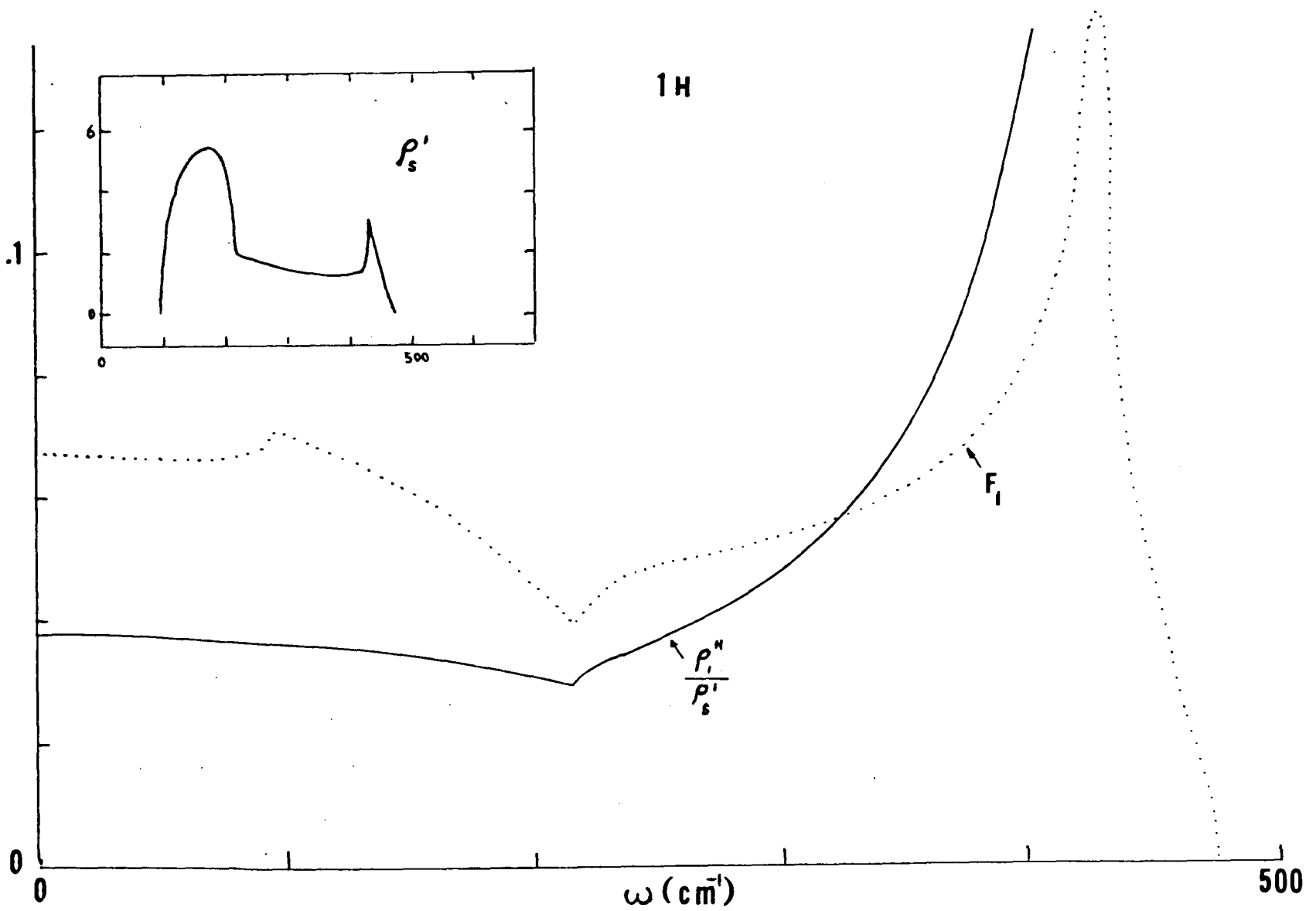

Fig.(II.6) F_1, ρ_s^1 and ρ_1^H/ρ_s^1 using the analytic continuation of the Bethe lattice Green's function ($\varepsilon \simeq 10^{-5}$). All quantities are defined in the text.

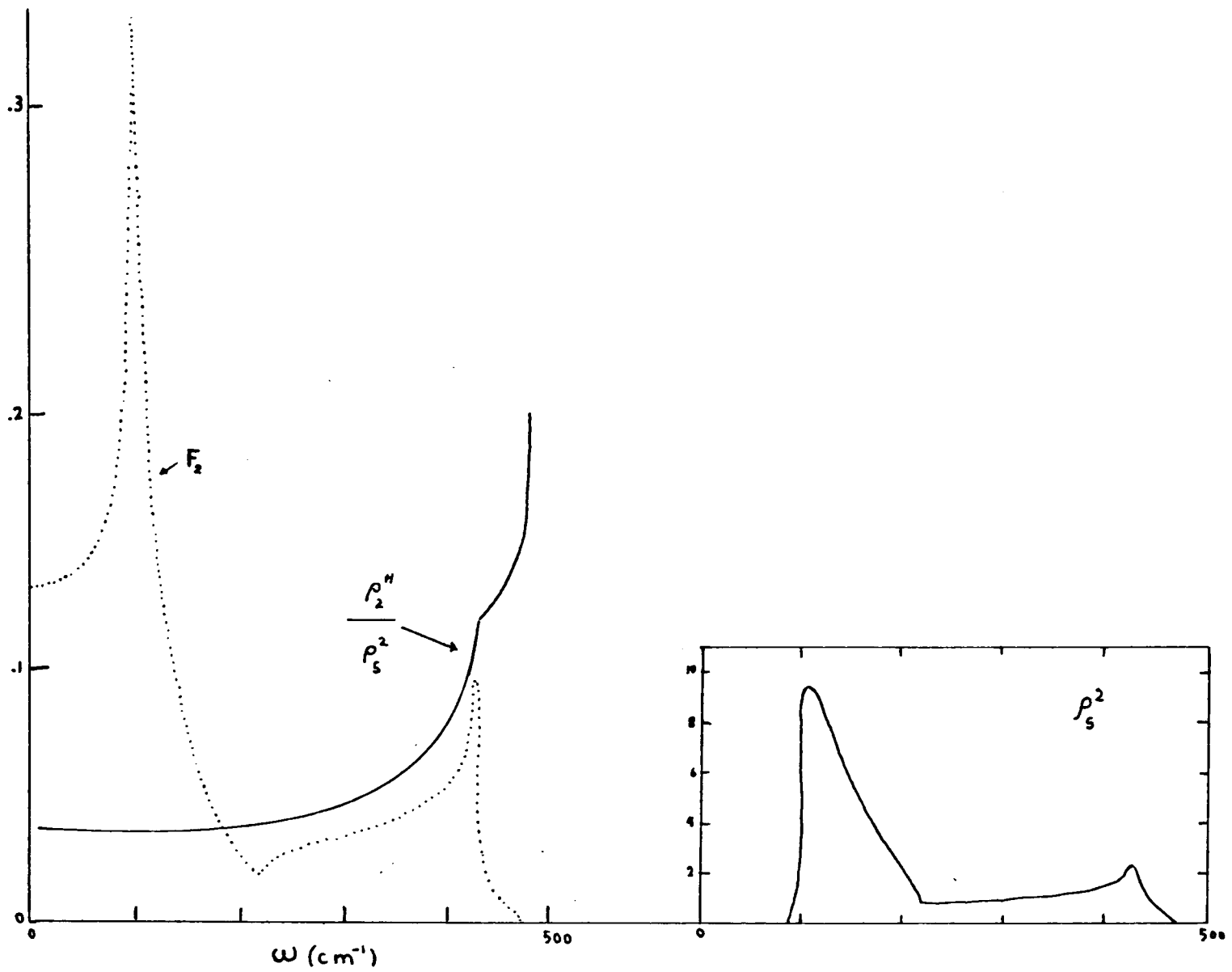

Fig(II.7) Same as Fig.(II.6) but for the 2H case

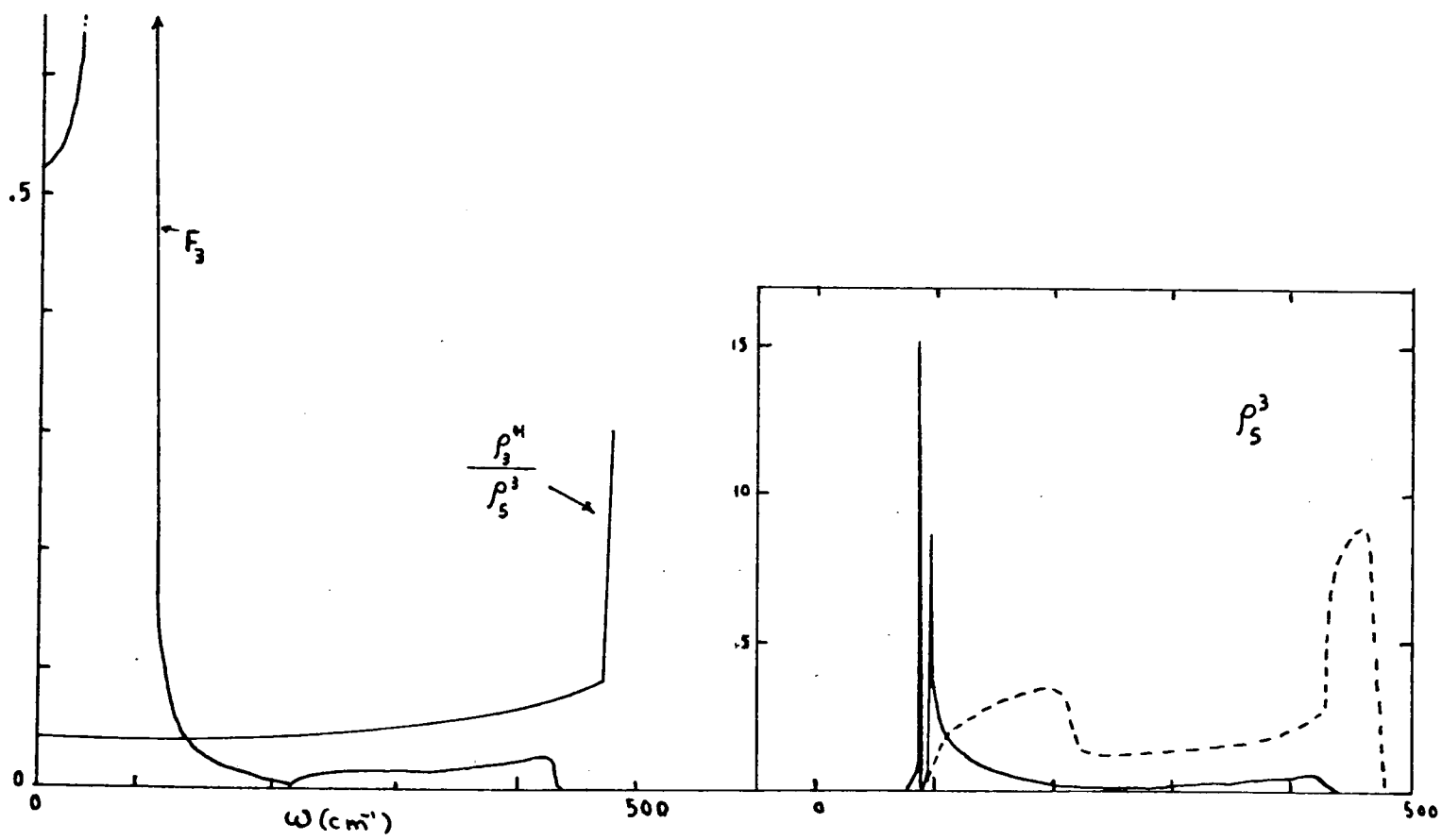

Fig,(II.8) Same as before but for the 3H case. The DOS for a bulk Si is also shown (---).

The important result is that ρ_i^H/ρ_s^i tends to m/M as $\omega \to 0$ in every case. This means that the hydrogens track exactly the motion of the surface Si atom, but not the motion in the bulk. On a real system the motion of surface and bulk atoms is the same at low frequencies, but this is not so in a Bethe lattice.

This general conclusion agrees with the results of E-NiFoo et al.(1976), where the DOS for atoms at and near the surface are calculated for the honeycomb, diamond and Bethe lattices.

In order to see how general this result is, the same method was applied to simpler models. In all of them the substitution $\omega^2 \to \omega^2 + i\varepsilon$ was made and functions of the form:

$$F_o = \lim_{\varepsilon \to 0} \lim_{\omega \to 0} \left(\frac{Im\, g_s}{Im\, g} \right) \quad , \qquad \text{(II.29)}$$

were calculated. The limits are taken in that order; g_s is the Green's function at the surface site and g is the Gn's function at any other site (next to the surface or in the bulk, as appropriate).

Five different models were considered:

i) Diatomic molecule . Two masses attached with a spring of stiffness α

$o\text{-}\overset{\alpha}{=}\text{--}o$ It is obvious that in this case $F_0 = 1$
$m_1 \quad m_2$

ii) Triatomic molecule. The situation is sketched as follows:

$o\text{-}\overset{\alpha}{=}o\text{-}\overset{\alpha}{=}o$. It is found that $F_0 = 1$ between any
$m_1 \quad m_2 \quad m_3$

pair of sites.

iii) Diatomic molecule attached to a wall. That is:

$o\text{-}\overset{\alpha}{=}o\text{-}\overset{\gamma}{-}\not\parallel$. In this case $F_0 = 1 + \dfrac{\gamma m_1 (2\alpha+\gamma)}{\alpha^2 (m_1+m_2)}$
$m_1 \quad m_2$

The last term arises because the wall is rigid, and a node is imposed in that position. If, instead, a moving wall (or an infinite network) is attached, then $\gamma = \gamma(\omega)$ and γ tends to zero as $\omega \to 0$. This means that the ratio F_0 between sites separated a finite distance is always 1, and that this result is quite general.

iv) Semi-infinite linear chain. Consider the following system:

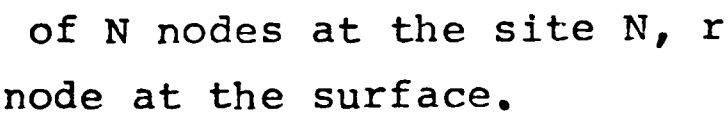

where all the masses and central forces are identical at every site. It is found that the ratio F_0 between the surface atom at 0 and a bulk one at ∞ is 2!.

By writing down the Green's function for the sites 0,1,2,etc... as a continued fraction

$$g_0 = \frac{1}{m\omega^2 - \Sigma}$$

$$g_1 = \frac{1}{m\omega^2 - \Sigma - \left(\alpha + \frac{\alpha^2}{m\omega^2 - \alpha}\right)} \qquad \text{(II.30)}$$

$$g_2 = \frac{1}{m\omega^2 - \Sigma - \left(\alpha + \frac{\alpha^2}{m\omega^2 - \alpha - \left(\alpha + \frac{\alpha^2}{m\omega^2 - \alpha}\right)}\right)}$$

$$\vdots$$

one is able to find the ratio F between the surface at 0 and the subsequent sites F(1), F(2), F(3), etc... The results are shown in Fig.(II.9). From here one can say that $F_0(N) = 1$ for any finite N, in agreement with the general result. The limit 2 for $N = \infty$ is due to the unphysical nature of the infinite system.

The N peaks found in F(N) arise because of the presence of N nodes at the site N, resulting from the forced antinode at the surface.

A linear chain is a Bethe lattice of coordination 2 and it is seen that the pathological behaviour of F at

low frequencies is already present in this system, and is undoubtedly a non-physical feature. In order to understand quantitatively the limits found in (II.28), let us examine a Bethe lattice of coordination 4, for central forces only.

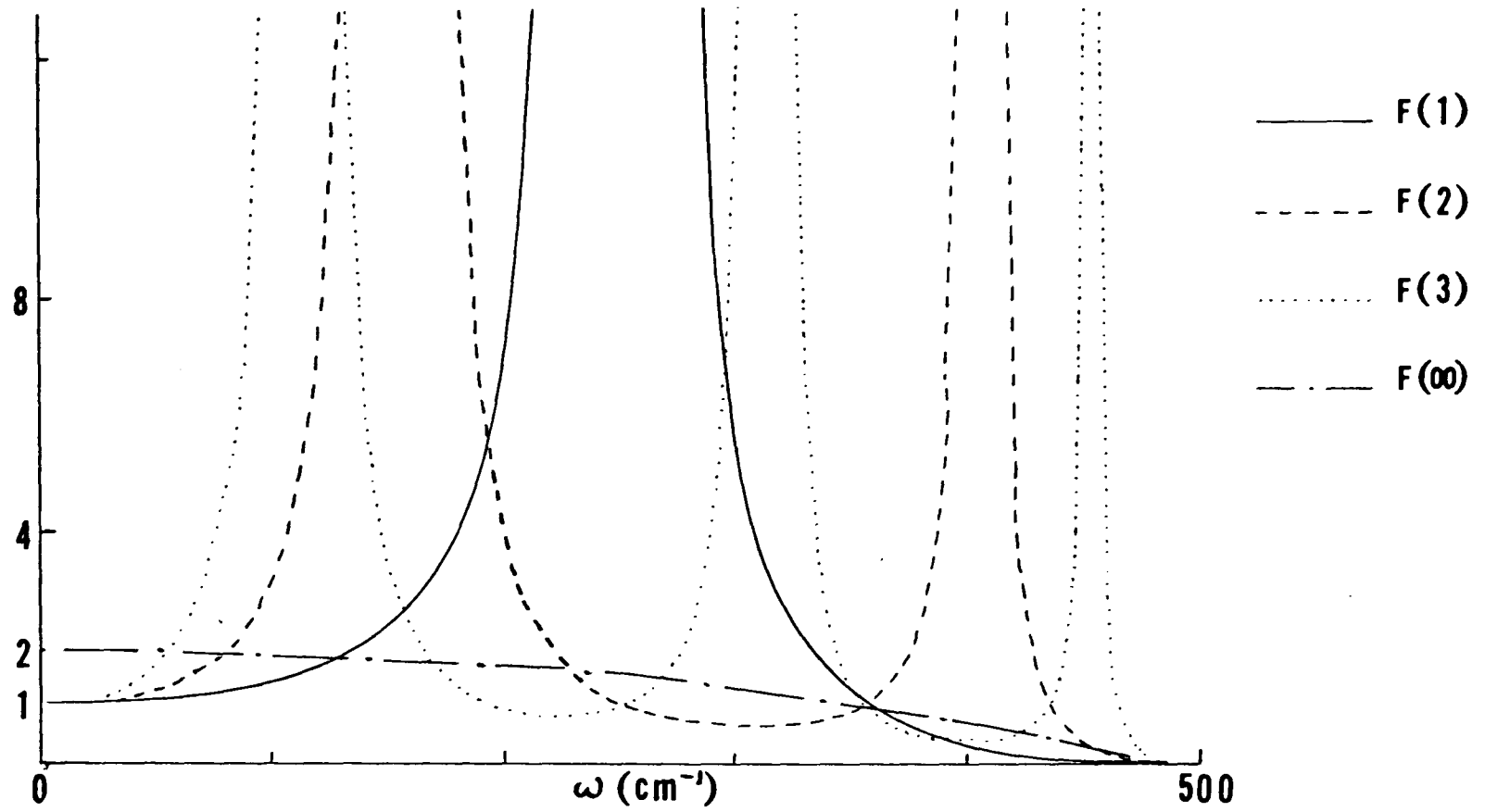

Fig.(II.9)Fraction of the surface atoms modes near $\omega=0$ for a semi-infinite linear chain.

v) Bethe lattice of coordination 4. Consider a surface atom at site O with n dangling bonds, if in the bulk

$$g_B = \frac{1}{M\omega^2 - 4\Sigma} \qquad \text{(II.31)}$$

then on the surface

$$g_o = \frac{1}{M\omega^2 - (4-n)\Sigma} \qquad \text{(II.32)}$$

For this model Σ is easily found by using equations(I.29), (I.30) and (I.31):

$$\zeta = \frac{M\omega^2}{2} - \frac{\alpha}{3} - \frac{1}{6}\sqrt{9(M\omega^2 - \frac{4}{3}\alpha)^2 - 12\alpha^2} \quad , \tag{II.33}$$

then

$$\lim_{\varepsilon \to 0} \lim_{\omega \to 0} \left(\frac{Im\, g_0}{Im\, g_B} \right) = \left(\frac{4}{4-n} \right)^2 \quad . \tag{II.34}$$

In Table II.3 these results are summarised and immediately seen is the good agreement between the last two columns.

Table II.3

Comparison between F_0 and the exact value for a Bethe lattice with only central forces.

configuration	n	$(\frac{4}{4-n})^2$	F_0 (from (II.28))
1H	1	1.78	1.87
2H	2	4	3.67
3H	3	16	14.56

The importance of this result is two-fold: 1) It enables one to understand the behaviour of F at low frequencies quantitatively and 2) supports the validity of equation (II.29) in the sense that the DOS could be analytically continued correctly in that way. Point (2) is not clear and some doubts have always arisen when the model is applied (Sen & Thorpe (1977)).

5.- BOUND STATES

Besides the band states some information can be extracted from the bound states outside the band. The oscillator strength of each one of those and the weight of the states in the band were calculated. The results are shown in Table II.4. Notice that the DOS comes out normalized properly, in each case.

Table II.4

Weights of the band and bound states for the hydrogen motion.

conf.	dir.	bound state at (cm^{-1})	oscil. strength (R_i)	$\sum_i R_i$	weight of band (W)	total weight $\sum_i R_i + W$
1H	⊥	640	.618			
	∥	2000	.320	.938	.060	0.998
2H	x	631.5	.049			
		890	.053			
		1999	.114			
		2011	.106			
	y	624	.168			
		654	.145			
	z	631.5	.114			
		890	.105			
		1999	.049			
		2011	.052	.956	.044	1.000
3H		624.2	.120			
		630.4	.219			
		794	.099			
		938	.214			
		1999	.112			
		2015.7	.210	.974	.020	0.994

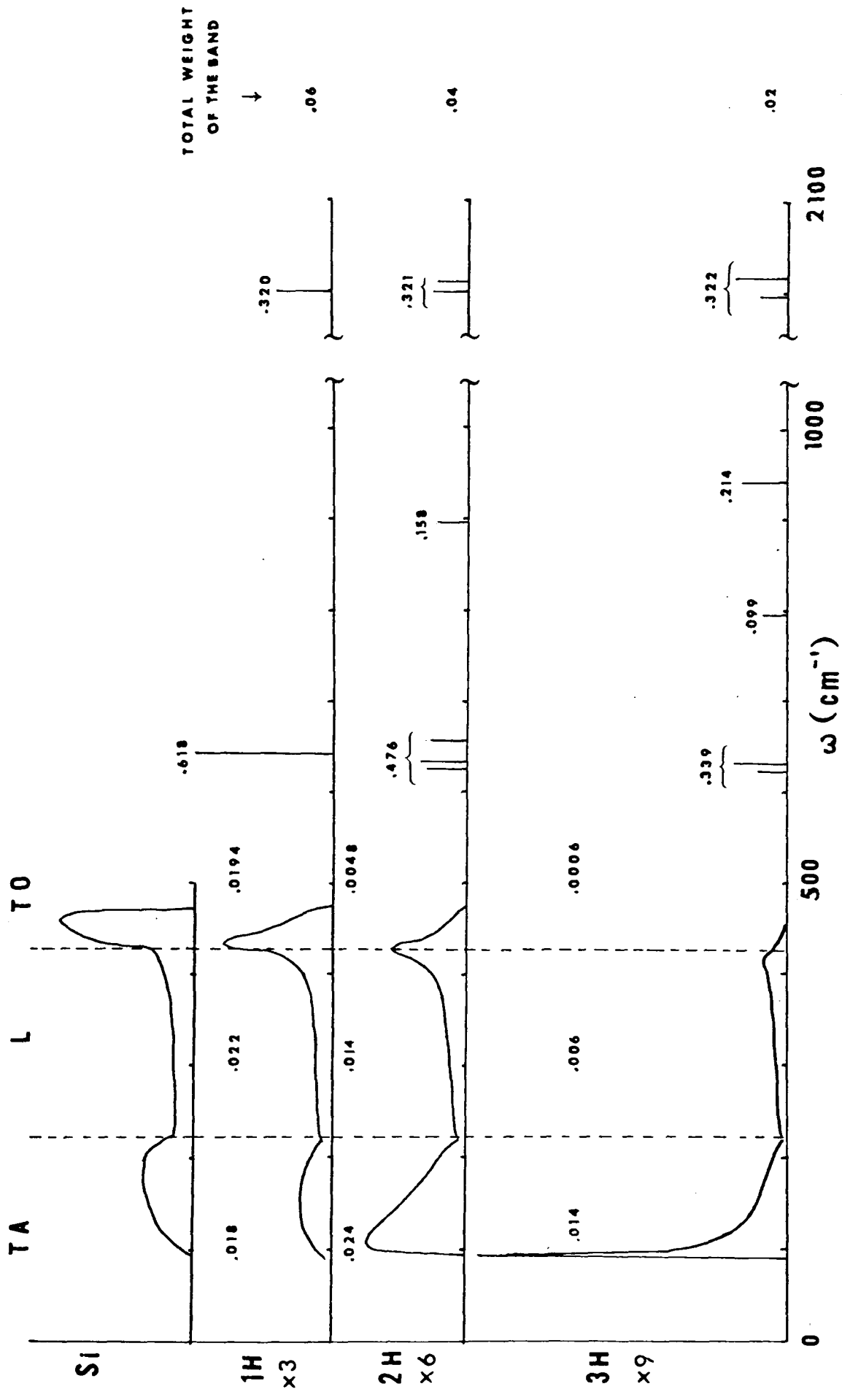

Fig. (II.10) Bands and localized states due to hydrogen motion. The numbers indicate the partial weight of each feature.

6.- RESULTS

All the results are collected in Fig.(II.10), where the band has been divided into three regions (TA,L,TO). Concerning the behaviour of the bands, the facts that are apparent from the figure are:

i) The weight of the band decreases with the number of hydrogens attached:

1H ≃ 0.06

2H ≃ 0.04

3H ≃ 0.02

ii) The fraction of the modes in the L region (ω_L/ω_B) remains constant:

1H ≃ .36

2H ≃ .35

3H ≃ .33

iii) The number of states in the TA region remains fairly constant, but the fraction of the modes (ω_{TA}/ω_B) increases

	ω	ω_{TA}/ω_B
1H	.018	.31
2H	.024	.56
3H	.014	.68

iv) The number of states in the TO region decreases, and also the fractional number ω_{TO}/ω_B

1H ∿ .33

2H ∿ .11

3H ∿ .03

Some splittings are observed in the wagging and stretching modes. In the 3H case a tremendous mixing of the bound states takes place and a very large splitting of the scissors modes is produced. Agrawal (1981a) calculated the frequencies for the 3H configuration and obtained 875, 910 and 2140 cm^{-1}, using an angular force constant model (Weber (1975)),but he adjusted its value with the 2H mode at 850 cm^{-1}.

Notice that nearly all the weight is in the bound states, this is because the large mass difference between Si and H. As more hydrogens are introduced, the weight of the bound states increases (as the band decreases) and the distribution of states changes.

It is worth noticing the following features:

v) The δ-function at 2000 cm^{-1} has constant weight

1H $\simeq$ .32

2H $\simeq$ .32

3H $\simeq$ .32

vi) The weight of the wagging modes decreases

1H $\simeq$ .62

2H $\simeq$ .48

3H $\simeq$ .34

vii) The weight of the scissors modes increases, as expected

1H = 0

2H $\simeq$ .16

3H $\simeq$ .31

The regularity of transfer of oscillator strength between the band states and the bound states in different regions is remarkable. In Fig.(II.11) it is noticed that the variation of the weights of all states is linear with the number of hydrogens (n) in the local configuration.

The importance of the interpolation made in Fig.(II.11) is that it provides a quantitative way for determining the fraction of sites with the 1H, 2H, or 3H configurations in a given sample of a-Si:H. The interpretation of the Raman scattering experiments (see for instance Shen et al. (1980)) is a little difficult, because information about the bands is needed. In infrared and Raman experiments the Si band dominates the spectrum due to the low weight of the H-band and the low concentration of hydrogen in the samples. However, the behaviour of the bands (fig,2 in

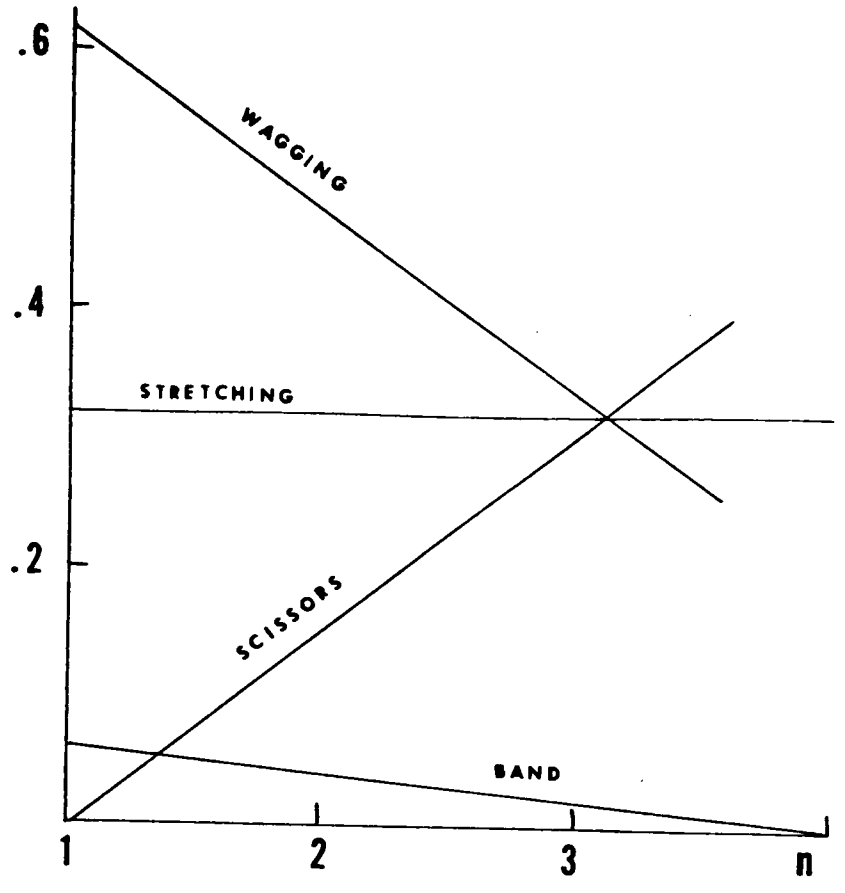

Fig.(II.11) Fraction of the hydrogen modes as a function of the number of H-atoms attached to a single Si atom. The sum of all of them is always unity.

Shen et al. (1980))with the concentration supports the idea that at higher concentration of H, clusters like 2H and 3H are formed (compare with Figs,(II.6),(II.7)and (II.8) for ρ_s^i).

As was mentioned above, inelastic neutron scattering in the ω range of the bands permits one to extract the hydrogen contribution and then, a quantitative study of them could be made. At the present moment some very recent experimental results are being examined in the light of the present theory (Axe et al.(1981)).

Let us go back to Fig(II.10) and try to find a relationship between the states in the bands and the bound states. It is seen that in the configuration nH, some

weight is transferred from the band and the wagging modes to the scissors modes as n increases. Of the total weight in the scissors modes, 1/7 comes from the band in every case. It is also apparent that this weight is taken from the upper part of the band.

7.- PHENOMENOLOGICAL MODEL

In order to understand this behaviour, we considered a simple phenomenological model to investigate the effect of the relative position of these bound states (with respect to the band) on the band itself.

Let us take a single mass defect with mass m in a host with mass M. If the local environment has cubic or tetrahedral symmetry, the response at the defect site (Elliott et al.(1974)) is the imaginary part of the Green's function

$$g_d = \frac{g_0}{1 - M\omega^2 \epsilon g_0} \quad , \tag{II.35}$$

where $\epsilon = \frac{(M-m)}{M}$, and g_0 is the Green's function for the host in the absence of a defect. This could be written in terms of the DOS of the host (ρ_0). Thus:

$$g_0(\omega) = \frac{1}{M}\left[\mathcal{P} \int_0^\infty \frac{\rho_0(\omega')\, d\omega'}{\omega^2 - \omega'^2} + \frac{i\pi}{2\omega} \rho_0(\omega) \right] \quad , \tag{II.36}$$

where $\mathcal{P}$ stands for the principal value of the integral. If one takes a simple ρ_0, one could investigate the fraction of the mode on the defect site

$$F = (Im\, g_d / Im\, g_0) \tag{II.37}$$

Two models for the DOS were considered: a Debye

spectrum (see for instance Dawber & Elliott (1963)) and a semicircular band. F is shown in Fig.(II.12a,b) for both models and for vàrious values of ϵ. The corresponding quantity for the 1H case is also shown in Fig.(II.12c).

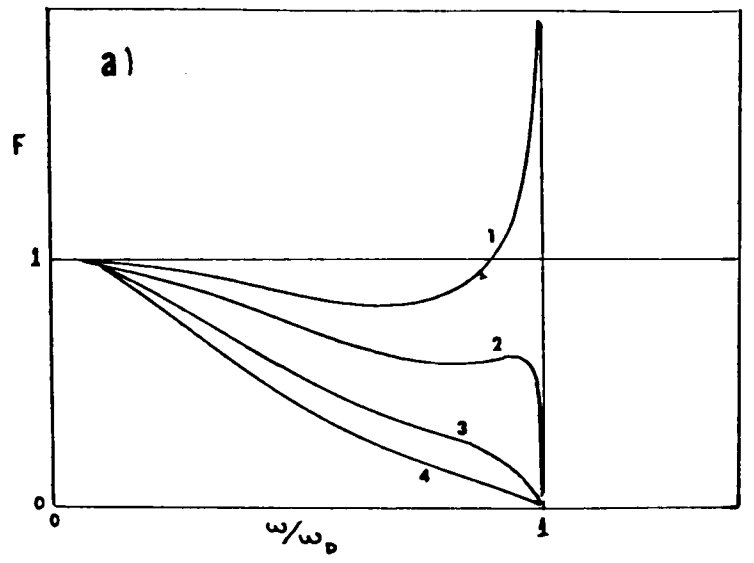

	ω_0/ω_D	ϵ
1	1	~.5
2	1.4	.7
3	2	.85
4	5	.98

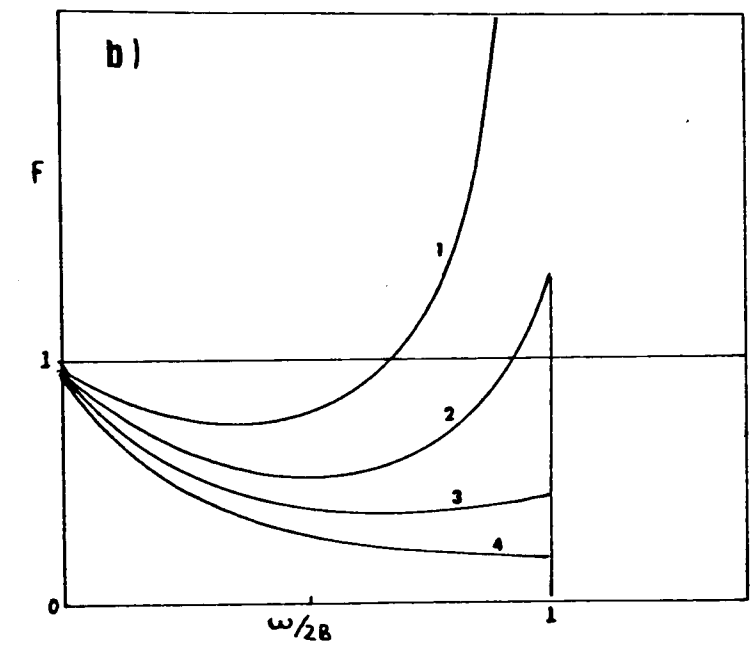

	$\omega_0/2B$	ϵ
1	1	.25
2	1.3	.46
3	2	.62
4	5	.82

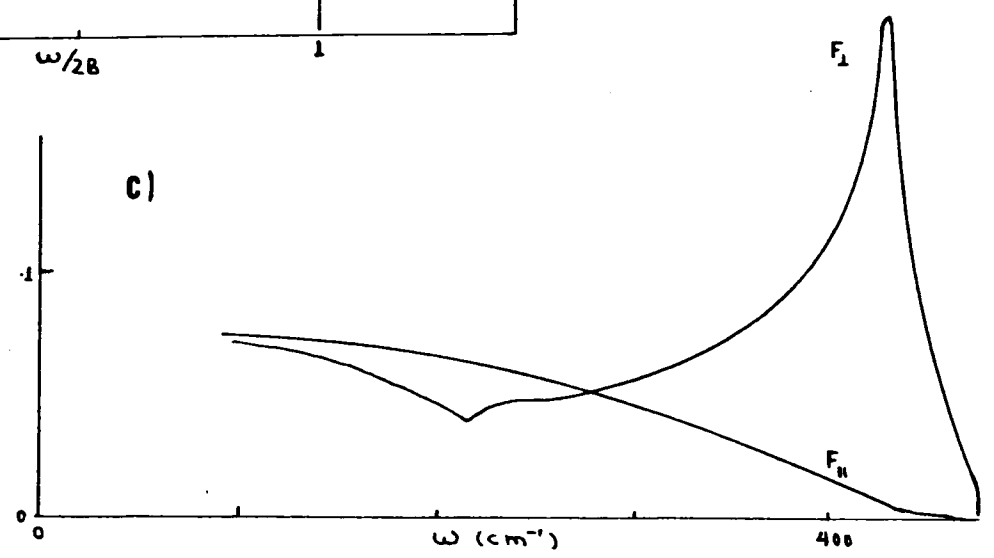

Fig.(II.12) a) Fraction of the mode on the defect site (F) for various values of ϵ using a Debye spectrum (ω_D = Debye frequency). b) Semicircular Band. ω_0 is the frequency of the bound state. c) $F_{\parallel}$, $F_{\perp}$ defined by eq.(II.26)

The position of the bound state $\omega(\omega_0)$ is obtained when the denominator of (II.35) vanishes.

The qualitative behavior of the three sets of graphs is similar. Particularly noticeable is the similarity between curves 1 and 4 on part a) and $F_\perp$ and $F_{||}$ on part c). The two important features are 1) The bottom of the band is quite independent of ω_0, as all the atoms vibrate with the same amplitude in this regime, and this just corresponds to sound waves; 2) The weight of the band decreases as e increases, and it is taken from the <u>top</u> of the band, Therefore the position of the bound states is crucial for determining the scattering from the band.

These conclusions are quite general because they do not depend on the details of the spectrum. In order to check if there is also quantitative agreement, we plotted the fractional weight of the band as a function of the position of the bound states, for both models Fig.(II.13).

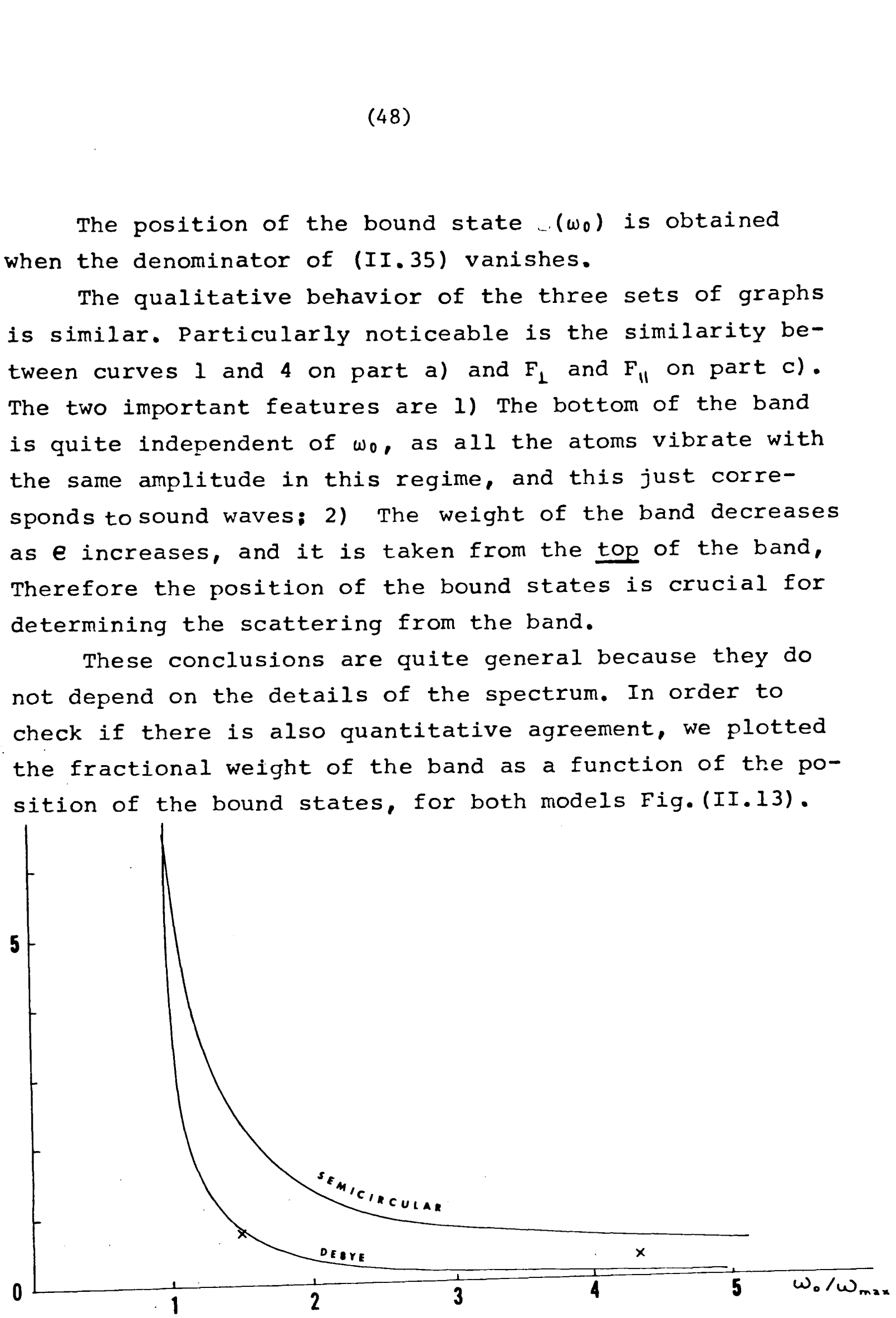

Fig.(II.13) Total weight in the band as a function of ω_0 for the two models considered. The weights of the partial DOS in the 1H case are marked ×.

In the 1H case, the bound states are at $\frac{\omega_0}{\omega_D} = 1.39$ and 4.35 for wagging and stretching respectively. The weights of the bands are 0.072 and 0.035 for each case. These are indicated also in Fig.(II.13). It is seen that the Debye model predicts roughly the same numbers, thus we conclude that the predictions made using the simple model are quite general and that the relative weight of the different regions of the bands is rather insensitive to the details of the spectrum but that the position of the bound states is what matters.

8.- CONCLUSIONS

In this Chapter the vibrational properties of three different clusters of hydrogen in amorphous silicon have been examined. Through the detailed study of both, the bound states and the band, some general facts have been pointed out. These provide information that enables one to know the way in which hydrogen is incorporated in a given sample of a-Si:H, and to interpret inelastic neutron scattering data.

The important conclusions are:

i) The position of the bound states determines the actual shape of the upper part of the band.

ii) The relative oscillator strength of the bound states and of the TO region of the band is very sensitive to the clustering of the hydrogen.

iii) The statements i) and ii) are quite general, and do not depend on the actual shape of the band.

iv) The TA region of the band cannot be studied properly with the Bethe lattice model and the pathological changes in the shape of the band are non-physical, but are due entirely to the drawbacks inherent in the model.

C H A P T E R I I I

CPA ON A Si-Ge AMORPHOUS ALLOY

1.- BASIC CONCEPTS

Amorphous random alloys are very interesting systems where both, structural and topological disorder are present. Among those, the Si_x-Ge_{1-x} alloy is particularly suitable to be treated theoretically, mainly because both materials have similar coordination and bonding character.

The electronic properties of such an alloy have been studied by Falicov & Yndurain (1975), assuming a tight-binding Hamiltonian and a Cluster-Bethe lattice method, and the results compared with a CPA calculation.

This method has been applied to the vibrational properties by Yndurain (1976),(1978) and the deduced DOS compares extremely well with the first order Raman spectrum (Fig.(III.1)

The Coherent Potential Approximation (CPA) is considered at present, to be the best single-site theory for a disordered system (for a review of CPA see Yonezawa & Morigaki (1973)), and has been applied successfully to a number of disordered systems (Elliott et al.(1974)) and, in particular, to random alloys (Velický et al.(1968)). CPA has been used also in systems where more than one type of disorder is present, for instance, in the problem of exciton exponential tails in mixed alkali-halides (Sawai et al.(1973)).

Therefore, it is interesting to investigate the Si-Ge amorphous alloy within the CPA. The similarity of both materials allows one to think that the mass defect approximation (Taylor (1975)) will give fairly good results.

The procedure is as follows: Assume an effective medium described by a Green's function G_0, which can be written in terms of the Green's function of the unperturbed system (P) and a self-energy (Σ), defined by

$$G_0 = P + P\Sigma G_0 \qquad \text{(III.1)}$$

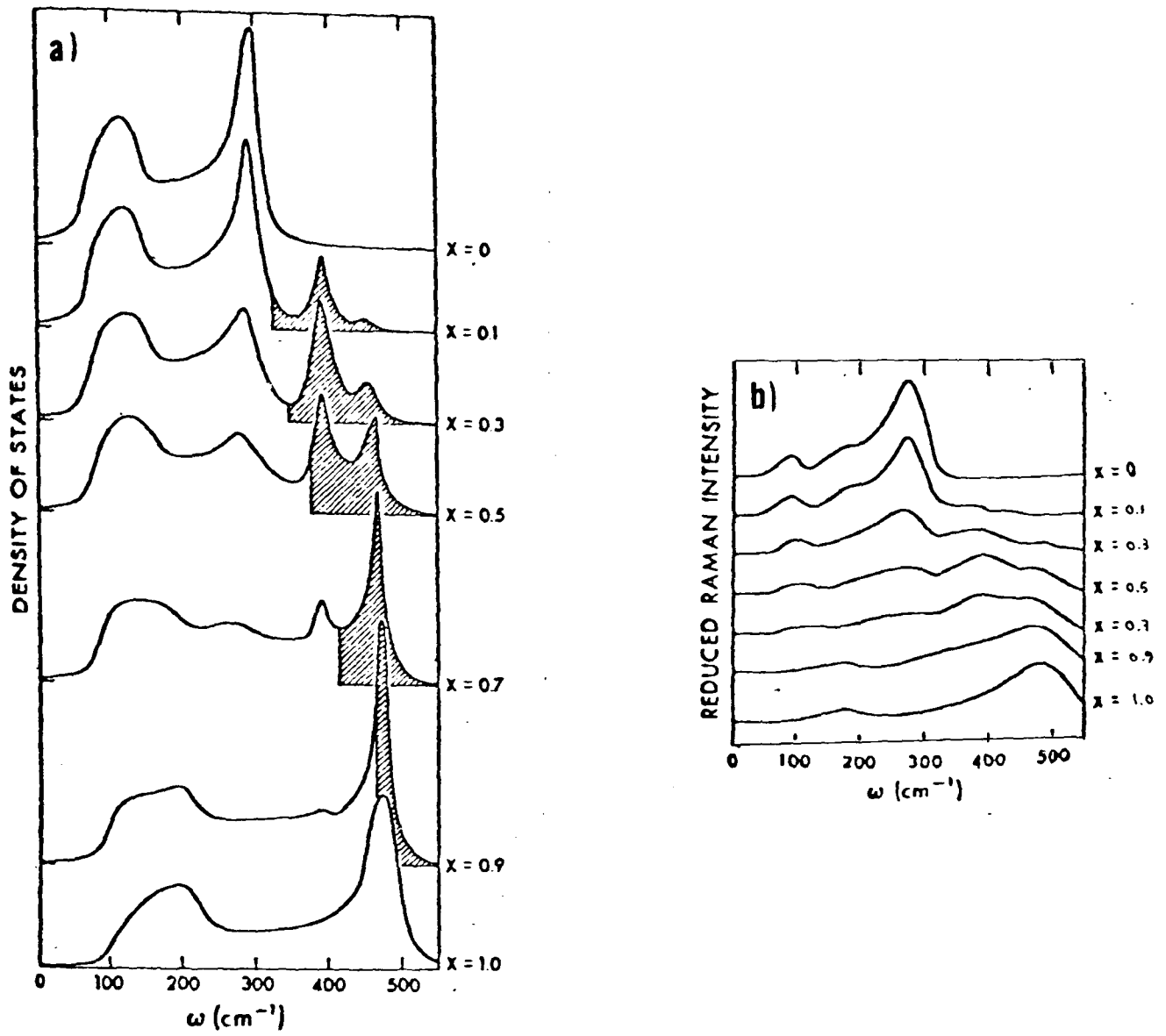

Fig.(III.1) a) Density of states for a Si_x-Ge_{1-x} amorphous alloy calculated with a Cluster-Bethe lattice method by Yndurain (1978). b) Reduced Raman intensity for various Si-Ge alloys taken by Lannin (1974).

If the model described in Chapter I is taken, P is nothing but the solution of equation (I.18), with $M=m_{Ge}$. The Green's function of the perturbed system obeys the Dyson equation

$$G = G_0 + G_0(V - \Sigma)G \qquad \text{(III.2)}$$

where the perturbation

$$V = m_{Ge}\omega^2\varepsilon \quad , \quad (\varepsilon = 1 - \frac{m_{Si}}{m_{Ge}}) \tag{III.3}$$

is put at random in each site. A self-consistent condition is found for Σ by demanding the single-site t-matrix to be zero on the average. The result is

$$\Sigma = \frac{xV}{1 - (V-\Sigma)\cdot G_0} \tag{III.4}$$

where x is the concentration of Si atoms. Equations (III.1) and (III.4) are solved simultaneously to give the best approximation for G.

Once G is obtained, the DOS is found by

$$\rho_x(\omega) = -\frac{2m_{Ge}\omega}{\pi}(1-x\varepsilon)\operatorname*{Im}_{\gamma\to 0+} G(\omega+i\gamma) \tag{III.5}$$

In principle the solution is straightforward, nevertheless, the actual calculation presents serious problems. Therefore it seems to be necessary to give a detailed description of the procedure and the way each problem encountered was solved.

2.- DETAILS OF THE CALCULATION AND RESULTS

First of all one obtains $P(\omega)$ in equation (III.1) as the solution of (I.18), which is g. Here we will make use of the symmetry properties of the CPA formula under interchange of x and (1-x); and use the Si lattice as the pure system (In the results all the parameters will be changed in order to compare with Fig,(III.1)). It is clear that

$$x \rightleftarrows (1-x); \quad m_{Ge} \rightleftarrows m_{Si}; \quad \varepsilon \rightleftarrows \frac{\varepsilon}{1-\varepsilon} \tag{III.6}$$

The correct root in (I.18) is selected using (I.13).

Then, in order to iterate (III.4), a first trial for Σ is needed. This was chosen to be the solution of (III.4) but substituting g instead of G_0:

$$\Sigma_{\pm} = \frac{1}{2g}(Vg - 1 \pm \sqrt{(1-Vg)^2+4Vgx}\ ) \qquad \text{(III.7)}$$

With this value one calculates G_0 using (III.1):

$$G_0(E) = P(E-\Sigma) = g(\omega^2-\Sigma/M) \qquad \text{(III.8)}$$

Observe that (III.7) has two roots, the physical one corresponding to taking the positive sign of the square root, because it gives the correct Virtual Crystal limits when x→0 or x→1. However, taking the square root of a complex number in the computer always gives the principal value (on the right half-plane), and it is very difficult to decide which root corresponds to the positive sign. One way of deciding between the roots is by calculating both Green's functions, G_{0_+} and G_{0_-} with the corresponding Σ_+ or Σ_- in (III.7), and by taking the numbers:

$$T_{\pm} = \Sigma_{\pm} - \left|\frac{xV}{1-(V-\Sigma_{\pm})G_{0_{\pm}}}\right| \qquad \text{(III.9)}$$

The correct root is the one that gives the smallest number, the reason is because the second term in (III.9) is nothing but the self-energy defined in (III.4). The DOS is calculated using g instead of G in (III.5), and also using G. Both are compared and if they differ by more than 1%, a new self energy is needed. This is exactly the second term in (III.9), thus it is inserted in (III.8) and the cycle repeats until the accuracy is attained, that is, until two succesive densities of states do not differ by more than 1%. Convergence is good for most of the values

of ω (less than 10 iterations are needed), but for some points (where Reg changes sign) this is not so. This is due to the fact that T_+ and T_- are equal, within the machine precision, and after few iterations an endless cycle of values appears, meaning that the wrong root has been chosen.

This problem is definitely a computational one and in order to avoid it , it is necessary to give new values to $\Sigma_\pm$ in order to get out of the vicious circle. Making the substitution $\Sigma_\pm \to \Sigma_\pm \mp (\Sigma_+ - \Sigma_-)/4$ proved to be helpful in all cases.

The final results are shown in Fig.(III.2), compare with the other figure.

3.- DISCUSSION

It is very difficult to make a precise quantitative comparison with experiment, because the data in Fig.(III.1b) are rather ambiguous. Furthermore, matrix elements effects in the Raman experiment have to be considered. It is not easy, at this stage, to calculate the Raman intensity for an alloy, but one could extrapolate the results in §4 of Chapter I and assume that the only effect is to enhance the upper part of the spectrum, and that there will be peaks in the Raman intensity wherever there are peaks in the DOS. This is in agreement with the observations and provides a justification for the neglect of matrix elements effects by Yndurain (1976). Taking this into account, let us compare Fig.(III.1a) and Fig (III.2)

At first glance they seem to be very similar, but a more careful look reveals some differences:

i) Notice that in Fig(III.2) (f2 form now on) the low frequency peak shifts continuously from 120 cm^{-1} to 190 cm^{-1} for pure Si. This does not happen in Fig.(III.1a) (f1),

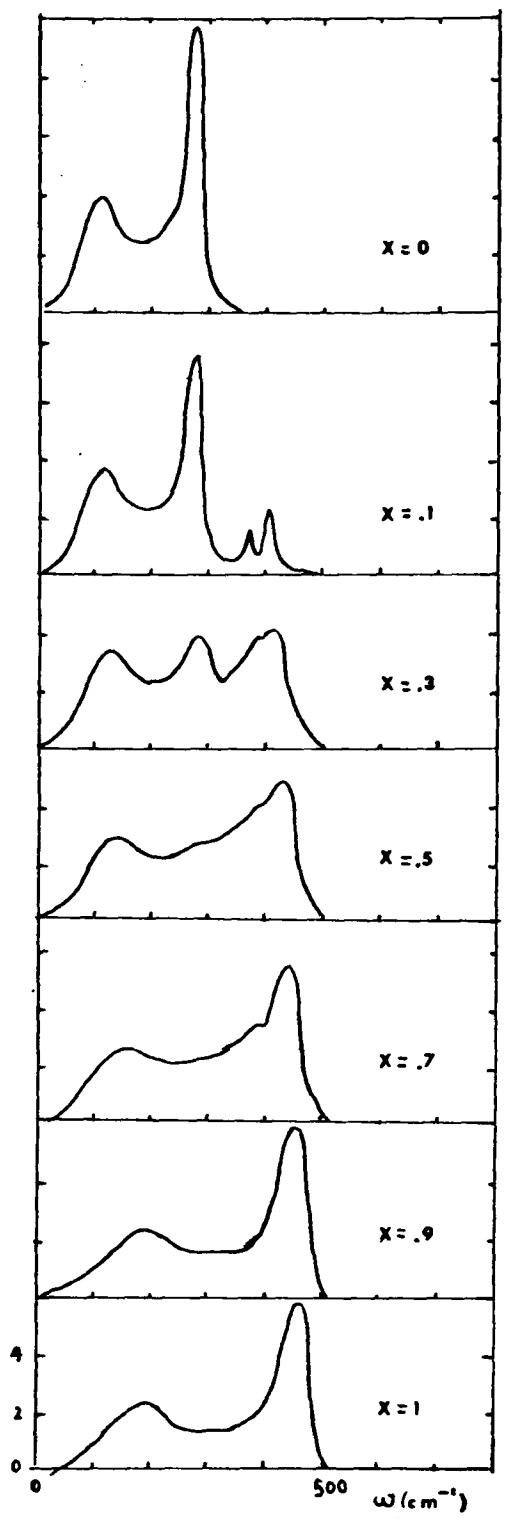

Fig.(III.2) CPA Density of states for a Si_x-Ge_{1-x} amorphous alloy.

where a sudden change occurs at x$\sim$.9. Therefore, the CPA calculation agrees better with experiment in this respect (see Agrawal (1981b), this paper will be Agr from now on).

ii) In the CPA, the peak at 280 cm^{-1} does not move with x, while in the other calculation it shifts towards lower frequencies with x. Yndurain (1978) (Y) attributes this peak to Ge-Ge bonds, and justifies its behaviour based on measurements by Feldman et al.(1971). However, one cannot see what really is happening in the experiment, because of

its poor resolution. It is worth mentioning that Agr states that this peak does not move with x. It is also noticed that in the CPA this peak diminishes too rapidly with x.

iii) The high frequency peak moves continuously from 470 cm^{-1} at x=1 to $\sim$420 cm^{-1} at x=.1. This agrees better with the experiment than the calculation by Y , where the peak remains stationary and only changes its intensity. Again, it is difficult to say something from the experiment, for instance, Agr is convinced that this Si-Si peak is x-independent and then forces his Cluster-Bethe lattice method to produce this result by making the Bethe lattices concentration independent!. This leads to a contradiction regarding the localization of the states in this peak: While Y shows that states in the Si-Si peak are localized for x <.7, Agr obtains extended states on the whole frequency range.

Notice that the intensity of this peak is always too large in f2 and that the peak itself cannot be ascribed to Si-Si bonds.

iv) There is a peak around 380 cm^{-1} in f2 for all intermediate concentrations. In (Y) this feature can be attributed to the presence of Si-Ge bonds in the cluster and its position is independent of x. In the CPA no pairing effects can be taken into account, and therefore the identification of one peak or the other as Si-Ge or Si-Si bonds is not possible. Not only that, but the very appearance of <u>two</u> impurity bands is very surprising.

This effect has never been observed in CPA but, curiously enough, the shifting of this peak with x is remarkably in agreement with experiment. It is, therefore, worthwhile to investigate the mechanism that produces such an unexpected feature.

In Fig.(III.3) we reproduce the typical behaviour of Σ for an intermediate concentration (x=.1). Notice that

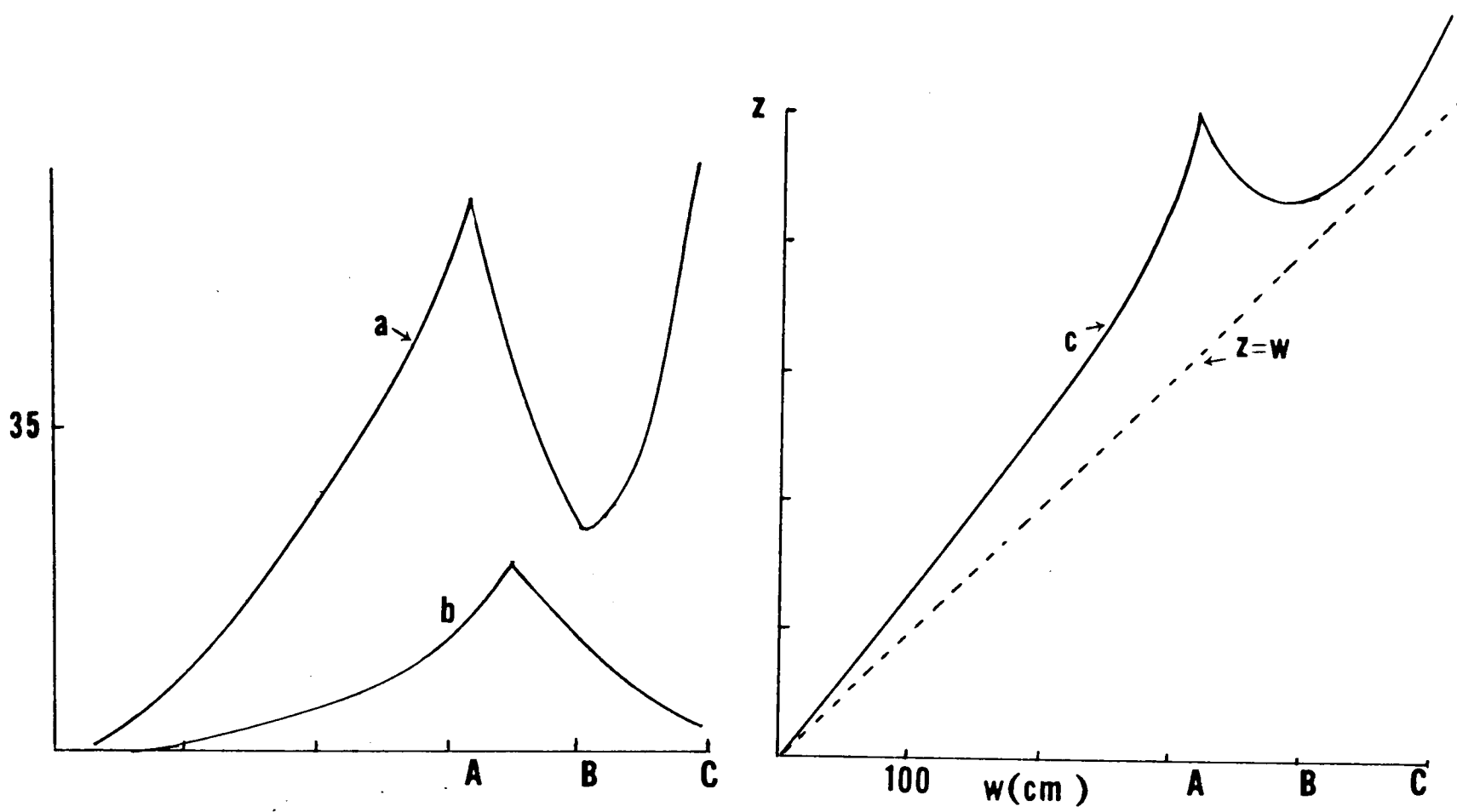

Fig.(III.3) a) Negative of the real part of the self energy. b) Negative of the imaginary part of the self energy. c) Real part of the effective frequency $z = \sqrt{(\omega^2 - \Sigma/M)}$, where g is evaluated to produce G_0 in the CPA.

the peak on $Re\Sigma$ occurs at a different frequency than the peak on $Im\Sigma$. This situation is very unusual and it is the very cause of the two peaks.

Formula (III.8) states that G_0 is simply g, calculated at an effective frequency $\sqrt{(\omega^2 - \Sigma/M)}$. When $Im\Sigma$ is very small, the DOS for the alloy will have the same value as the one for the pure system calculated for an energy shifted by Σ. If $Im\Sigma$ is large, g must be calculated very far from the real axis, where the spectrum becomes flat.

Looking at Fig.(III.3c) one can reproduce the spectrum for x=.1 (in fact x=.9 in the calculation) in f2. Going from ω=O to ω=A, the whole spectrum for pure Si is spanned. The TO peak is less intense because ImΣ is increasing steadily in this range. From A to B the TO peak is scanned again backwards. The same peak is reproduced once more while going from B to C. The last peak is higher because ImΣ is smaller in the interval B-C than in the interval A-B.

This situation is also encountered in the disordered linear chain (Taylor (1967)), but there the peak is washed out by a singularity in ImΣ precisely at the point where the peak on ReΣ occurs. There is no obvious reason to expect the shift in the peak on ImΣ but, in any case, one must conclude that the double peak on the upper part of the alloy spectrum is spurious and is due, perhaps, to the pathological band edges on the Bethe lattice.

4.- CONCLUSIONS

The results from the present CPA calculation are, at least, as useful as the ones from the Cluster-Bethe lattice by Y , and better than the ones by Agr. The position of the main peaks on the DOS, and their dependence on the concentration proved to be closer to the experiment than in the other calculations.

The upper part of the CPA spectrum shows a double peak that is believed to be spurious and cannot be attributed to pairs, as in the cluster calculation. However, we decided to show this phenomenon mainly for two reasons: First, it is rather puzzling that the structure resembles very closely the peak found in the experiments; and second, it has never been observed in a CPA calculation before. We leave this as an open question.

Quantitative comparison with the experiment is impossible, due to the poor resolution of the Raman spectra. Furthermore, the way the DOS is modified by the Raman tensor is not known, although one could extrapolate the result of Chapter I and expect that in the alloy a similar effect could occur, that is, that the TO peak would be enhanced.

C H A P T E R I V

DEFECTS IN AX_2 GLASSES

The interest of the study of point defects in AX_2 glasses is two-fold: 1) Raman scattering experiments present features that can be ascribed to defects and which, up to now, are not understood; and 2) The theoretical treatment of the problem can be performed satisfactorily by generalizing the model in Chapter I. Therefore, let us begin by revising in detail the experimental situation.

1.- EXPERIMENTAL BACKGROUND

The vibrational spectra of AX_2 glasses covers a wide range of situations, from nearly molecular-like spectra, as in chalcogenide glasses (GeS_2, $GeSe_2$), to band-like ones as in SiO_2 or GeO_2. This fact has been explained by Sen & Thorpe (1977) as a consequence of the value of the A-X-A angle (between the AX_4 tetrahedra). When this angle is near 90^0 one obtains a molecular-like behaviour, and when it is near 180^0, band-like modes appear.

Silica (SiO_2) belongs to the latter group, whose vibrational properties cannot be explained in terms of molecular modes.

Inelastic neutron scattering data in SiO_2 have been taken by Leadbetter & Stringfellow (1974) and the main features of the spectra nave been reproduced very satisfactorily by the numerical calculations of Bell et al. (1970) and by the Cluster-Bethe lattice model of Laughlin & Joannopoulos (1977). In Fig.(IV.1) a comparison between the experimental and theoretical DOS is shown.

The interpretation of the Raman and Infrared spectra is a little more complicated, because of unknown matrix-element effects. The spectra of SiO_2, GeO_2 and BeF_2 glasses have been studied thoroughly by Galeener (1979) and the

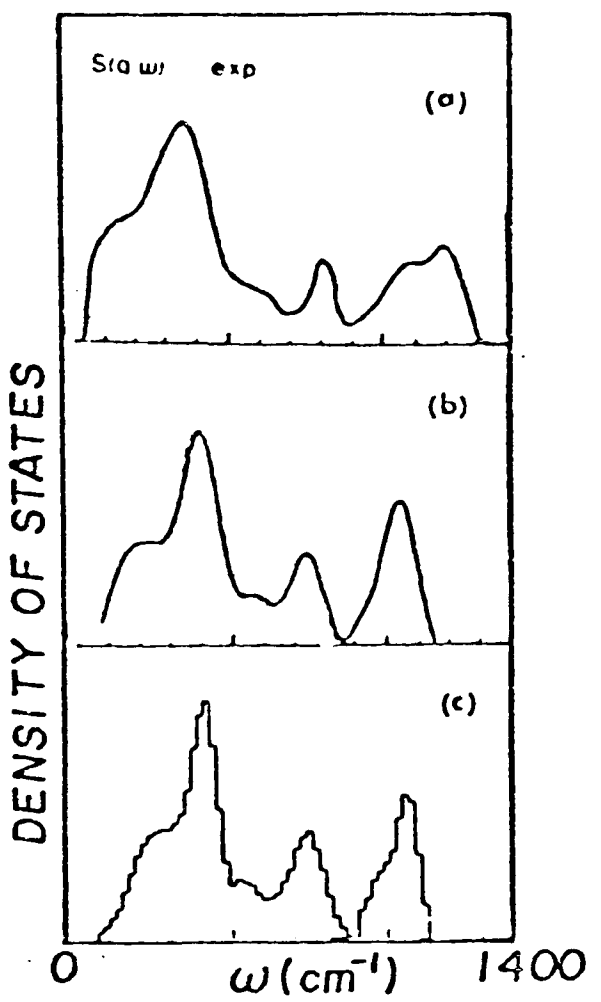

Fig.(IV.1) a) Scattering law from neutron measurements in Silica by Leadbetter & Stringfellow (1974). b) Cluster-Bethe lattice DOS (Laughlin & Joannopoulos (1977)). c) Numerical calculation using a 330 atom cluster by Bell et al.(1968).

main Raman active peaks have been interpreted in terms of the Sen & Thorpe (1977) theory. It is peculiar that the most intense Raman peak is not associated with a peak on the DOS, but with a band edge. This is somewhat surprising and leads one to admit that the accepted assumption that the Raman tensor is nearly independent of ω (Shuker & Gammon (1970)) fails, and hence the Raman tensor must be strongly frequency dependent near the band edge. This matter is discussed by Galeener & Sen (1978), but we postpone this subject until we consider the effect of matrix elements in § 6.

There are several interesting features in the Raman spectrum of these glasses. In Fig.(IV.2) the Raman and Infrared spectra of SiO_2 are shown.

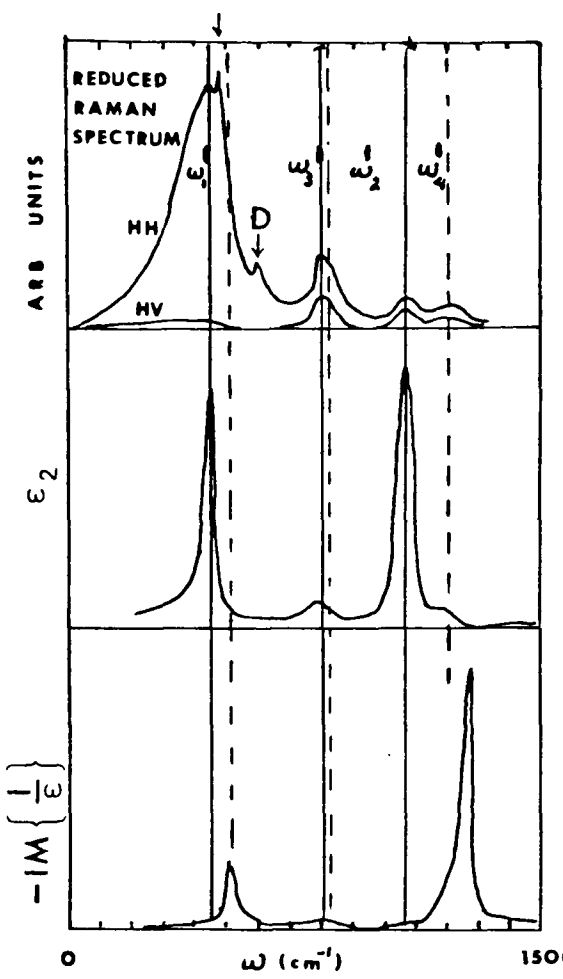

Fig.(IV.2) Comparison of the Raman and Infrared responses of a v-SiO_2 sample at room temperature (Galeener & Lucovsky (1976)). H-H is the configuration where the incident and scattered electric vectors are parallel, while H-V indicates that they are perpendicular. ω_i are the positions of the band edges calculated from Sen & Thorpe (1977).

First of all, the optic modes show a clear transverse-longitudinal splitting, as is demonstrated by the infrared response, because the longitudinal modes resonate at zeros of ε (or poles of $\mathrm{Im}(-1/\varepsilon)$), while the resonant frequencies of the transverse modes are determined

by the poles of $\varepsilon_2=Im\varepsilon$. This means that the long range Coulomb interactions are important in this material, but at present it is not known how to introduce these forces in a theory that could predict the number of TO-LO splittings in a glass.

Besides these broad features that are fairly well understood, there are two sharp features (marked with arrows in Fig.(IV.2)) that are totally unexpected. It is clear that their nature is different from those of the other peaks, not only because their sharpness, but their behaviour with temperature changes is also different. Not only that, but the two lines marked by arrows prove not to be similar: while the line at 606 cm^{-1} (labeled D) increases in intensity when the material is bombarded with fast neutrons (>10 Kev), the line at 495 cm^{-1} remains unchanged.

It seems evident that both lines are due to local defects in the regular coordination in the glass, but they have different origins. The peak D is the one that has received more attention since its discovery by Stolen et al.(1970), and was ascribed to a non-bridging oxygen defect by Bates et al.(1974). This interpretation was supported by Stolen & Walrafen (1976), who discovered that the strength of the line varied with water content. However, this assignment has been questioned recently by a more careful study of the line with water content by Mikkelsen & Galeener (1980) that proved that the observed variations in intensity were due to the inequivalent thermal histories of the samples. Furthermore, a Cluster-Bethe lattice calculation of the surface modes due to Si-O broken bonds, performed by Laughlin et al.(1978) to study the surface phonons of porous-SiO_2 (Vycor), showed that this sort of defect cannot be responsible for the D line. They rather suggest that the D line is due to Si-Si bonds.

This very reasonable suggestion is refuted by Galeener

(1980), who studied a similar feature in GeO_2 when the material is bombarded by neutrons and when there is a Ge excess in it. He concluded that, because there was no change in the feature with the deviation from stoichiometry, the line could not be due to Ge-Ge bonds, and extrapolated this conclusion to SiO_2. Galeener (private communication) suggested the possibility that four-atom rings (that is, two tetrahedra sharing an edge) will produce noticeable effects in the spectrum, as is observed in B_2O_3 glasses (Galeener et al.(1980)), where boroxil rings are present.

However, a general study of the effect on the DOS of a Si network (Thorpe(1974b)) due to 5 and 6-fold rings, shows that they produce broad and hardly noticeable features.

It is clear that a complete theoretical study is needed to decide which defects are good candidates to produce the sharp lines and which are not. We think that the model described in Chapter I provides a suitable method to study systematically all sorts of possible local defects, although some modifications and generalizations are needed.

2.- THEORETICAL MODEL

A theory whose predictions could be compared with Raman scattering experiments must include a study of the Raman polarizability as well as that of the DOS. Raman scattering is a complicated process and, at present, there is no neat way to treat it properly in an amorphous material. Therefore let us concentrate on finding the DOS and worry about matrix-element effects afterwards. If a defect is to be treated as a perturbation of a pure system, it is essential to start by finding a Green's function that represents this pure system.

An AX_2 network is far more complicated than the simple

tetrahedral network which we have considered up to now. However, Sen & Thorpe (1977), using a central force model Hamiltonian (eq.(I.2) with $\beta=0$), have shown that the complete problem of the AX_2 network maps into one involving only the cation motion, and thus, into a simple tetrahedral network. The procedure is as follows: Fix one's attention on a A-X-A unit

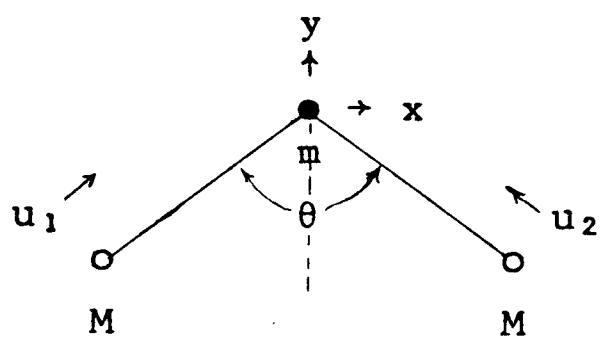

and play with the equations of motion to eliminate the coordinates of the bridging X atom. It is easily found that

$$(M\omega^2-\alpha_d)\,u_1 = \alpha' u_2 \quad , \tag{IV.1}$$

where

$$\alpha_d = \alpha + \frac{\alpha^2(m\omega^2-\alpha\sin^2\theta)}{(m\omega^2-\alpha)^2-\alpha^2\cos^2\theta} \tag{IV.2}$$

and

$$\alpha' = \frac{-m\omega^2\alpha^2\cos\theta}{(m\omega^2-\alpha)^2-\alpha^2\cos^2\theta} \quad . \tag{IV.3}$$

Equation (IV.1) connects the displacements of a renormalized mass at site 1 with the ones at site 2 through an effective force constant α'. Hence, following the mapping discussed in Weaire & Alben (1972), the normal modes are given, instead of (I.23), by

$$M\omega^2 = \frac{4}{3}(\alpha_d - \alpha'\varepsilon) \qquad \text{(IV.4)}$$

The eigenvalues ε of the connectivity matrix are bounded by the theorem of Perron-Frobenius ($|\varepsilon| \leq 1$). Therefore, the band edges are found by substituting (IV.2) and (IV.3) into (IV.4). There are two bands, whose edges are at

$$\omega_1^2 = \frac{\alpha}{m}(1+\cos\theta), \qquad \omega_2^2 = \frac{\alpha}{m}(1-\cos\theta) \qquad \text{(IV.5)}$$

$$\omega_3^2 = \omega_1^2 + \frac{4\alpha}{3M} \quad \text{and} \quad \omega_4^2 = \omega_2^2 + \frac{4\alpha}{3M}$$

These frequencies are marked in Fig.(IV.2) for SiO_2.

In order to investigate the displacement-displacement Green's function, it is convenient to separate the displacements of the cation ($\bar{u}$) from the ones of the anion ($\bar{X}$). The displacement $\bar{X}$ could be decomposed into a stretching part (along the y-direction) and a bending part (along x). From the former sketch, it is clear that

$$\chi = x\sin\frac{\theta}{2} + y\cos\frac{\theta}{2}, \qquad \text{(IV.6)}$$

Thus, we have the following equations of motion:

$$(M\omega^2 - \tfrac{4}{3}\alpha)\, g_{uu} = 1 - \tfrac{4}{3}\alpha\, g_{xu} = 1 - \tfrac{4}{3}\alpha\left(\sin\tfrac{\theta}{2}\, g_{xu} + \cos\tfrac{\theta}{2}\, g_{yz}\right) \qquad \text{(IV.7)}$$

$$m(\omega^2 - \omega_2^2)\, g_{xx} = 1 - 2\alpha\sin\tfrac{\theta}{2}\, g_{ux} \qquad \text{(IV.8)}$$

$$m(\omega^2 - \omega_1^2)\, g_{yy} = 1 - 2\alpha\cos\tfrac{\theta}{2}\, g_{uy} \qquad \text{(IV.9)}$$

These equations enable one, with a little algebraic manipulation, to express the self-correlations at the anion site in terms of g_{uu}:

$$g_{xx} = \frac{-3M\sin^2\theta/2}{2m\cos\theta}\,\frac{(\omega^2-\omega_3^2)}{(\omega^2-\omega_2^2)}\,g_{uu} + \frac{\omega^2(\omega_2^2+2\omega_1^2)-3\omega_1^2\omega_3^2}{4\omega^2\alpha\cos\theta(\omega^2-\omega_2^2)} \qquad \text{(IV.10)}$$

$$g_{yy} = \frac{3M\cos^2\theta/2}{2m\cos\theta}\,\frac{(\omega^2-\omega_4^2)}{(\omega^2-\omega_1^2)} - \frac{\omega^2(\omega_1^2+2\omega_2^2)-3\omega_1^2\omega_2^2}{4\omega^2\alpha\cos\theta(\omega^2-\omega_1^2)} \qquad \text{(IV.11)}$$

With these equations one can find the DOS per AX_2 unit as

$$\rho(\omega) = \frac{-2\omega}{\pi}\,Im\,(3M\bar{g}_{uu} + 2m\bar{g}_{xx} + 2m\bar{g}_{yy}), \qquad \text{(IV.12}$$

where the bar means a configurational average. This treatment is completely general in the sense that no assumptions have been made about the topological nature of the network. Before choosing a specific model for the lattice, let us describe the way one could treat the simplest defect, that is , a missing A-X bond.

3.- MISSING A-X BOND

If one considers that there are no force constant changes around the defect, the perturbation is

$$-\frac{1}{2} \propto [(\bar{u}-\bar{X})\cdot\hat{r}_{AX}]^2. \qquad \text{(IV.13)}$$

The displacement-displacement Green's function of the perturbed system is

$$G = g + gVG = g(1-Vg)^{-1} \qquad \text{(IV.14)}$$

where all matrices are 6×6 in principle (three coordinates at each side of the bond),however, if one chooses a coor-

dinate along the direction of the bond (i.e. parallel to $\hat{r}_{AX}$), they reduce to a 2×2 size, where

$$V = \begin{pmatrix} -\alpha & \alpha \\ \alpha & -\alpha \end{pmatrix} . \qquad \text{(IV.15)}$$

Poles in G will appear whenever

$$\Delta = Det\,(1 - V g) = 0 . \qquad \text{(IV.16)}$$

If the separation (IV.6) is made

$$\Delta = 1 + \alpha\,(g_{uu} + g_{\bar{X}\bar{X}} - g_{u\bar{X}} - g_{\bar{X}u}) , \qquad \text{(IV.17)}$$

where

$$g_{\bar{X}\bar{X}} = \sin^2\frac{\theta}{2}\, g_{xx} + \cos^2\frac{\theta}{2}\, g_{yy} , \qquad \text{(IV.18)}$$

All quantities are written in terms of g_{uu} (see eqs, (IV.7), (IV.10) and (IV.11)). The response on the defect site can be investigated

$$\Delta G = \begin{pmatrix} g_{uu} & g_{u\bar{X}} \\ g_{\bar{X}u} & g_{xx} \end{pmatrix} \begin{pmatrix} 1+\alpha(g_{\bar{X}\bar{X}} - g_{u\bar{X}}) & \alpha(g_{\bar{X}\bar{X}} - g_{u\bar{X}}) \\ \alpha(g_{uu} - g_{\bar{X}u}) & 1+\alpha(g_{uu} - g_{u\bar{X}}) \end{pmatrix} = \qquad \text{(IV.19)}$$

$$= \begin{pmatrix} g_{uu} + Q & g_{u\bar{X}} + Q \\ g_{\bar{X}u} + Q & g_{\bar{X}\bar{X}} + Q \end{pmatrix} = \begin{pmatrix} G_{uu} & G_{u\bar{X}} \\ G_{\bar{X}u} & G_{\bar{X}\bar{X}} \end{pmatrix} ,$$

where

$$Q = \alpha\,(g_{uu}\, g_{\bar{X}\bar{X}} - g_{u\bar{X}}^2) . \qquad \text{(IV.20)}$$

At this point a model for g_{uu} is needed, and it is adequate to choose a Bethe lattice. For an AX_2 tree, the Green's function obeys the equation

$$g_{uu}^2 \left[9 \left(M\omega^2 - \tfrac{4}{3}\alpha_d \right)^2 - 16\alpha'^2 \right] - 6 \left(M\omega^2 - \tfrac{4}{3}\alpha_d \right) g_{uu} - 3 = 0 \; ; \qquad \text{(IV.21)}$$

instead of eq.(I.22).

Perhaps it is instructive to derive (IV.21) explicitly, in order to show the method used in detail. Fig. (IV.3) represents schematically the transformation to the AX_2 Bethe lattice.

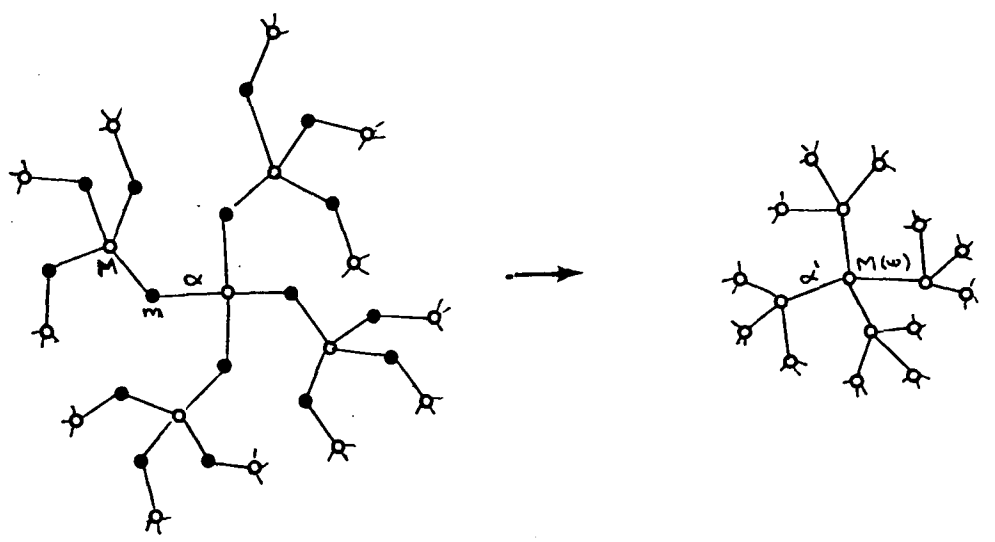

Fig.(IV.3) Transformation of the AX_2 Bethe lattice into a simple Bethe lattice of coordination 4.

The equation of motion (IV.1) can be written

$$\left(-3M\omega^2 + 4\alpha_d \right) u_1 = \sum_{i=1}^{4} \alpha_i' u_{2i} = 4\alpha' u_2 \, . \qquad \text{(IV.22)}$$

If $\varepsilon = -3M\omega^2 + 4\alpha_d$, the equation of motion for the Green's functions are

$$
\begin{aligned}
\varepsilon\, g_{u,u_1} &= 1 + 4\alpha' g_{u,u_2} \\
\varepsilon\, g_{u_2 u_1} &= \alpha' g_{u,u_1} + 3\alpha' g_{u_3 u_1} \\
&\vdots \\
\varepsilon\, g_{u_n u_1} &= \alpha' g_{u_{n-1},u_1} + 3\alpha' g_{u_{n+1},u_1}
\end{aligned}
\qquad \text{(IV.23)}
$$

which could be solved for g_{uu} defining the transfer matrix κ (equation (I.27)). The result is

$$
g_{uu} = \frac{\varepsilon \pm 2\sqrt{\varepsilon^2 - 12\alpha'^2}}{16\alpha'^2 - \varepsilon^2} = \frac{1}{-(M\omega^2 - \frac{4}{3}\alpha_d) \pm 2\sqrt{(M\omega^2 - \frac{4}{3}\alpha_d)^2 - \frac{4}{3}\alpha'^2}} \qquad \text{(IV.24)}
$$

which is exactly the solution of (IV.21). The subscript in the u's has been dropped because all sites are equivalent in a Bethe lattice.

The sign of the square root must be chosen to give the correct DOS. Notice also the delta functions at $|\varepsilon| = 4\alpha'$, each with weight 1.

Fig. (IV.4) shows the allowed regions for the bands as a function of the angle θ. The position of the bound states and resonances ($\Delta = 0$), when a bond is missing, is also shown.

Notice that the band edges are not reached by the Bethe lattice. A typical band shape is shown in Fig. (IV.5).

It is seen that the defect produces two resonances (one in each band) and one localized state in the gap. This result is completely general and it is obtained when a semicircular band model is used for g. In order to understand the origin and nature of these defect modes, we considered a simple molecular model in which there is only one A-X-A molecule attached to rigid walls by a spring

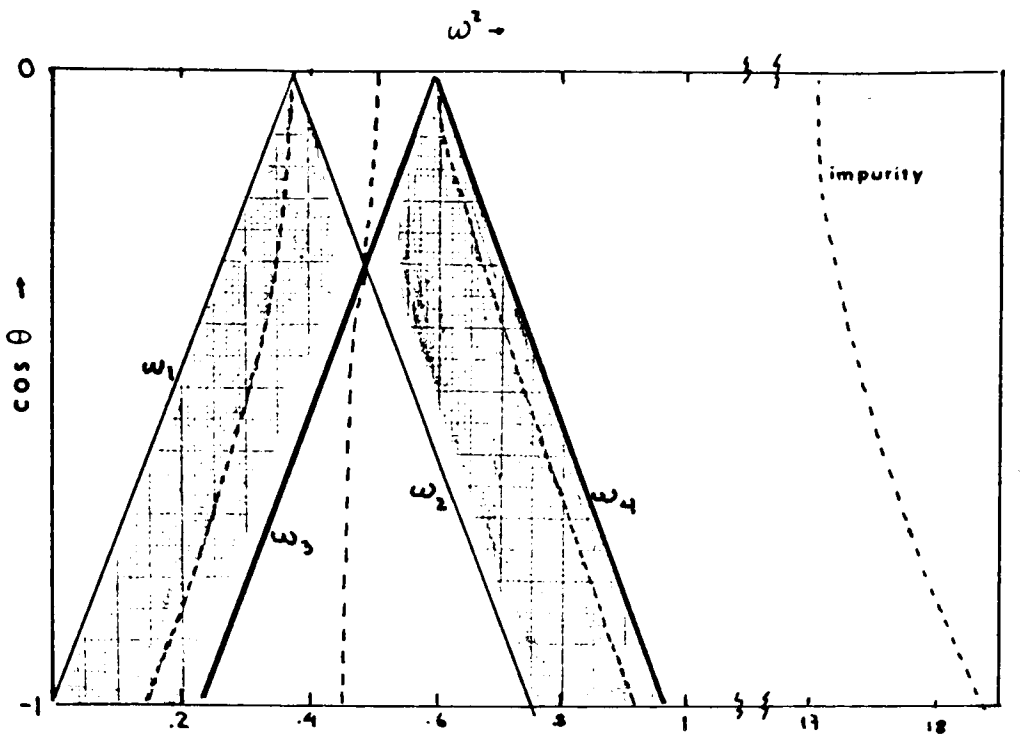

Fig.(IV.4) Bands of a GeS_2 Bethe lattice (shaded). The limits of the bands are the straight lines marked ω_1, ω_2, ω_3, and ω_4. The dotted lines are the zeros of Δ. An impurity state appears at very high frequency when an atom of mass 2 is attached to the dangling bond. There are δ-functions at ω_3 and ω_4.

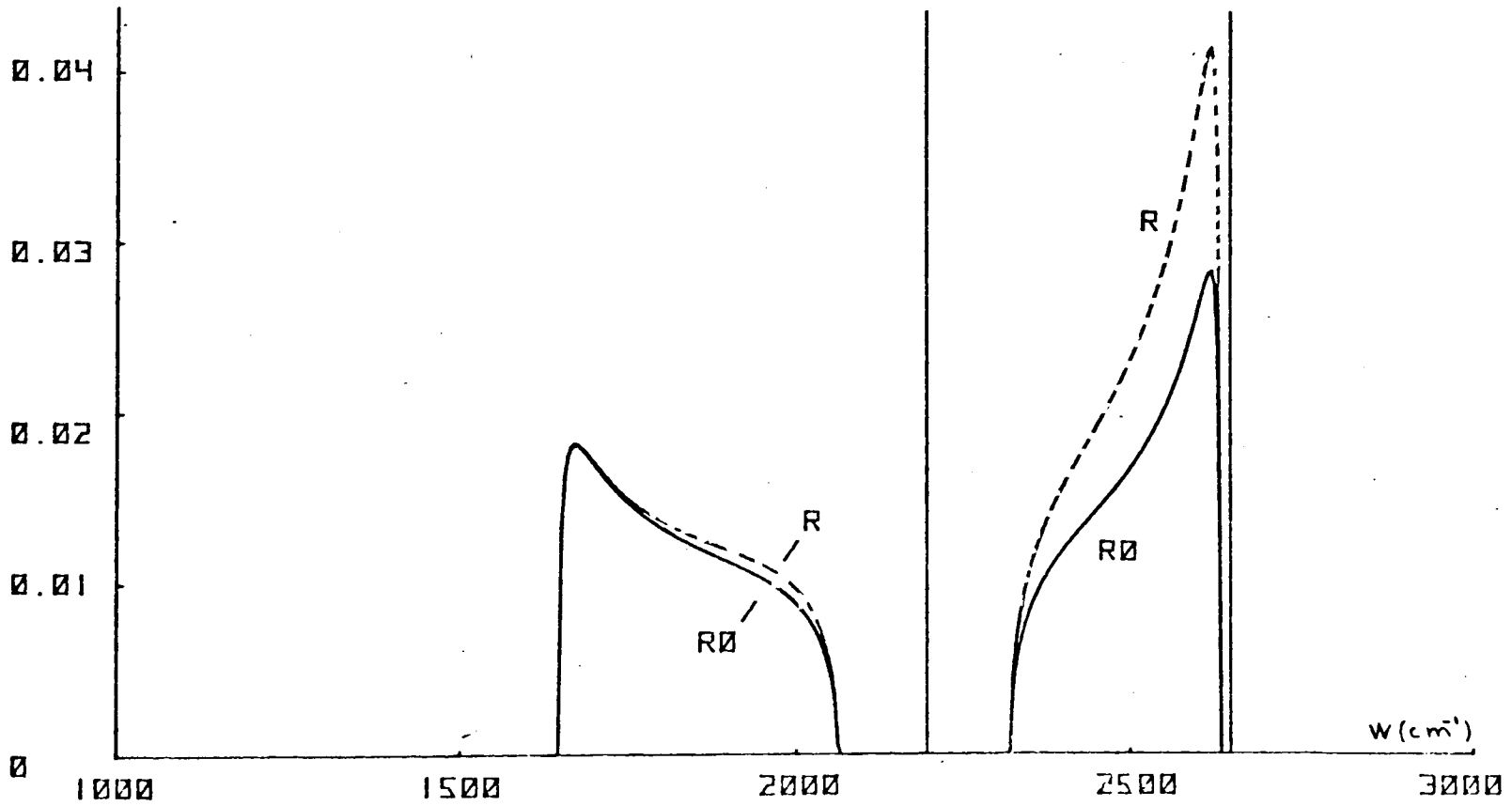

Fig.(IV.5) Density of states for a Bethe lattice (parameters for GeS_2, and $\theta=107^{o}$). The dotted line is the response at the defect site.

of stiffness γ. A graph similar to Fig.(IV.4) is shown in Fig.(IV.6) for this model.

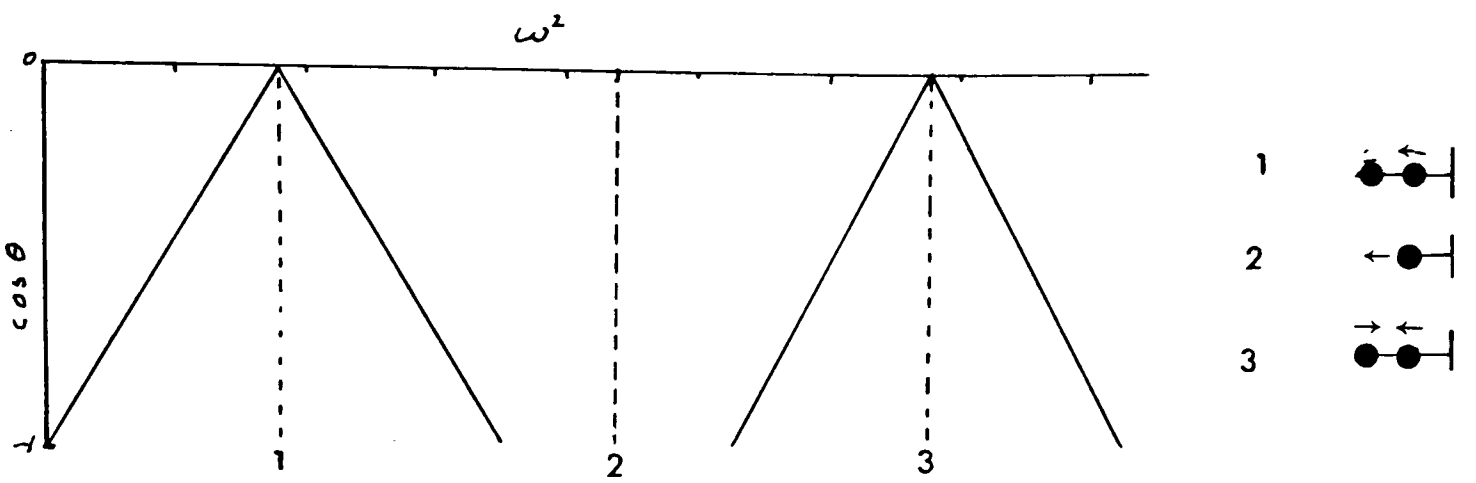

Fig.(IV.6) Normal modes of the molecule shown schematically on the right-hand side. The dashed lines are the modes that appear when one α-bond is missing.

Notice that there is no crossing of the lines as in Fig.(IV.4), because the crossing is due to band-like behaviour. The mode in the "gap" at $\omega^2=\gamma/m$ is the vibration of the isolated atom (←●-|), while the other two correspond to acoustic and optical vibrations of the A-X pair, and all of them are independent of θ, of course.

Hence, it can be said that, at least for the molecule-like glasses, the state in the gap in Fig.(IV.4) corresponds to parallel motion of the surface A-atom. This might not be true for a band-like glass. This is supported by the fact that when a light mass is attached to the dangling bond, the state in the gap disappears and goes to a very high frequency, while the other two resonances in the bands do not change their position.

It is rather easy to study the case when a mass (m') is coupled to the surface atom by

$$\frac{1}{2}\, a\, [(\bar{u}-\bar{u}')\cdot \hat{r}_{aa'}]^2 . \qquad \text{(IV.25)}$$

Then, the Green's function at the defect site will be

$$G' = G_0 + G_0 V G' \,, \qquad \text{(IV.26)}$$

with $V = \begin{pmatrix} a & -a \\ -a & a \end{pmatrix}$ and $G_0 = \begin{pmatrix} G_{uu} & 0 \\ 0 & G_{u'u'} \end{pmatrix}$;

where $G_{uu'} = \frac{1}{m'\omega^2}$

The position of the poles of G' as a function of θ is shown in Fig.(IV.4) labeled "impurity".

These results bear a close resemblance with the electronic problem in a-Si, where it is believed that the dangling bonds introduce states in the gap, which are taken out by saturating the dangling bonds with hydrogen.

The picture does not depend on the type of atoms chosen and is valid for SiO_2 also. However, we need another method, if we want to study other defects, because this procedure becomes very complicated if the perturbation is not as simple as a missing bond.

4.- DEFECTS IN SiO_2. METHOD.

The method described in Chapter I is particularly suitable for dealing with local defects in a Bethe lattice, because it allows one to find a solution for a local configuration and to attach it to a Bethe lattice in a simple way.

According to the experimental facts*, the defects which one must consider are

1) O-Si broken bond (≻o-● o≺)
2) Si-Si bond (≻o-o≺)
3) O-Si double bond (≻o=●)
4) Square ring (≻o≺●≻o≺)

*sec §1

All these can be treated in a similar way, the procedure is as follows:

i) Consider the equations of motion for the atoms joining the defect, and close the equations by attaching Bethe lattices on the proper bonds. This can be done by using self energies similar to those given by equation (I.10). The geometry is chosen so as to take full advantage of the symmetry in each configuration.

ii) Once the normal modes are found, the displacement-displacement Green's functions at the defect site (g_{ii}) are obtained.

iii) The local DOS is related to g_{ii} by

$$\rho_i(\omega) = \frac{-2M_i\omega}{\pi} Im\, g_{ii} \quad . \tag{IV.27}$$

iv) bound states and resonances are found at the poles of g_{ii}.

Let us describe each case:

1) 

For the part with the oxygen atom, a suitable geometry is

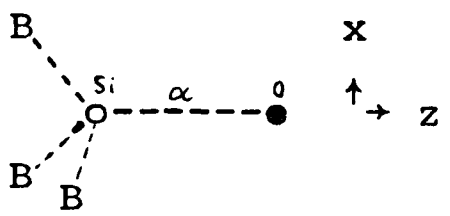

where B stands for the Bethe lattices attached to the remaining bonds.

Solving the equations of motion for the cartesian components of the displacement of the Si atom

$$\left(M\omega^2 - B_{\parallel} - \alpha - \frac{\alpha^2}{m\omega^2 - \alpha}\right) Z = 0 \,,$$

$$\left(M\omega^2 - B_{\perp}\right)\begin{pmatrix} x \\ y \end{pmatrix} = 0 \,, \tag{IV.27}$$

where $B_{\parallel}$ and $B_{\perp}$ are the parallel and perpendicular components of the potential due to B. Define:

$$g_{\perp} = \langle\langle x ; x \rangle\rangle = \langle\langle y ; y \rangle\rangle = \frac{1}{M\omega^2 - B_{\perp}} \quad , \tag{IV.28}$$

$$g_{\parallel} = \langle\langle z ; z \rangle\rangle = \frac{1}{M\omega^2 - B_{\parallel} - \frac{m\omega^2\alpha}{m\omega^2 - \alpha}} \quad .$$

From equations (I.10) with $\beta_{eff}=0$, one finds

$$B_{\perp} = 4 B_{\parallel} = \frac{4}{3}\alpha_{eff} \quad , \tag{IV.29}$$

which can be written in terms of g_{uu} using (I.10) and (IV.4):

$$B_{\parallel} = M\omega^2 - \alpha_d - \frac{1}{2g_{uu}} \pm \sqrt{\frac{1}{4g_{uu}^2} + \alpha'^2} \quad , \tag{IV.30}$$

the sign of the square root is chosen as to satisfy an equation like (I.13) identically. The poles of g are at

$$M\omega^2 - 4B_{\parallel} = 0 \tag{IV.31a}$$

and

$$M\omega^2 - B_{\parallel} - \frac{\alpha m\omega^2}{m\omega^2 - \alpha} = 0 \quad , \tag{IV.31b}$$

and the local DOS is

$$\rho_{Si}(\omega) = \frac{-2M\omega}{\pi} Im(2g_{\perp} + g_{\parallel}) \tag{IV.32}$$

At the Si site with the dangling bond the procedure is exactly the same, except that m=0 in equations (IV.28) and (IV.31).

2) 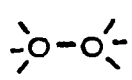

This defect is treated in the same way as the broken bond, except that instead of an oxygen, one puts an exact replica of the lattice coupled by a central force γ. It is clear that

$$g_{\perp} = \frac{1}{M\omega^2 - 4B_{\perp}} \quad , \tag{IV.33}$$

$$g_{\parallel} = \frac{1}{M\omega^2 - B_{\parallel} - \gamma - \frac{\gamma^2}{M\omega^2 - B_{\parallel} - \gamma}} \quad . \tag{IV.34}$$

3) ;o=●

Here the geometry has to be changed

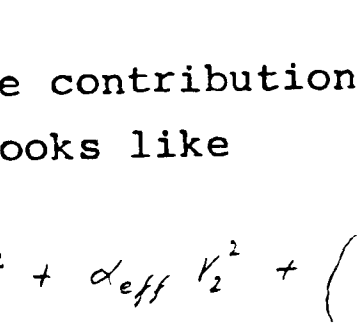

Every thing could be combined to obtain an effective potential at the Si site which could be written

$$\frac{1}{2}\left(V_x x^2 + V_y y^2 + V_z z^2\right) . \tag{IV.35}$$

All the V's have contributions from the oxygen and Si atoms. The potential looks like

$$\alpha_{eff} r_1^2 + \alpha_{eff} r_2^2 + \left(\alpha_0 + \frac{\alpha_0^2}{m\omega^2 - \alpha_0}\right) z^2 . \tag{IV.36}$$

Therefore

$$V_x = \frac{4}{3}\alpha_{eff} \quad , \quad V_z = \frac{2}{3}\alpha_{eff} + \frac{\alpha_0 m\omega^2}{m\omega^2 - \alpha_0} \quad , \tag{IV.37}$$

$$V_y = 0 .$$

In terms of the quantities defined before, the components of the Green's function at the Si site are

$$g_{xx} = \frac{1}{M\omega^2 - 4B_{\parallel}} \quad , \tag{IV.38}$$

$$g_{yy} = \frac{1}{M\omega^2} \quad , \tag{IV.39}$$

$$G_{zz} = \frac{1}{M\omega^2 - 2B_{\perp} - \frac{\alpha m \omega^2}{m\omega^2 - \alpha}} \quad , \tag{IV.40}$$

and the local DOS is

$$\rho(\omega) = \frac{-2M\omega}{\pi} Im\left(G_{xx} + G_{yy} + G_{zz}\right) . \tag{IV.41}$$

4) 

Using the same frame of reference as in 3), the sites are labelled

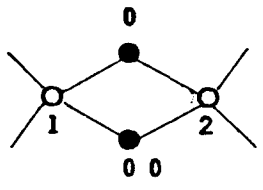

It is easier to solve the equations for symmetrised combinations of the displacements, thus we define:

$$\begin{aligned}
G_{ox}^{x\pm} &= \langle\langle x_0 \pm x_{00} \,;\, x_0 \pm x_{00} \rangle\rangle \\
G_{ox}^{y} &= \langle\langle y_0 \,;\, y_0 \rangle\rangle = \langle\langle y_{00} \,;\, y_{00} \rangle\rangle \\
G_{ox}^{z\pm} &= \langle\langle z_0 \pm z_{00} \,;\, z_0 \pm z_{00} \rangle\rangle \\
G_{si}^{x\pm} &= \langle\langle x_1 \pm x_2 \,;\, x_1 \pm x_2 \rangle\rangle \\
G_{si}^{y} &= \langle\langle y_1 \,;\, y_1 \rangle\rangle = \langle\langle y_2 \,;\, y_2 \rangle\rangle \\
G_{si}^{z\pm} &= \langle\langle z_1 \pm z_2 \,;\, z_1 \pm z_2 \rangle\rangle .
\end{aligned} \tag{IV.42}$$

Hence one finds:

$$\begin{aligned}
G_{ox}^{x+} &= 1 \Big/ \left(m\omega^2 - \tfrac{4}{3}\alpha - \frac{16\alpha^2}{9(M\omega^2 - \frac{4}{3}\alpha)} \right) \\
G_{ox}^{x-} &= 1 \Big/ \left(m\omega^2 - \tfrac{4}{3}\alpha - \frac{8\alpha^2}{9(M\omega^2 - \frac{2}{3}\alpha - 2B_{\perp})} \right) \\
G_{ox}^{y} &= 1/m\omega^2
\end{aligned} \tag{IV.43}$$

$$g_{ox}^{z+} = 1/\left(m\omega^2 - \frac{2}{3}\alpha - \frac{4\alpha^2}{9(M\omega^2 - \frac{2}{3}\alpha - 2B_{11})} \right)$$

$$g_{ox}^{z-} = 1/\left(m\omega^2 - \frac{2}{3}\alpha - \frac{8\alpha^2}{9(M\omega^2 - \frac{2}{3}\alpha)} \right) \qquad \text{(IV.43)}$$

$$g_{si}^{x+} = 1/\left(M\omega^2 - \frac{4}{3}\alpha - \frac{16\alpha^2}{9(m\omega^2 - \frac{4}{3}\alpha)} \right)$$

$$g_{si}^{x-} = 1/\left(M\omega^2 - \frac{4}{3}\alpha - \frac{8\alpha^2}{9(m\omega^2 - \frac{2}{3}\alpha)} \right) \qquad \text{(IV.44)}$$

$$g_{si}^{y} = 1/\left(M\omega^2 - 4B_{11} \right)$$

$$g_{si}^{z+} = 1/\left(M\omega^2 - 2B_{11} - \frac{2}{3}\alpha - \frac{4\alpha^2}{9(m\omega^2 - \frac{2}{3}\alpha)} \right)$$

$$g_{si}^{z-} = 1/\left(M\omega^2 - 2B_{11} - \frac{2}{3}\alpha - \frac{8\alpha^2}{9(m\omega^2 - \frac{4}{3}\alpha)} \right).$$

The response of the oxygen is

$$\rho_{ox}(\omega) = \frac{-2m\omega}{\pi} \frac{Im}{2} \left(g_{ox}^{x+} + g_{ox}^{x-} + 2g_{ox}^{y} + g_{ox}^{z+} + g_{ox}^{z-} \right) \qquad \text{(IV.45)}$$

and that of the silicon

$$\rho_{si}(\omega) = \frac{-2M\omega}{\pi} \frac{Im}{2} \left(g_{si}^{x+} + g_{si}^{x-} + 2g_{si}^{y} + g_{si}^{z+} + g_{si}^{z-} \right) \qquad \text{(IV.46)}$$

We checked these results by finding the full dynamical matrix and solving for the cartesian components of the displacements.

The poles are found when the denominators vanish and the participation of the oxygen (silicon) atom in each mode is easily investigated, thanks to the symmetrization

of the problem.

5.- RESULTS AND DISCUSSION

1) -o-● o- The local densities at the two Si-atoms are plotted in Fig.(IV.7). The parameters were chosen so as to fit the experimental frequencies ω_1 and ω_3 (see Fig.(IV.2)), and their values are:

$M = 28$

$m = 16$

$\alpha = 9.17$ (same units as usual)

$\theta = 130^0$.

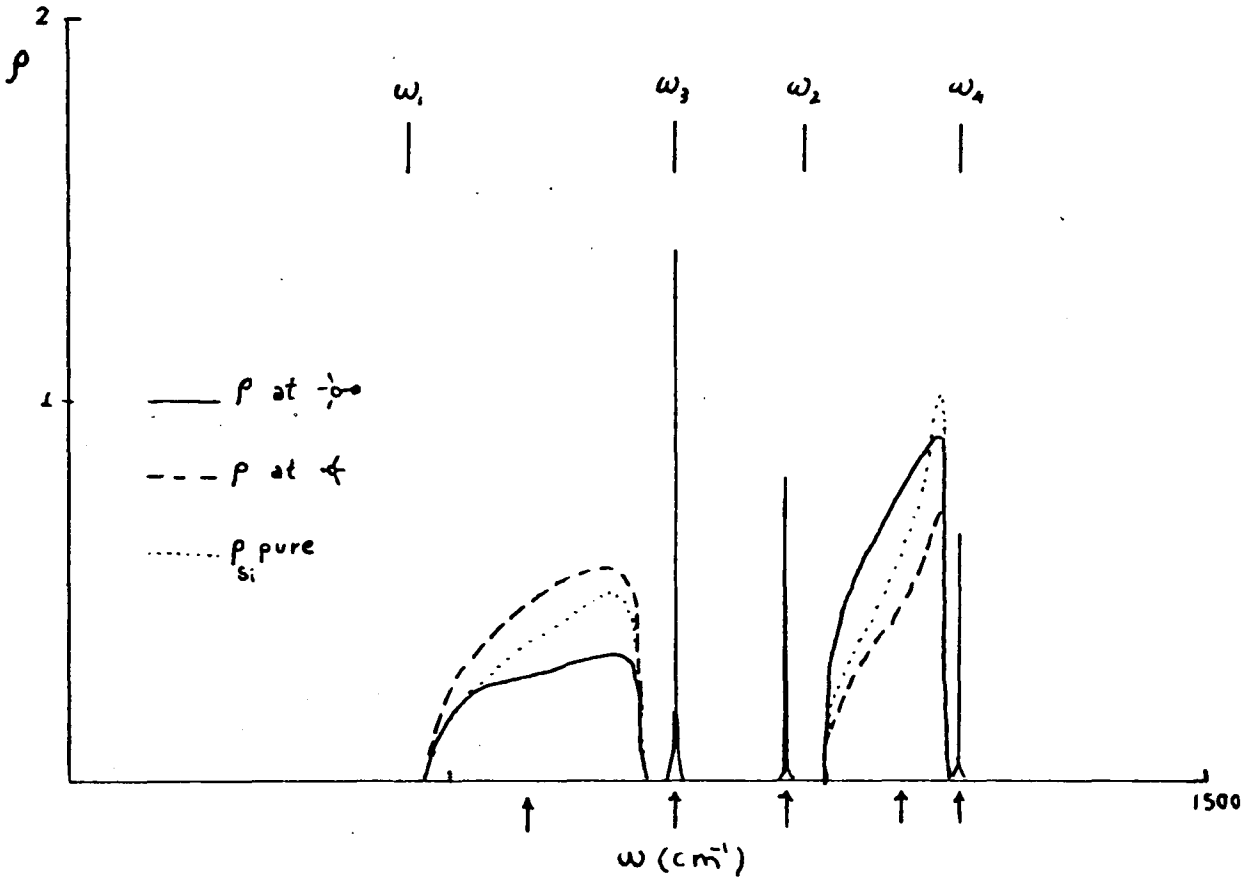

Fig.(IV.7) DOS at the Si atoms joining a broken bond. The position of the poles of g are marked by arrows.

The overall picture agrees extremely well with Fig. (IV.4), in the sense that there is a bound state in the gap and two resonances in the bands. Furthermore, the shapes of the local DOS on the two surface atoms are very similar to the ones obtained by Laughlin et al.(1978) by

a similar model including non-central forces. Fig (IV.7) is practically identical to their fig.2, if one ignores the lower part of the latter, which arises because of the non-central forces.

From the analysis of the poles of each g, it is seen that the state in the gap at 940 cm^{-1} is the Si-O stretching mode, while the resonances at 610 and 1100 cm^{-1} are due to perpendicular motion of the two Si atoms adjoining the defect. They are at the same frequencies because the presence of the oxygen in one of them does not affect the perpendicular motion. There are two δ-functions at ω_3 and ω_4 , as expected.

This picture is somewhat different from the one given by the molecular model. This is reasonable because in SiO_2 solid-state-effects are important, and its spectrum is more band-like. It is interesting to notice that, although the poles appear in the same region, their nature changes drastically with θ.

In any case, it seems that dangling oxygens are unlikely to produce the D peak in the Raman spectrum. Two facts support this statement:1) The resonance at 610 cm^{-1} (which coincides with the D peak frequency) does not appear as a sharp feature in the band, even when an imaginary part is added to the frequency. It is very unlikely that the Raman matrix elements would show a sharp feature there, because the motion is perpendicular and the polarizability could be thought to be minimum in that case. 2) There is no evidence of the bound state at 940 cm^{-1} in the Raman spectrum, although one could expect this mode to be very Raman active, because there is a maximum stretching of the Si-O bond.

2) $\dot{O}-O\dot{}$ In Fig.(IV.8) the DOS at the defect site (for γ=2.5) is compared with the bulk density of states. It is noticed that the weight of the lower band has in-

creased considerably, reflecting the fact that the atoms adjoining the defect are looser. Also, some weight is taken from the δ-functions at ω_3 and ω_4 and put into the bands.

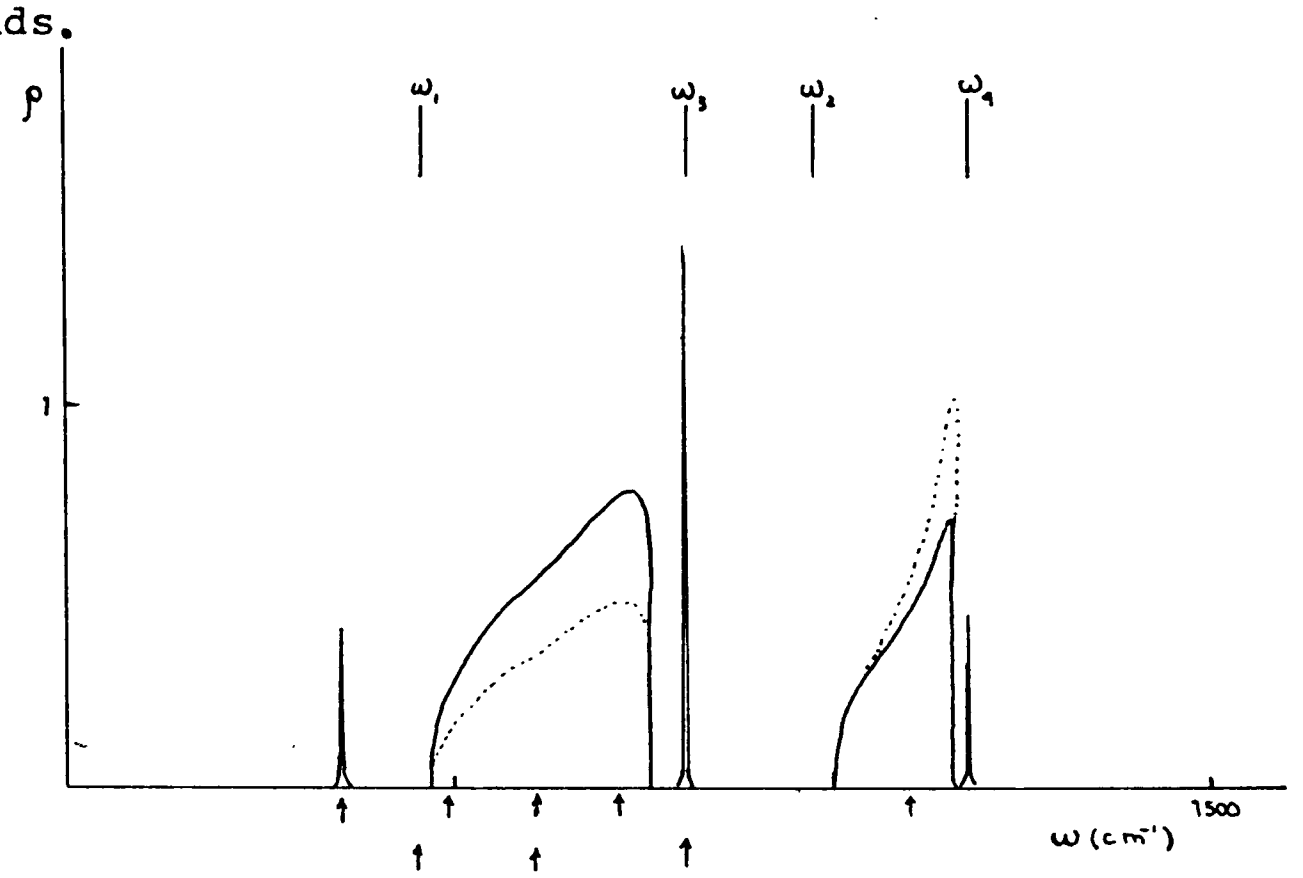

Fig.(IV.8) Local DOS for the Si-Si bond defect. The value of γ was chosen to fit the high frequency peak of pure a-Si ($\gamma=3M\omega_0^2/8$). The poles of g are shown by the upper set of arrows. The lower set indicate the poles of g when $\gamma=4.6$.

Besides the poles already found for the perpendicular motion at 610, ω_3, 1100 and ω_4, there are three poles due to parallel motion at 355, 495 and 715 cm^{-1}. Of these, the poles on the extremes are similar, for they involve a stretch of the Si-Si bond, and therefore their position varies with the value of γ. A very schematic way of visualizing these modes could be

←⊘---→O-←O---⊘→ at 355

→⊘---→O-←O---⊘← at 715

←⊘---→O-→O---⊘← at 495

where ⊘ represents the lattice and o the two Si atoms.

Although resonances do not show up in the DOS, the Raman activity of these modes could be different from zero due to the local polarization produced at the defect site (see §6). It is also apparent from the sketch of the modes that the Raman activity of each one should be different, because the mode at 355 cm^{-1} only involves Si-Si stretching, the one at 495 cm^{-1} only produces Si-O stretching (through the lattice) and the one at 715 cm^{-1} stretches all the bonds. Hence, their relative intensities must be different and one could say in a naïve way, the ones involving Si-O stretching must be the most intense.

Then, it is natural to think that the peak at 495 cm^{-1} would appear in the Raman spectrum, so it is tempting to attribute the experimental peak at the same frequency to the Si-Si defect. However, there is no sign of a peak at 715 cm^{-1} despite the fact that the mode should be present. In this respect we notice that the position of this mode depends very strongly on the value of γ, which could be fitted as to make it coincide with ω_3 (see lower part of Fig.(IV.8)). It is remarkable that in that situation the mode at 355 cm^{-1} shifts to match ω_1 exactly. Although the value of γ needed to have this fit (4.6) is nearly twice as large as the central force constant for a-Si.

3) ⊘=● This is not very interesting in the sense that it does not show features that could be related with any of the observed ones. The local DOS for two values of α_0 is shown in Fig.(IV.9). Notice that a bound state appears on the high frequency side of the spectrum and moves when α_0 changes. Its weight increases with α_0 and is taken mainly from the upper part of the spectrum, in agreement with the results of Chapter II for a-Si:H.

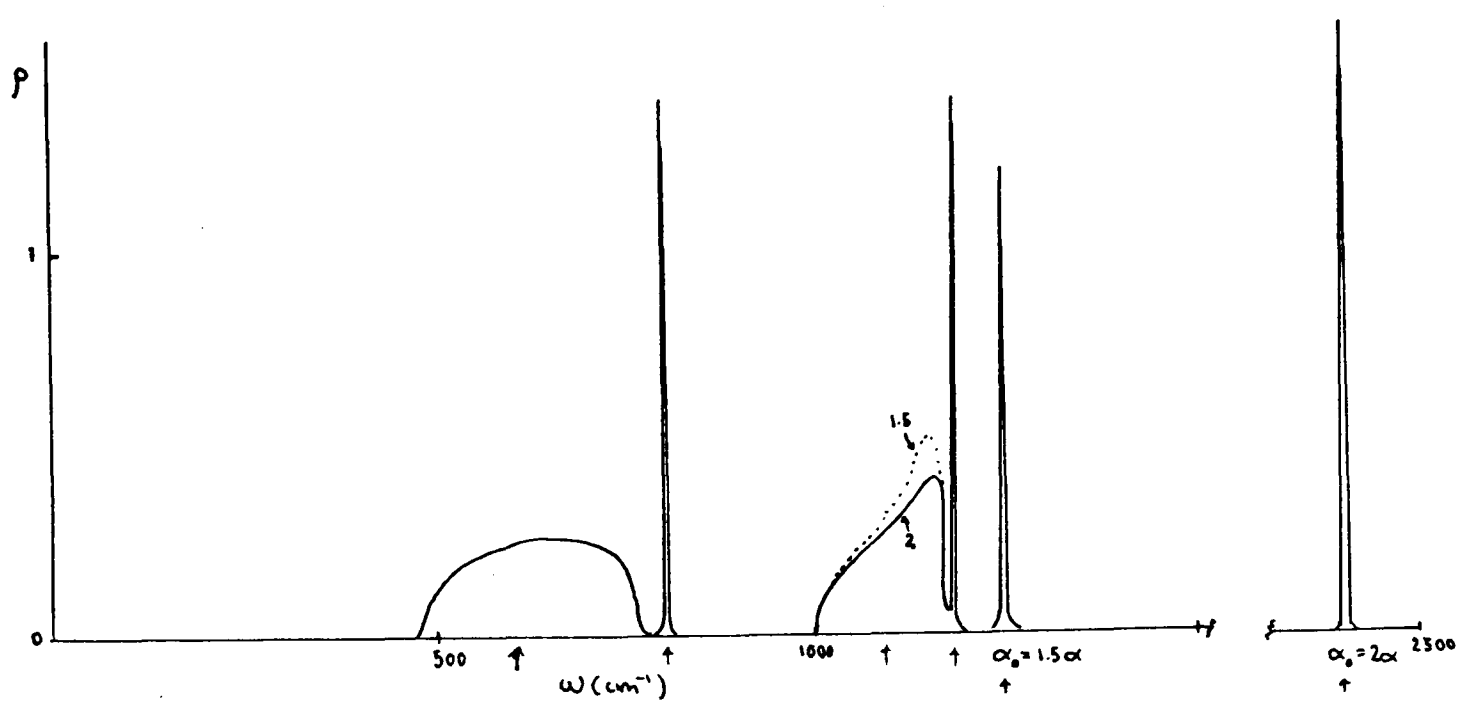

Fig.(IV.9) Local DOS at the Si atom doubly bound to an oxygen. Two values of the double bond force constant are shown. The poles of g are marked by arrows.

4) 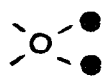 Fig.(IV.10) shows the local DOS at the defect site $\rho(\omega)=\frac{1}{2}(\rho_{Ox}+\rho_{Si})$ (see equations (IV.45) and (IV.46)).This defect produces a lot of structure: several states in the gap, and a resonance , which is sharp and visible, in the upper part of the spectrum (in band). In the experiment there is nothing that looks like this, therefore one must conclude that it is very unlikely that this sort of defect is present in the glass.

The nature of the poles is discovered by analysing the poles of the partial Green's functions (equations (IV.43) and (IV.44)). With this knowledge one could imaging the motion of the atoms in the ring at each one of the frequencies. These are sketched pictorially on Table IV.1.

It is seen that the resonance at 1095 cm^{-1}, which is

the only one that appears visible in the band, arises from a motion that is not coupled to the lattice. Something similar happens with the state at 905 cm^{-1}.

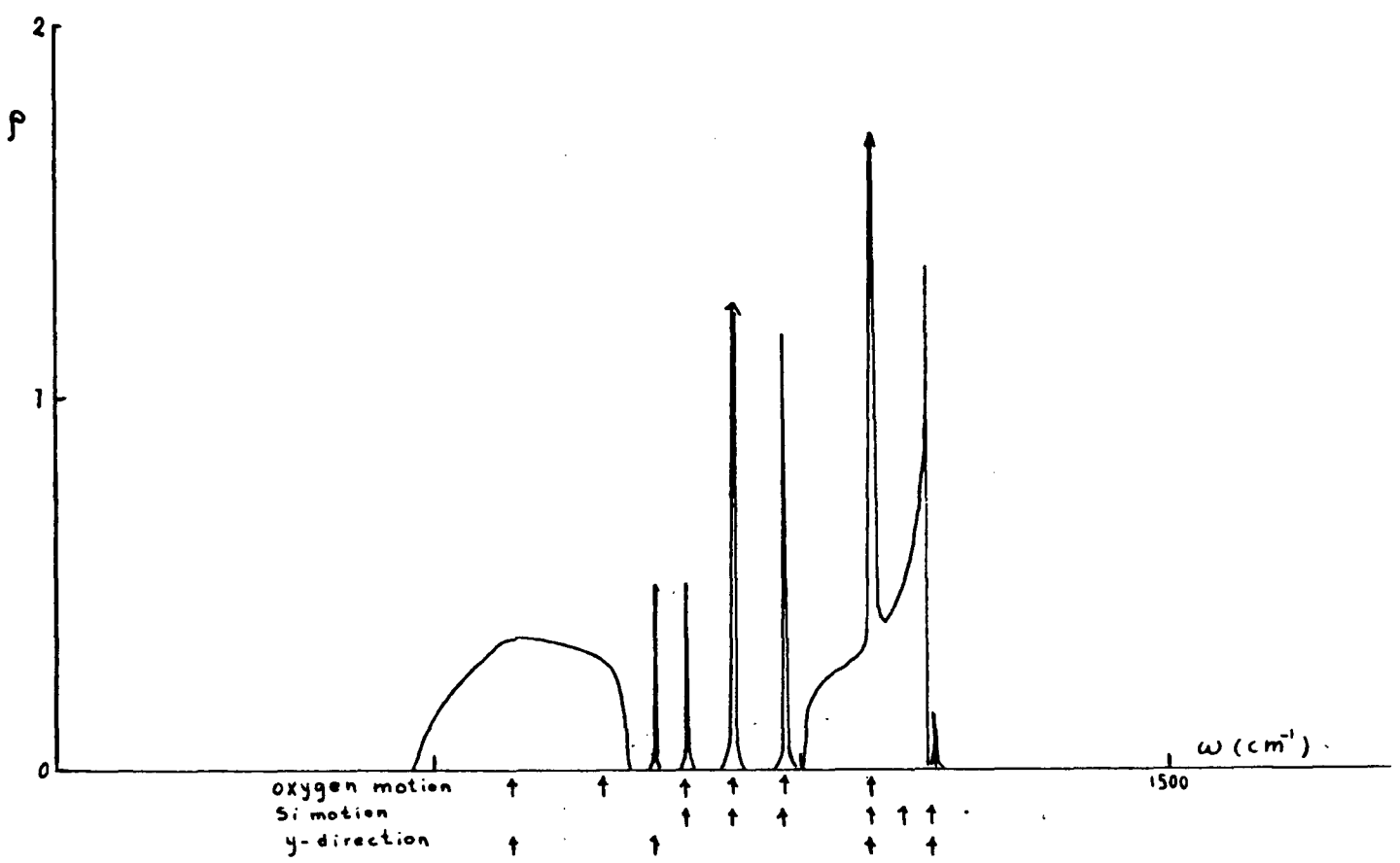

Fig.(IV.10) Local DOS for the square ring. The poles of the partial Green's functions are marked by arrows.

Unlike the case for the former two defects, there are no adjustable parameters in this case, so the frequencies of the bound states must be right. Of course, there is the assumption that the square ring is planar, and that the tetrahedral angles remain the same. This configuration is very unlikely because it gives a value of θ less than 90^0 for the oxygens in the ring. Hence, one can imagine that if there are any rings of this sort in the real material, they must be distorted, in order to have a less strained topology. The reason we considered such a regular ring was only for simplicity. Nevertheless, as it was stated before, rings are poor candidates for responsibility for the experimental features and this cal-

culation agrees with that statement.

In any case, no conclusions drawn by looking only at the DOS are valid, and some study must be made of the Raman response.

Table (IV.1)

Normal Modes of the Square Ring.

pole at ω (cm^{-1})	Mode	pole at ω (cm^{-1})	Mode
610		970	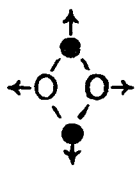 ω_2
730		1095	
800	ω_3	1135	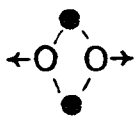
845	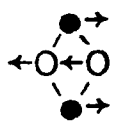	1175	ω_4
905		● Oxygen ○ Silicon	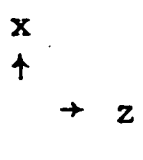

6.- RAMAN SCATTERING IN SILICA

The model for Raman scattering described in Chapter I §4 is not suitable, as it stands, for SiO_2 because, although the mapping discussed between the two lattices is still possible, the assumption that the polarizability is maximum when the two Si atoms move so as to compress bonds is not reasonable any more. In SiO_2 a similar model must introduce the assumption that the polarizability is greater when the Si-O bonds are stretched. This means that, appart form the long range correlation in equation (I.26), the local motion in each A-X-A unit has to be studied carefully. The model described below separates neatly the local contributions to the polarizability within the unit from the correlations between units. Let us start with an expresion for the Raman cross section similar to (I.24):

$$\frac{d^2\sigma}{d\Omega\, d\omega} \propto \sum_{i,j} \int \langle \vec{\nabla}_i \alpha_i \cdot \bar{x}_i(0);\ \bar{x}_j(t) \cdot \vec{\nabla}_j \alpha_j \rangle e^{i\omega t} dt \qquad \text{(IV.47)}$$

where $\vec{\nabla}_i \alpha_i$ is the gradient of the electronic polarizability on the atom i with respect to $\bar{x}_i$. Consider a local geometry at the unit ℓ:

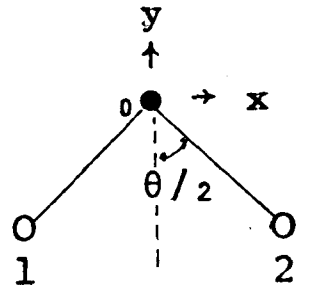

and use the following notation:

$\bar{u}_i(\ell)$ is the displacement of the Si atom 1 (or2) in the unit ℓ.

$\bar{u}_0(\ell)$ is the displacement of the O atom in the same unit ℓ

Assume that there is an isotropic dilatation of a scalar polarizability when the atoms move along the bonds. Then

$$\alpha_1 = A\,(\bar{u}_1 - \bar{u}_0)\cdot\hat{r}_1$$

$$\alpha_2 = A\,(\bar{u}_2 - \bar{u}_0)\cdot\hat{r}_2 \qquad \text{(IV.48)}$$

$$\alpha_0 = A\,\{(\bar{u}_0 - \bar{u}_1)\cdot\hat{r}_1 + (\bar{u}_0 - u_2)\cdot\hat{r}_2\}$$

where $\hat{r}_1=(\sin\frac{\theta}{2},\cos\frac{\theta}{2},0)$ and $\hat{r}_2=(-\sin\frac{\theta}{2},\cos\frac{\theta}{2},0)$, and these relations are valid in any unit. Thus, one has

$$\begin{aligned}\vec{\nabla}_1\alpha_1 &= A\,\hat{r}_1\\ \vec{\nabla}_2\alpha_2 &= A\,\hat{r}_2\\ \vec{\nabla}_0\alpha_0 &= -A\,(\hat{r}_1+\hat{r}_2)\end{aligned} \qquad \text{(IV.49)}$$

and equation (IV.47) is explicitly

$$A^2\sum_{\ell,\ell'}\int\Big\{\langle u_{1x}(\ell)\sin\tfrac{\theta}{2}+u_{1y}(\ell)\cos\tfrac{\theta}{2}\,;\,u_{1x}(\ell')\sin\tfrac{\theta}{2}+u_{1y}(\ell')\cos\tfrac{\theta}{2}\rangle + \qquad \text{(IV.50)}$$

$$+\langle u_{1x}(\ell)\sin\tfrac{\theta}{2}+u_{1y}(\ell)\cos\tfrac{\theta}{2}\,;\,-2u_{0y}(\ell')\cos\tfrac{\theta}{2}\rangle +$$

$$+\langle u_{1x}(\ell)\sin\tfrac{\theta}{2}+u_{1y}(\ell)\cos\tfrac{\theta}{2}\,;\,-u_{2x}(\ell')\sin\tfrac{\theta}{2}+u_{2y}(\ell')\cos\tfrac{\theta}{2}\rangle +$$

$$+\langle -2u_{0y}(\ell)\cos\tfrac{\theta}{2}\,;\,u_{1x}(\ell')\sin\tfrac{\theta}{2}+u_{1y}(\ell')\cos\tfrac{\theta}{2}\rangle +$$

$$+\langle -2u_{0y}(\ell)\cos\tfrac{\theta}{2}\,;\,-2u_{0y}(\ell')\cos\tfrac{\theta}{2}\rangle +$$

$$+\langle -2u_{0y}(\ell)\cos\tfrac{\theta}{2}\,;\,-u_{2x}(\ell')\sin\tfrac{\theta}{2}+u_{2y}(\ell')\cos\tfrac{\theta}{2}\rangle +$$

$$+\langle -u_{2x}(\ell)\sin\tfrac{\theta}{2}+u_{2y}(\ell)\cos\tfrac{\theta}{2}\,;\,u_{1x}(\ell')\sin\tfrac{\theta}{2}+u_{1y}(\ell')\cos\tfrac{\theta}{2}\rangle +$$

$$+\langle -u_{2x}(\ell)\sin\tfrac{\theta}{2}+u_{2y}(\ell)\cos\tfrac{\theta}{2}\,;\,-2u_{0y}(\ell')\cos\tfrac{\theta}{2}\rangle +$$

$$+\langle -u_{2x}(\ell)\sin\tfrac{\theta}{2}+u_{2y}(\ell)\cos\tfrac{\theta}{2}\,;\,-u_{2x}(\ell')\sin\tfrac{\theta}{2}+u_{2y}(\ell')\cos\tfrac{\theta}{2}\rangle\Big\}$$

$$e^{i\omega t}\,dt\,\Big]$$

where the displacements on the right hand side of the brakets <> are taken at time t and the ones on the left are at t=0.

Let us make a connection with the old notation for the Green's functions

$$\int \langle u_i(\ell);\, u_j(\ell')\rangle e^{i\omega t}\,dt = \frac{-2\omega f(\omega)}{\pi} Im\, g_{uu}(\ell,\ell');\quad i,j=1,2$$

$$\int \langle u_{oy}(\ell)\cos\tfrac{\theta}{2};\, u_{oy}(\ell')\cos\tfrac{\theta}{2}\rangle e^{i\omega t}\,dt = \frac{-2\omega f(\omega)}{\pi} Im\, g_{yy}(\ell,\ell') \qquad \text{(IV.51)}$$

$$\int \langle u_i(\ell);\, u_{oy}(\ell')\cos\tfrac{\theta}{2}\rangle e^{i\omega t}\,dt = \frac{-2\omega f(\omega)}{\pi} Im\, g_{uy}(\ell,\ell'),$$

where $f(\omega)$ is a slowly varying function of frequency and we shall consider it as a constant absorbed into A. Therefore, equation (IV.50) is

$$\frac{d\sigma}{d\Omega\, d\omega} \propto \frac{-2\omega}{\pi} \sum_{\ell,\ell'} Im\Big\{ g_{uu}(\ell,\ell')\left(1+2\sin\tfrac{\theta}{2}\cos\tfrac{\theta}{2}\right) - \qquad \text{(IV.52)}$$

$$-2g_{uy}(\ell,\ell')\left(\sin\tfrac{\theta}{2}+\cos\tfrac{\theta}{2}\right) + g_{uu}(\ell,\ell')\left(\cos^2\tfrac{\theta}{2}-\sin^2\tfrac{\theta}{2}\right) - 2g_{yu}(\ell,\ell')\left(\sin\tfrac{\theta}{2}+\cos\tfrac{\theta}{2}\right) +$$

$$+4g_{yy}(\ell,\ell') + 2g_{yu}(\ell,\ell')\left(\sin\tfrac{\theta}{2}-\cos\tfrac{\theta}{2}\right) + g_{uu}(\ell,\ell')\left(\cos^2\tfrac{\theta}{2}-\sin^2\tfrac{\theta}{2}\right) +$$

$$+2g_{uy}(\ell,\ell')\left(\sin\tfrac{\theta}{2}-\cos\tfrac{\theta}{2}\right) + g_{uu}(\ell,\ell')\left(1-2\sin\tfrac{\theta}{2}\cos\tfrac{\theta}{2}\right)\Big\} =$$

$$= \frac{-2\omega}{\pi} \sum_{\ell,\ell'} \left\{ 2g_{uu}(\ell,\ell') + 2g_{uu}(\ell,\ell')\cos\theta + 4g_{yy}(\ell,\ell') - 8g_{uy}(\ell,\ell')\cos\theta/2 \right\}.$$

All the g's could be written in terms of $g_{uu}(\ell,\ell')$. From (IV.11)

$$Im\, g_{yy}(\ell,\ell') = \Gamma(\omega)\, Im\, g_{uu}(\ell,\ell'), \qquad \text{(IV.53)}$$

where

$$\Gamma(\omega) = \frac{3M\omega^2\cos^3\theta/2}{2m\cos\theta}\,\frac{(\omega^2-\omega_4^2)}{(\omega^2-\omega_3^2)}. \qquad \text{(IV.54)}$$

Form the equations of motion is easy to see that

$$2\alpha\, g_{uy}(l,l')\cos\frac{\theta}{2} = (m\omega^2 - 2\alpha\cos^2\frac{\theta}{2})\, g_{yy}(l,l') - \delta_{ll'} \quad , \qquad \text{(IV.55)}$$

or

$$Im\, g_{uy}(l,l')\cos\frac{\theta}{2} = \frac{m}{2\alpha}(\omega^2-\omega_1^2)\,\Gamma(\omega)\, Im\, g_{uu}(l,l') \quad . \qquad \text{(IV.56)}$$

Now, we could use the model in chapter I if we write

$$g_{uu}(l,l') = K_s^{l-l'}\, g_{uu}(l,l') = K_s^{l-l'}\, g_{uu} \quad , \qquad \text{(IV.57)}$$

where, from (IV.24):

$$K_s = \pm\frac{3}{2\alpha}\sqrt{(M\omega^2 - \tfrac{4}{3}\alpha_1)^2 - \tfrac{4}{3}\alpha'^2} \quad . \qquad \text{(IV.58)}$$

Hence, the equation analogous to (I.28) is

$$\frac{d\sigma}{d\Omega\, dE} \propto -\omega\, R(\omega)\, Im\left(\frac{g_{uu}}{1+fK_s}\right) \quad , \qquad \text{(IV.59)}$$

where

$$R(\omega) = 1 + \cos\theta + 2\Gamma(\omega)\left[1 - \frac{m}{\alpha}(\omega^2-\omega_1^2)\right] . \qquad \text{(IV.60)}$$

Equation (IV.59) is plotted for various values of f in Fig.(IV.11).

It is seen that the effect of f is very weak: the spectrum for f=0 is practically identical to the one with f=.75, except in the relative weights of the bands and δ-functions. One can conclude that the local configuration is more important than the long distance correlations in SiO_2.

The factor R(ω) is responsible for the large Raman activity around ω_1 and arises from the Si-O stretching motion (through Γ(ω)). The proposal made by Galeener(1979) concerning the strong dependence of the Raman polarizability on ω around the band edge ω_1 is supported by the

results of the present model.

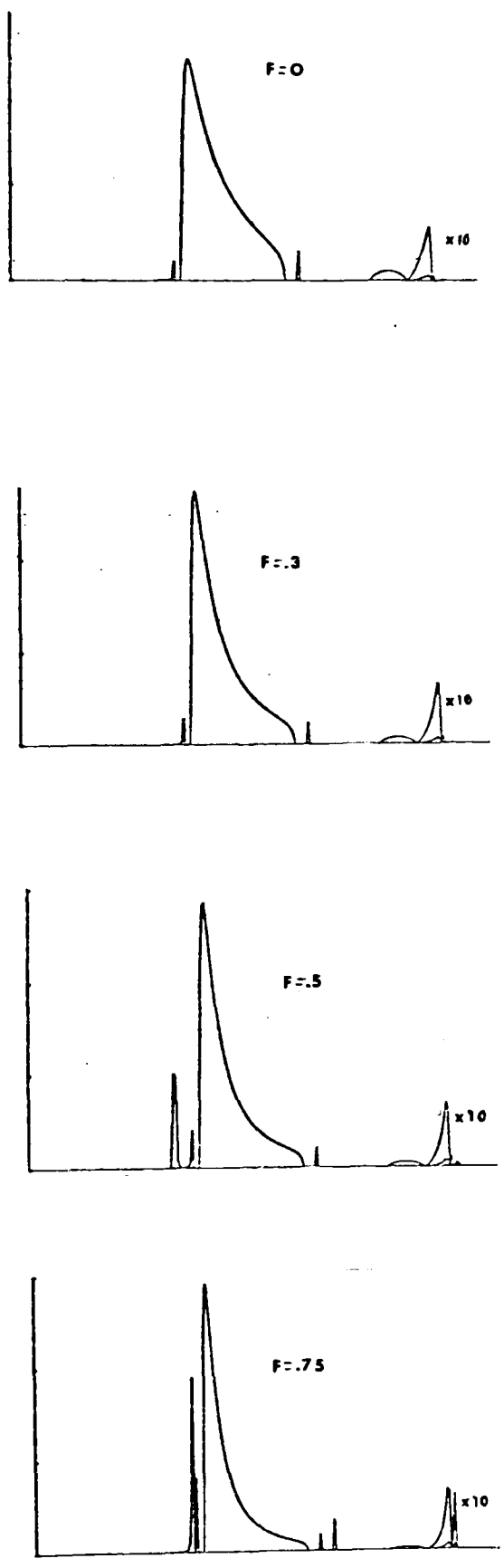

Fig.(IV.11) Raman intensity for a SiO_2 glass for various values of f.

The δ-function at ω_1 arises from the pole of $\Gamma(\omega)$ which is also present in g_{xx}. In the DOS of the glass, the weight of this state is 1/N, if the weight of the state at ω_3 is unity (so the weight of the bands is (N-1)/N), and is negligible for large N. However, the factors in equation (IV.59) modify the relative weight of the state at ω_1 and make it appear very strong. This could be due to the unsound band edges in the Bethe lattice and must not be taken too seriously.

The main feature exhibited by (IV.59) is that the local response at the defect site will be very strong whenever a particular mode involves opposite motion of the extremes of a Si-O bond. This response should be weighted by the concentration of defects if the response is supposed to be additive.

A revision of the different features in each defect leads to the conclusion that the best candidate for the observed defect peaks is the Si-Si bond (and, perhaps, O-O bonds). We agree with Laughlin et al.(1978), who discard the oxygen dangling bond, because no mode is observed in the gap (at 940 cm^{-1}). For the same reason the oxygen double bond is also a bad candidate, not to mention the square ring, which has several states in the gap involving Si-O stretch.

We believe that the present work presents a coherent and useful picture of the effects produced by simple local defects in Silica. The inclusion of non-central forces is not very useful, because it only modifies substantially the lower part of the spectrum, which is bad for a Bethe lattice in any case. Therefore, we did not pursue that direction.

It will be very desirable to extend the treatment to include long range Coulomb forces in order to explain the LO-TO splittings. Notice that Fig.(IV.11) also exhibits the extra δ-functions discussed on page 87, but these are

definitely spurious (Joannopoulos & Yndurain (1974)).

Taking advantage of the versatility of the model presented here, one could carry on studying other more complex defects, like 3-bound oxygens (Lucovsky (1979)) or 6-fold rings (Galeener et al.(1980)).

P A R T I I

O N E X C I T O N S

INTRODUCTION.

The optical absorption edge of Cuprous Oxide exhibits a remarkably rich structure due to excitons. Four series of excitons are found in the yellow, green, blue and violet regions of the spectrum. The first two are very well defined hydrogenic spectra, and for this reason, have received particular attention by the experimentalists for more than thirty years now (for a review see Washington et al.(1977) or Agekyan (1977)). Most of the interest has been directed to the yellow series, in which the hydrogenic lines, up to n=9, are clearly seen. Detailed studies of these lines under the action of external magnetic, electric and strain fields have been developed, mainly by Gross and co-workers in Leningrad (Gross et al.(1960a), (1960b), (1961),(1962a),(1962b)) and by Nikitine and his group in Strasbourg (Nikitine et al.(1961),(1969), Merle et al.(1973), Brahms et al.(1966)). Other important experiments worth mentioning are those by Sasaki & Kuwabara (1973), Petroff et al.(1975), Kuwabara et al.(1977), Frölich et al.(1979), Bloch & Shwab (1978) and Waters et al. (1980).

In spite of this huge experimental information, little theoretical work has been done, mainly because of two reasons: i) The nearly perfect hydrogenic nature of the spectrum allows one to think that cuprous oxide (Cu_2O) is the ideal material, where the simplest theory for excitons, the Wannier Model (Wannier(1937)), is suitable. This model is based on the Effective Mass Approximation and assumes that the excited states arise from isotropic and non-degenerate bands (for details see Elliott(1963)). ii) The theory developed by Elliott(1961) was able to explain, based on symmetry considerations, most of the important features observed experimentally, up to that date.

However, despite this well equilibrated picture of the situation, several questions were left without a clear answer, two of which are of paramount importance and form the core of this dissertation. These could be described briefly in the following way:

1) The limits of the green and yellow series are separated by 1064 cm^{-1} and their energy gaps show similar dependence on temperature ($\partial E_y/\partial T \sim \partial E_g/\partial T \sim -3cm^{-1}/^oK$). With these facts, the anisotropic absorption shown by the lines and symmetry relations, Elliott(1961) concluded that both series arise because a spin-orbit splitting of the valence band (of symmetry Γ_{25}^+ at the centre of the zone) into a 2-fold degenerate band (Γ_7^+) and a 4-fold degenerate one (Γ_8^+). Then, the yellow series corresponds to transitions between the Γ_7^+ band and a simple conduction band Γ_6^+ while the green series arises from $\Gamma_8^+ \rightarrow \Gamma_6^+$ transitions. If this is so, the Γ_7^+ component must be above the Γ_8^+ one. This situation is the reverse of what it is usually found in cubic semiconductors with the diamond or zinc-blende structures. Furthermore, an APW band calculation by Dahl & Switendick(1966) gives an upper Γ_8^+.

It seems reasonable to believe that the higher valence band should be Γ_7^+, because the symmetry-break splittings expected from a Γ_8^+ band would not agree with the observations. At the time this work started there were no calculations that could favour one of the two configurations.

A simple method for estimating the order of magnitude and sign of the spin-orbit splitting is described in Chapter I. This is done by using the Wigner-Eckart Theorem and by calculating a reduced matrix element of the operator l_z between properly symmetrised wave functions. The wave functions are found within the spirit of a Tight-Binding Approximation. This estimate is discussed and compared with very recent calculations.

2) The other problem is related to the shifts of some levels in the excitonic spectrum from the hydrogenic values. As a matter of fact, the hydrogenic law is well reproduced by the states with $n \geq 3$ in both series, but substantial deviations are exhibited by the lowest excited states. For example, the n=1 exciton of the yellow series ($1S_y$) lies 333 cm^{-1} below the expected value; the n=2 S-like exciton ($2S_y$) is not found at all, and the $2P_y$ exciton is slightly shifted ($\sim$4 cm^{-1} above). The green excitons also present anomalies, eg. the $1S_g$ level is found 191 cm^{-1} below the Rydberg law.

Two possible causes may be thought to produce such effects: i) The effective mass theory breaks down for the lowest states because their small Bohr radii ($\sim 9a_0$). ii) There is a strong interaction between the green and yellow excitons due to the nearly degenerancy of the $1S_g$ and the $2P_y$ levels.

It is true that both, i) and ii) are equally important, but it is convenient to examine ii) first and, possibly, introduce the effects of i) later on.

Admixtures of the S_y and S_g excitons are possible because both have components (orthoexcitons) with the same symmetry (Γ_{25}^+):

$$S_y \rightarrow \Gamma_7 \times \Gamma_6 = \Gamma_2 + \Gamma_{25}$$

$$S_g \rightarrow \Gamma_8 \times \Gamma_6 = \Gamma_{12} + \Gamma_{15} + \Gamma_{25}$$

This may occur by different mechanisms and all of them have to be explored: First of all, there is a direct Coulomb interaction that could mix the yellow and green excitons. This matter is considered in Chapter II, where second-order perturbation theory is used.

One might expect effects of this sort arising from the complexity of the valence band. In Chapter III a perturbative approach to the kinetics of the hole is used and a rough estimate of the shifts is then possible. As it is seen, no one of these methods provides a full ex-

planation of the situation. Therefore, in Chapter IV exchange terms between the electron and the hole are introduced in the formalism. The results obtained are in excellent agreement with the observations and some relevant conclusions are drawn.

C H A P T E R I

SPIN-ORBIT SPLITTING

The purpose is to estimate the spin-orbit splitting of the electronic states at the top of the valence band. This occurs at the point Γ of the reciprocal space (k=0) and it is known that the eigenfunctions form a basis for the Γ_{25}^{+} representation of the cubic group. In order to achieve this, one needs to find a set of wave functions for the states in the valence band, and this could be done (avoiding a complicated band calculation) by adopting a simple tight-binding model.

1.- TIGHT-BINDING APPROXIMATION.

In general, one must solve the eigenvalue problem:

$$H \bar{\Phi}_m = \varepsilon_m \bar{\Phi}_m \quad . \tag{I.1}$$

Due to the translational symmetry of the crystal, the Bloch's theorem holds and, in the tight-binding approximation, the eigenfunctions Φ_m could be written as Bloch sums

$$\bar{\Phi}_m(\bar{r}) = \frac{1}{N} \sum_{R_i} (R_i) e^{i\bar{k}\cdot\bar{R}_i} \Psi_m(\bar{r}-\bar{R}_i) \quad , \tag{I.2}$$

where m stands for all the quantum numbers characterizing the state, N is a normalization factor and the Ψ_m's are atomic orbitals centered at the atom located at $\bar{R}_i$. The sum runs over all equivalent atoms in the unit cell. This leads to the secular equation

$$| H_{mn} - \varepsilon_{mn} \delta_{mn} | = 0 \quad . \tag{I.3}$$

The order of this equation is the same as the number of orbitals considered. Knowing that there are no matrix elements between Bloch sums with different k, a typical

matrix element is

$$H_{mn} = \langle \Phi_n \mid H \mid \Phi_m \rangle = \frac{1}{N^2} \sum_{R_i} \sum_{R_j} (R_i, R_j) e^{i\bar{k}\cdot(\bar{R}_i - \bar{R}_j)} \int \Psi_n^*(\bar{r} - \bar{R}_i) H \Psi_m(\bar{r} - \bar{R}_j)\, d^3r \quad \text{(I.4)}$$

At this point further simplifications are needed: First, one must restrict the number of orbitals forming the Bloch sums. It is physically sound to consider only the copper 3d-orbitals and the oxygen 2p-orbitals. Noticing that there are four copper and two oxygen atoms per unit cell, the size of the secular equation (I.3) is 26×26. One could also assume that the only important interactions are between nearest neighbours; in the present case this means that the only non-vanishing off-diagonal matrix elements are between chemically different atoms.

Let H_{cu} and H_{ox} be the matrix elements between Cu and O respectively, then the equation (I.3) takes the form

$$\left\{\begin{array}{l} \text{20 rows} \\ \text{6 rows} \end{array}\right. \left|\begin{array}{c|c} \begin{array}{cc} H_{cu}-E & 0 \\ & \ddots \\ 0 & H_{cu}-E \end{array} & \begin{array}{c} \text{non-} \\ \text{vanishing elements} \end{array} \\ \hline \begin{array}{c} \text{non-vanishing} \\ \text{elements} \end{array} & \begin{array}{cc} H_{ox}-E & 0 \\ & \ddots \\ 0 & H_{ox}-E \end{array} \end{array}\right| = 0 \quad \text{(I.5)}$$

This equation could be written in a more convenient form at the point Γ, where direct transitions take place, if one chooses as the Bloch sums the combinations of atomic orbitals that transform like the irreducible representations (IR) of the space group of the crystal. At Γ the space group of Cu_2O (O_h^4) is isomorphous to the cubic point group (O_h), and the IR spanned by the atomic orbitals at Γ are easy to find (Table 1 in Dahl & Switendick (1966)).

The advantage of this representation is that there will not be any non-zero matrix elements between Bloch sums

belonging to different IR or between different partners of the same IR.

The results on Table 1 of Dahl & Switendick(1966) were verified by applying the standard theorem that states that if a reducible representation Γ^{red} is written as a linear combination of IR (Γ^j), the coefficients a_j are

$$a_j = \frac{1}{h} \sum_R \chi^j(R)\,\chi^{red}(R)$$

where R are all the h operations of the group and χ are the characters. Considering the IR spanned by the copper 3d and oxygen 2p orbitals, one could write (I.5), in a symbolic form, as

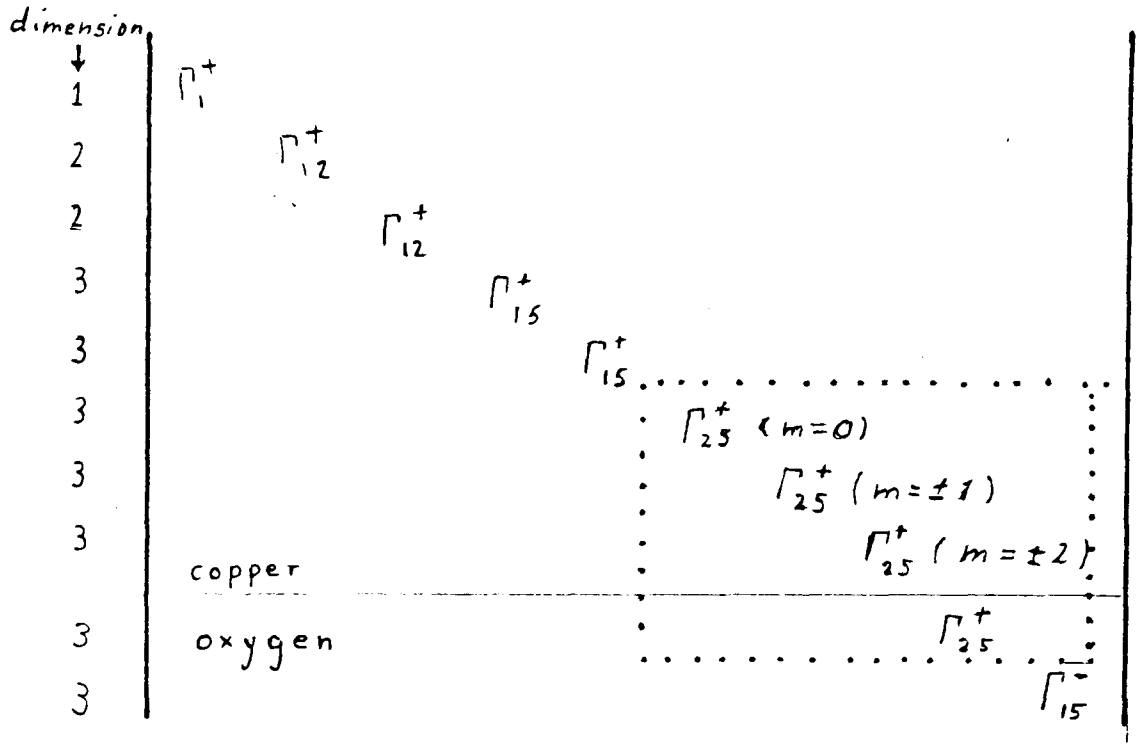

When the quantization axes are chosen along the Cu-O bonds, orbitals with different quantum number m do not mix, thus m is indicated in (I.6).

Let us concentrate on the 12×12 block inside the dotted square in (I.6), and parametrize the non-zero matrix elements. Let t_0 be the matrix element between the copper d-functions with orbital magnetic number m=0 and the oxygen p-functions. Analogously, t_1 will be the matrix elements between the copper d-functions with m=±1 and the oxygen p-functions. The copper orbitals with m=±2 do not mix with the oxygen ones. After some rearrangements, one

is left with 3 sets of 4×4 equations (one for each collection of partners) of the form

$$\begin{vmatrix} H_{cu}-E & 0 & 0 & t_0 \\ 0 & H_{cu}-E & 0 & t_1 \\ 0 & 0 & H_{cu}-E & 0 \\ t_0 & t_1 & 0 & H_{ox}-E \end{vmatrix} = 0 \quad . \qquad \text{(I.7)}$$

The roots of (I.7) are the energies of the 4 Γ_{25}^{+} bands. Labeling arbitrarily the eigenvalues, these are

$$\begin{aligned} E_1 &= H_{cu} \\ E_2 &= H_{cu} = E_1 \\ E_3 &= \tfrac{1}{2}(H_{cu} + H_{ox}) + G \\ E_4 &= \tfrac{1}{2}(H_{cu} + H_{ox}) - G \end{aligned} \qquad \text{(I.8)}$$

where $G = \{\tfrac{1}{4}(H_{cu} - H_{ox})^2 + (t_0^2 + t_1^2)\}^{\frac{1}{2}}$

The situation looks like:

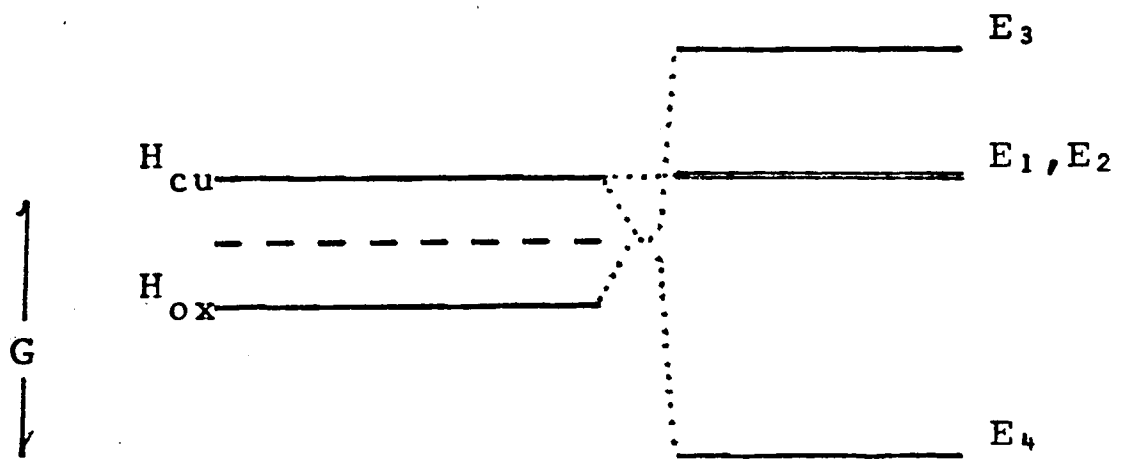

The picture could be matched with the one given in the two band calculations available (Kleinman & Mednick (1980), Dahl & Switendick (1966)), except that the two degenerate levels E_1 and E_2 are split. The reason might be that we oversimplified the problem neglecting Cu-Cu interactions that must, certainly, cause the splitting of E_1 and E_2 which are built from Cu 3d (m=2) orbitals.

But, since we are interested mostly in E_3 which is the top of the valence band, this will not bother us very much.

We must investigate now the eigenvectors corresponding to each one of the eigenvalues, we define these as

$$H\,\Phi^i = E_i\,\Phi^i \,. \tag{I.9}$$

This is easily accomplished by substituting each of the eigenvalues in (I.7). One set of orthonormal eigenvectors is

$$\Phi^1 = \begin{pmatrix} 0 \\ 0 \\ 1 \\ 0 \end{pmatrix} \;;\; \Phi^2 = \frac{1}{a}\begin{pmatrix} t_1 \\ -t_0 \\ 0 \\ 0 \end{pmatrix} \;;\; \Phi^3 = \frac{1}{\sqrt{a^2+b_3^2}}\begin{pmatrix} -t_0 \\ -t_1 \\ 0 \\ b_3 \end{pmatrix} \;;\; \Phi^4 = \frac{1}{\sqrt{a^2+b_4^2}}\begin{pmatrix} -t_0 \\ -t_1 \\ 0 \\ b_4 \end{pmatrix} \tag{I.10}$$

where $a^2 = t_0^2 + t_1^2$

$b_3 = H_{cu} - E_3$

$b_4 = H_{cu} - E_4$ also $b_3 b_4 = -a^2$

Now, define a 4×4 unitary matrix S which has Φ^i as columns. Then, the Hamiltonian in (I.7) is diagonalized by the similarity transformation

$$S^{-1} H S = \begin{pmatrix} E_1 & 0 & 0 & 0 \\ 0 & E_2 & 0 & 0 \\ 0 & 0 & E_3 & 0 \\ 0 & 0 & 0 & E_4 \end{pmatrix} \tag{I.11}$$

Accordingly, the vectors ξ used to write (I.7), transform to

$$\Psi_j = S^{-1}\xi_j \tag{I.12}$$

The subscript j refers to a particular partner of a Γ_{25}^+ IR. In fact:

partner 1 transforms like xy

partner 2 transforms like zx

partner 3 transforms like yz

Remember that ξ must be formed with the four symmetrized functions that transform in the same way. These can be found in Appendix I. The representation in which equation (I.7) was written is then:

$$\xi_j = \begin{pmatrix} d_0^j \\ d_1^j \\ d_2^j \\ p^j \end{pmatrix} , \qquad \text{(I.13)}$$

where d or p represent functions built with copper 3d or oxygen 2p respectively. The subscripts indicate that only orbitals with m=0,±1 or ±2 are present in each case. In this notation,

$$\begin{aligned} \langle d_0^j | H | p^j \rangle &= t_0 \\ \langle d_i^j | H | p^j \rangle &= t_1 \qquad i = 0,1,2 \\ \langle d_i^j | H | d_i^j \rangle &= H_{cu} \qquad j = 1,2,3 \\ \langle p^j | H | p^j \rangle &= H_{ox} \end{aligned} \qquad \text{(I.14)}$$

The eigenfunctions are found by substituting (I.13) into (I.12) and are listed in Table I.1 .

Table I.1

Eigenfunctions for the Γ_{25}^+ bands in Cu_2O.

Band		Eigenfunction	Partner	Name
$\Gamma_{25}^+(1)$	E_1	d_2^1	xy	Ψ_1^1
		d_2^2	zx	Ψ_2^1
		d_2^3	yz	Ψ_3^1
$\Gamma_{25}^+(2)$	E_2	$(t_1 d_0^1 - t_0 d_1^1)/a$	xy	Ψ_1^2
		$(t_1 d_0^2 - t_0 d_1^2)/a$	zx	Ψ_2^2
		$(t_1 d_0^3 - t_0 d_1^3)/a$	yz	Ψ_3^2
$\Gamma_{25}^+(3)$	E_3	$\{b_3 p^1 - (t_0 d_0^1 + t_1 d_1^1)\}/\sqrt{(a^2+b_3^2)}$	xy	Ψ_1^3
		$\{b_3 p^2 - (t_0 d_0^2 + t_1 d_1^2)\}/\sqrt{(a^2+b_3^2)}$	zx	Ψ_2^3
		$\{b_3 p^3 - (t_0 d_0^3 + t_1 d_1^3)\}/\sqrt{(a^2+b_3^2)}$	yz	Ψ_3^3
$\Gamma_{25}^+(4)$	E_4	$\{b_4 p^1 - (t_0 d_0^1 + t_1 d_1^1)\}/\sqrt{(a^2+b_4^2)}$	xy	Ψ_1^4
		$\{b_4 p^2 - (t_0 d_0^2 + t_1 d_1^2)\}/\sqrt{(a^2+b_4^2)}$	zx	Ψ_2^4
		$\{b_4 p^3 - (t_0 d_0^3 + t_1 d_1^3)\}/\sqrt{(a^2+b_4^2)}$	yz	Ψ_3^4

2.- SPIN-ORBIT COUPLING

It is known from Group Theory that a state with symmetry Γ_{25}^{+} splits, when spin-orbit interactions are considered, into a two-fold degenerate state Γ_{7}^{+} and a four-fold degenerate state Γ_{8}^{+}. If one wants to know the difference in energy between these two states ($\Delta\varepsilon$), one must calculate the matrix elements of the operator

$$H_{so} = \sum_{i} \zeta(\tilde{r}_i)\, \tilde{\ell}_i \cdot \tilde{s}_i \quad , \tag{I.15}$$

where the operators $\tilde{\ell}_i$ and $\tilde{s}_i$ act on the atom situated at $\tilde{r}_i$.

The Wigner-Eckart theorem (see for instance Brink & Satchler(1971)) allows one to accomplish this by calculating only one simple matrix element. This theorem states that the matrix elements of an operator that transforms in a particular way are proportional to those of another operator that transforms exactly in the same way. In this case

$$\langle | H_{so} | \rangle = \Lambda \langle | \bar{L} \cdot \bar{S} | \rangle \quad , \tag{I.16}$$

where $\bar{L}$ and $\bar{S}$ are the effective angular momentum and spin operators respectively, and Λ is a constant to be determined and that contains all the physics of the problem. In general, if there is a state with pseudo angular momentum L', spin S and total angular momentum J, the matrix elements of the operator $\bar{L}\cdot\bar{S}$ are

$$\Delta\varepsilon(J) = \langle L', S, J | \bar{L} \cdot \bar{S} | L', S, J \rangle = \frac{\eta}{2}\left[J(J+1) - L'(L'+1) - S(S+1)\right] \tag{I.17}$$

In the present case the Γ_{25}^{+} states have L'=1 and S=½, therefore J=1/2,3/2. For these states η=-1 (see Zeiger & Pratt(1973) p.137). Then it is easy to see that

$$\Delta\varepsilon = \varepsilon(3/2) - \varepsilon(1/2) = -\frac{3}{2}\Lambda \qquad \text{(I.18)}$$

To determine Λ one evaluates a single matrix element chosen in a convenient way. If one chooses states with maximum spin and $a_j = iyz_j$ and $b_j = zx_j$ (Kubic harmonics), then $\langle ia_j | L_z S_z | b_j \rangle = 1(\frac{1}{2})$ and then

$$\Lambda_j = \sum_i \langle\zeta\rangle_i \langle i a_j | \ell_i^2 | b_j \rangle \qquad \text{(I.19)}$$

where $\langle\zeta\rangle_i$ is a one-electron radial integral and could take the value ζ if there is a copper on site i, or $q\zeta$ if the site i is occupied by an oxygen atom.

One cannot evaluate (I.19) using the Ψ's in TableI.1 because the operator ℓ_i^z is referred to a fixed z-axis, while the Ψ's are linear combinations of spherical harmonics quantized in four different directions. It is convenient to transform the basis functions to a single quantization axis, because it only involves rotations of the eigenfunctions of the full rotation group. The transformation that gives a particular spherical harmonic in one frame ($Y_\ell^m(\theta,\phi)$) in terms of spherical harmonics in another frame ($Y_\ell^m(\theta',\phi')$) is

$$Y_\ell^m(\theta,\phi) = \sum_n^\ell Y_\ell^n(\theta',\phi')\ \mathcal{D}_{nm}^\ell(\alpha,\beta,\gamma) \qquad \text{(I.20)}$$

where α,β,γ are the Euler angles between the two frames and the rotation matrices

$$\mathcal{D}_{nm}^\ell = e^{-in\alpha}\, d_{nm}^\ell(\beta)\, e^{-im\gamma}$$

could be found in Tables (Brink & Satchler(1971) p.24). We choose the axis (001) as the unique quantization direction. The old axes were:

copper site A z-axis (111)
B ($\bar{1}\bar{1}1$) (for oxygen sites the
C ($\bar{1}1\bar{1}$) z-axis was (001))
D ($1\bar{1}\bar{1}$)

Applying (I.20) to the states in Appendix I, and from Table I.1, a new set of eigenfunctions referred to the (001) axis is obtained:

(I.21)

$$\Psi_2' = \frac{1}{6}\{(xy+yz)_A-(xy-yz)_B-(xy+yz)_C+(xy-yz)_D - \frac{\sqrt{3}}{2}[(3z^2-r^2)_A-(3z^2-r^2)_B+(3z^2-r^2)_C-(3z^2-r^2)_D] - 2(zx_A+zx_B+zx_C+zx_D)\}$$

$$\Psi_3' = \frac{1}{6}\{(xy+zx)_A-(xy-zx)_B+(xy-zx)_C-(xy+zx)_D - \frac{\sqrt{3}}{2}[(3x^2-r^2)_A-(3x^2-r^2)_B-(3x^2-r^2)_C+(3x^2-r^2)_D] - 2(yz_A+yz_B+yz_C+yz_D)\}$$

$$\Psi_2^2 = \frac{1}{a}\left\{\left[\frac{t_1}{2\sqrt{3}}-\frac{t_0}{3\sqrt{2}}\right](zx_A+zx_B+zx_C+zx_D)+\left[\frac{t_1}{2\sqrt{3}}+\frac{t_0}{6\sqrt{2}}\right][(xy+yz)_A-(xy-yz)_B-(xy+yz)_C+(xy-yz)_D] + \frac{t_0}{6}[(3y^2-r^2)_A-(3y^2-r^2)_B+(3y^2-r^2)_C-(3y^2-r^2)_D]\right.$$

$$\Psi_3^2 = \frac{1}{a}\left\{\left[\frac{t_1}{2\sqrt{3}}-\frac{t_0}{3\sqrt{2}}\right](yz_A+yz_B+yz_C+yz_D)+\left[\frac{t_1}{2\sqrt{3}}+\frac{t_0}{6\sqrt{2}}\right][(xy+zx)_A-(xy-zx)_B+(xy-zx)_C-(xy+zx)_D] + \frac{t_0}{6}[(3x^2-r^2)_A-(3x^2-r^2)_B-(3x^2-r^2)_C+(3x^2-r^2)_D]\right.$$

$$\Psi_2^3 = \frac{1}{\sqrt{a^2+b_3^2}}\left\{c_3\rho^2-\left[\frac{t_0}{2\sqrt{3}}+\frac{t_1}{3\sqrt{2}}\right](zx_A+zx_B-zx_C+zx_D)-\left[\frac{t_0}{2\sqrt{3}}-\frac{t_1}{6\sqrt{2}}\right][(xy-yz)_A-(xy-yz)_B-(xy+yz)_C+(xy-yz)_D]+\frac{t_1}{6}[(3y^2-r^2)_A-(3y^2-r^2)_B+(3y^2-r^2)_C-(3y^2-r^2)_D]\right\}$$

$$\Psi_3^3 = \frac{1}{\sqrt{a^2+b_3^2}}\left\{b_3\rho^3-\left[\frac{t_0}{2\sqrt{3}}+\frac{t_1}{3\sqrt{2}}\right](yz_A-yz_B+yz_C-yz_D)-\left[\frac{t_0}{2\sqrt{3}}-\frac{t_1}{6\sqrt{2}}\right][(xy+zx)_A-(xy-zx)_B+(xy-zx)_C-(xy+zx)_D]+\frac{t_1}{6}[(3x^2-r^2)_A-(3x^2-r^2)_B-(3x^2-r^2)_C+(3x^2-r^2)_D]\right\} \quad \ldots$$

Ψ_j^4 are of the same form as Ψ_j^3 replacing b_4 for b_3 (these equations agree with the ones found by Kleinman & Mednick (1980)).

The subscripts in equations (I.21) indicate the site at which the functions are centered. The notation for the functions is as follows

$$xy = \frac{i}{\sqrt{2}} \left(Y_2^{-2} - Y_2^2 \right) \qquad \text{(I.22)}$$

$$yz = \frac{i}{\sqrt{2}} \left(Y_2^{-1} - Y_2^1 \right)$$

$$zx = \frac{1}{\sqrt{2}} \left(Y_2^{-1} + Y_2^1 \right)$$

$$x^2 - y^2 = \frac{1}{\sqrt{2}} \left(Y_2^{-2} + Y_2^2 \right)$$

$$3z^2 - r^2 = Y_2^0$$

$$3y^2 - r^2 = \frac{1}{2} \left(-Y_2^0 - \frac{\sqrt{3}}{\sqrt{2}} \left(Y_2^{-2} + Y_2^2 \right) \right)$$

$$3x^2 - r^2 = \frac{1}{2} \left(-Y_2^0 - \frac{\sqrt{3}}{\sqrt{2}} \left(Y_2^{-2} + Y_2^2 \right) \right)$$

where Y_ℓ^m is properly normalized. Operating with ℓ_z gives

$$\ell_i^z \, |xy\rangle_i = -2i \, |x^2 - y^2\rangle_i \qquad \text{(I.23)}$$
$$\ell_i^z \, |yz\rangle_i = -i \, |zx\rangle_i$$
$$\ell_i^z \, |zx\rangle_i = i \, |yz\rangle_i$$
$$\ell_i^z \, |x^2 - y^2\rangle_i = 2i \, |xy\rangle_i$$
$$\ell_i^z \, |3z^2 - r^2\rangle_i = 0 \, |3z^2 - r^2\rangle_i$$
$$\ell_i^z \, |3y^2 - r^2\rangle_i = -\sqrt{3} i \, |xy\rangle_i$$
$$\ell_i^z \, |3x^2 - r^2\rangle_i = \sqrt{3} \, |xy\rangle_i$$

Substituting the functions (I.21) in equations (I.19) and using (I.23) it is found

$$a) \quad \Lambda_1 = \zeta$$
$$b) \quad \Lambda_2 = -\zeta \left(t_0^2/2 + \sqrt{6} t_0 t_1 \right) / a^2 \qquad \text{(I.24)}$$
$$c) \quad \Lambda_3 = -\zeta \left(t_1^2/2 - \sqrt{6} t_0 t_1 - 4 b_3 \right) / \left(a^2 + b_3^2 \right)$$
$$d) \quad \Lambda_4 = -\zeta \left(t_1^2/2 - \sqrt{6} t_0 t_1 - 4 b_4 \right) / \left(a^2 + b_4^2 \right)$$

$$\Delta \varepsilon_i = \frac{-3}{2} \Lambda_i$$

3.- DISCUSSION

The parameters in (I.24) are related to the energies at Γ, from the band calculation by Kleinman& Mednick(1980) the following values (in eV) are estimated:

$$H_{cu} = E_1 = -2.35 \qquad (I.25)$$
$$E_3 = 0$$
$$E_4 = -6.03$$
$$G = 3.02$$
$$b_3 = -2.35$$
$$b_4 = 3.60$$
$$a^2 = 8.65\ eV^2$$

It is reasonable to set q=0 in (I.24) because the spin-orbit splitting of p-orbitals is very small indeed. Now the problem is to give separate values to the integrals t_0 and t_1. This could be done from (I.24a) and (I.24b) if the ratio Δ_1/Δ_2 were known. In the present calculation these bands are degenerate, therefore let us assume that their splitting is the same, that is $\Delta_1/\Delta_2=1$. If this is done, equation (I.24b) gives

$$t_1 = -\sqrt{\tfrac{3}{2}}\, t_0 \qquad (I.26)$$

and with (I.18),(I.24),(I.25) and (I.26) the numbers are

$$a) \quad \Delta\varepsilon_1 = -\tfrac{3}{2}\zeta \qquad (I.27)$$
$$b) \quad \Delta\varepsilon_2 = -\tfrac{3}{2}\zeta$$
$$c) \quad \Delta\varepsilon_3 = 1.28\,(\tfrac{3}{2}\zeta)$$
$$d) \quad \Delta\varepsilon_4 = 0.82\,(\tfrac{3}{2}\zeta)\,.$$

The value of $(3\zeta/2)$ can be found for copper on page 210 of Condon & Shortley (1953) and is $-820\ cm^{-1}$ (more than half-filled shell). Therefore, the band 3, which is the one of interest, will show a splitting

$$\Delta\varepsilon_3 = -1050\ cm^{-1} \qquad (I.28)$$

The order of magnitude and sign of the splitting (I.28) is correct and almost identical to the one found by Kleinman & Mednick(1980). However, attemps to fit our (I.24) with their splittings for all the bands were unsuccessful. It is believed that this discrepancy is due to the crudeness of our model, neglecting further neighbours interactions and hybridization of the Cu-4S orbitals, which turns out to be important in the band calculation.

At the present time a band calculation using a generalization of the LCAO (CNDO) Method is in progress and it is expected that a more precise estimate of the splitting will be available, as the drawbacks of the present model are minimised.

C H A P T E R I I

DIRECT COULOMB INTERACTION

The yellow excitons in Cu_2O are formed by states belonging to simple valence and conduction bands. The regularity of the series also suggests that these bands are isotropic, and therefore they could be treated theoretically by the effective mass approximation. The hydrogenic nature of the green series also allows one to think that this approximation is valid, if it is generalized so as to include a degenerate valence band.

The anomalies found in the lowest states of both series are sketched in Fig.(II.1). A rapid inspection of this figure let us think that this effects are due to an interaction between excitons belonging to different series.

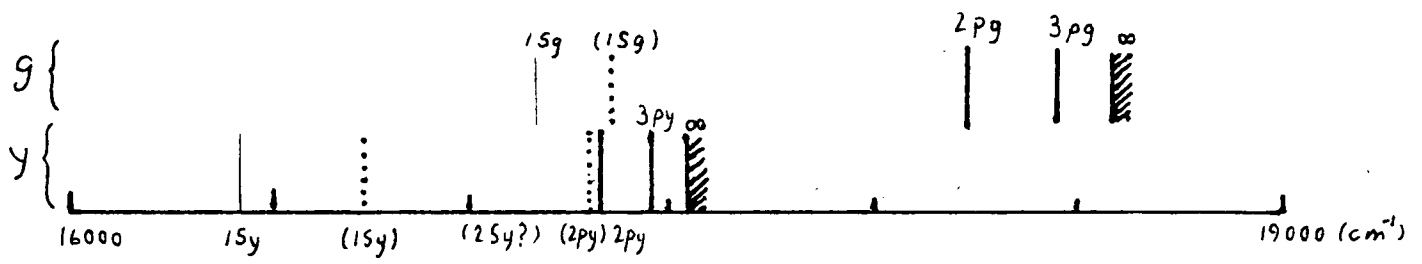

Fig.(II.1) Lowest states of the yellow (Y) and green (G) excitonic spectra in Cu_2O, represented by solid lines. The nomenclature nℓ indicates the principal and orbital quantum numbers of the envelope of the exciton wave function. The dotted lines and names in () indicate the expected position of the states from the Rydberg law. The 2sy exciton is not found. The s-lines are weak because they are dipole forbidden transitions.

These effects might be explained within the effective mass approximation, if one takes into account higher-order Coulomb interactions between the excitons. Let us start with a brief review of this theory (for details see Knox (1963)). An excited state in a crystal can be written

$$\Psi^i(\bar{k}_e, \bar{k}_h) = \frac{1}{\sqrt{N!}} \mathcal{P}\{\Psi_{v\bar{k}_1}(\bar{r}_1)\ldots\Psi_{c\bar{k}_e}(\bar{r}_e)\Psi^i_{vk_h}(\bar{r}_h)\ldots\Psi_{v\bar{k}_N}(\bar{r}_N)\}\,. \qquad \text{(II.1)}$$

for a N-electron system. Here P denotes the antisymmetric combination of one-electron wave functions of the type

$$\Psi_{n\bar{k}}(\bar{r}) = \frac{1}{\sqrt{NB}} e^{i\bar{k}\cdot\bar{r}} u_{n\bar{k}}(\bar{r}) \quad , \qquad \text{(II.2)}$$

where B is the volume of a unit cell and u has the periodicity of the lattice.

Equation (II.1) is the Hartree-Fock wave function of a state in which a single electron at $\bar{r}_e$ has been promoted with momentum $\bar{k}_e$ to the conduction band c, leaving a hole in the valence band v_i with momentum $-\bar{k}_h$.

The electron-hole interaction in the exciton problem could be approximated by a screened Coulomb potential

$$\frac{-e^2}{\varepsilon|\bar{r}_e-\bar{r}_h|} \quad , \qquad \text{(II.3)}$$

in which the factor ε takes into account the effects of the electronic and lattice polarization (Haken(1963)). When (II.3) is introduced into the two-particle Hamiltonian, the exciton states are linear combinations of the states (II.1):

$$\phi^i = \sum_{\bar{k}_e}\sum_{\bar{k}_h} A^i(\bar{k}_e,\bar{k}_h)\Psi^i(\bar{k}_e,\bar{k}_h) = \sum_{\bar{k}_e,\bar{k}_h} A^i(\bar{k}_e,\bar{k}_h)\Psi(\bar{k}_e)\Psi^i(\bar{k}_h) \qquad \text{(II.4)}$$

(the last step is just a short-hand notation for states (II.1)). The matrix elements of (II.3) could be written in terms of integrals involving only pairs of single-particle states.

For the time being exchange terms will be neglected (see Chapter IV), and any deviations from the Coulomb law due to the small size of the excitons will not be considered. Using (II.4) in the Schrödinger equation, an equation for the A's is obtained:

$$(E_c(\bar{k}_e)-E_{v_i}(\bar{k}_h)-\bar{E})A^i(\bar{k}_e,\bar{k}_h) + \sum_{\bar{k}_e',\bar{k}_h'}\left[\int_{\text{cryst.}}\Psi^*(\bar{k}_e')\Psi^*(\bar{k}_h')\frac{e^2}{\varepsilon|\bar{r}_e-\bar{r}_h|}\Psi(\bar{k}_e)\Psi(\bar{k}_h)\,d\bar{r}_e\,d\bar{r}_h\right]A^i(\bar{k}_e',\bar{k}_h') = 0 \qquad \text{(II.5)}$$

It is at this point where the crucial assumptions are usually made. If one supposes that the interaction potential does not vary greatly over a unit cell, and that $\bar{u}_k$ varies slowly in the range of $\bar{k}$ where A is appreciable, one obtains the effective mass equation by Fourier transforming (II.5). In the case of having non-degenerate spherical bands near k=0, i.e.

$$\bar{E}_c(\bar{k}_e) - \bar{E}_{v_i}(\bar{k}_h) = \bar{E}_G + \frac{\hbar^2 k_e^2}{2m_e} + \frac{\hbar^2 K_h^2}{2m_h} \quad , \tag{II.6}$$

the effective mass equation becomes the hydrogen atom one and therefore the A's are known exactly. When the valence band is degenerate, the solution is not exact, finding the coefficients is a rather complicated task, although it could be done.

Let the excitons arising from the Γ_7^+ valence band be ϕ^i and the excitons from the degenerate band Γ_8^+

$$\phi^j = \sum_{\bar{k}_e, \bar{k}_h} B^j(\bar{k}_e, \bar{k}_h)\, \Psi(\bar{k}_e)\, \Psi^j(\bar{k}_h) \tag{II.7}$$

and assume that the A's and B's are known. The perturbation (II.3) does not mix the states (II.4) and (II.7), to zero order, therefore

$$\langle \phi^i | \phi^j \rangle = 0 \tag{II.8}$$

At higher order there will be non-zero off-diagonal matrix elements, thus one is interested in calculating terms like

$$\frac{-e^2}{\varepsilon} \langle \phi^i | \frac{1}{|\bar{r}_e - \bar{r}_h|} | \phi^j \rangle \tag{II.9}$$

and the eigenstates will be admixtures of the exciton functions

$$\Psi = a\,\phi^i + b\,\phi^j \tag{II.10}$$

Now, let us write

$$\frac{1}{|\bar{r}_e-\bar{r}_h|} = \frac{1}{|(\bar{r}_e-\bar{R}_1)-(\bar{r}_h-\bar{R}_2)+(\bar{R}_1-\bar{R}_2)|} = \frac{1}{|(\bar{r}_1-\bar{r}_2)+(\bar{R}_1-\bar{R}_2)|}, \quad \text{(II.11)}$$

where $\bar{R}_1$ is the position of the unit cell containing the electron and $\bar{R}_2$ labels the cell where the hole is. Expanding (II.11) in powers of $(\bar{r}_1-\bar{r}_2)$

$$\frac{1}{|\bar{r}_e-\bar{r}_h|} = \frac{1}{|\bar{R}_1-\bar{R}_2|} - \frac{(\bar{r}_1-\bar{r}_2)\cdot(\bar{R}_1-\bar{R}_2)}{|\bar{R}_1-\bar{R}_2|^3} + \frac{1}{2}\left[\frac{3[(\bar{r}_1-\bar{r}_2)\cdot(\bar{R}_1-\bar{R}_2)]^2}{|\bar{R}_1-\bar{R}_2|^5} - \frac{|\bar{r}_1-\bar{r}_2|^2}{|\bar{R}_1-\bar{R}_2|^3}\right]+\dots \quad \text{(II.12)}$$

The matrix element (II.9) vanishes for the first term in (II.12), by virtue of (II.8). Therefore let us concentrate on the second term in (II.12). We introduce it in (II.9) and write explicitly the eigenfunctions using (II.4) and (II.7). Realize that for direct excitons $\bar{K} = \bar{k}_e + \bar{k}_h \simeq 0$, and substituting into (II.2) the definitions

$$\begin{cases} \bar{K} \equiv \bar{k}_e \simeq -\bar{k}_h \\ \bar{K}' \equiv \bar{k}'_e \simeq -\bar{k}'_h \end{cases}, \quad \text{(II.13)}$$

it is obtained an expression in which one can write $\bar{r}_e$ and $\bar{r}_h$ in terms of $\bar{r}_1$ and $\bar{r}_2$ and take advantage of the periodicity of the u's ($u(\bar{r})=u(\bar{r}+\bar{R}_n)$), in order to write the integral over the whole crystal as an integral over the unit cells. The result is:

$$-\langle\phi^i|\frac{1}{|\bar{r}_e-\bar{r}_h|}|\phi^j\rangle \simeq \langle\phi^i|\frac{(\bar{r}_1-\bar{r}_2)\cdot(\bar{R}_1-\bar{R}_2)}{|\bar{R}_1-\bar{R}_2|^3}|\phi^j\rangle = \quad \text{(II.14)}$$

$$= \sum_{K,K'} A^i(K')\,B^j(K)\left\{\frac{1}{N^2}\sum_{\bar{R}_1,\bar{R}_2}\frac{e^{i(\bar{K}-\bar{K}')\cdot(\bar{R}_1-\bar{R}_2)}}{|\bar{R}_1-\bar{R}_2|}\left[\frac{1}{B^2}\int_{cell} e^{i(\bar{K}-\bar{K}')\cdot(\bar{R}_1-\bar{R}_2)} u^*_{cK'}(\bar{r}_1)u^*_{jK'}(\bar{r}_2)[(\bar{r}_1-\bar{r}_2)\cdot(\bar{R}_1-\bar{R}_2)]\,u_{cK}(\bar{r}_1)u_{jK}(\bar{r}_2)\,d\bar{r}_1 d\bar{r}_2\right]\right\}$$

Periodic boundary conditions permit one to extend the double summation over lattice vectors to infinity, and write it as N times a single sum over $\bar{R}=\bar{R}_1-\bar{R}_2$. Observe that $\bar{R}$ could be taken out of the integral in square brackets. Let us investigate the nature of this factor: it

could be written as $\bar{R}\cdot(I_1-I_2)$ by defining

$$I_1 = \langle c k' | \bar{r}_1 e^{i\Delta\bar{k}\cdot\bar{r}_1} \langle i k' | e^{-i\Delta\bar{k}\cdot\bar{r}_2} | j k \rangle_2 | c k \rangle_1 \qquad \text{(II.15)}$$

$$I_2 = \langle i k' | \bar{r}_2 e^{i\Delta\bar{k}\cdot\bar{r}_2} \langle c k' | e^{i\Delta\bar{k}\cdot\bar{r}_1} | c k \rangle_1 | j k \rangle_2 \,,$$

where $\Delta\bar{k} = k - k'$ and

$$\langle n k' | \hat{O} | m k \rangle_\ell = \frac{1}{B} \int_{cell} u^*_{nk'}(\bar{r}_\ell)\, \hat{O}\, u_{mk}(\bar{r}_\ell)\, d\bar{r}_\ell \qquad \text{(II.16)}$$

Near the centre of the Brillouin Zone one can expand all functions around $\bar{k}=0$, retaining only linear terms in $\bar{k}$:

$$e^{\pm i\Delta\bar{k}\cdot\bar{r}} \sim 1 \pm i\Delta\bar{k}\cdot\bar{r} \qquad \text{(II.17)}$$
$$u_{nk}(\bar{r}) \sim u_{no} + \sum_{n'\neq n} u_{n'o}\, \frac{\hbar}{m}\, \bar{k}\cdot\frac{\langle n'|\bar{p}|n\rangle}{E_n - E_{n'}}$$

With (II.17) and (II.16) one detects at once that $I_1 \sim O(k^2)$ because of the orthonormalization condition (II.8) and hence it is negligible. The integral with respect to $\bar{r}_2$ in I_2 is $1+O(k^2)$, because $\langle c|\bar{r}_2|c\rangle=0$, by symmetry, and therefore

$$I_2 = \langle i|\bar{r}_2|j\rangle + \frac{\hbar}{m}\Delta\bar{k}\cdot\sum_n \left[\frac{\langle i|\bar{r}|n\rangle\langle n|\bar{r}_2|j\rangle}{E_i - E_n} + \right. \qquad \text{(II.18)}$$
$$\left. + \frac{\langle i|\bar{r}_2|n\rangle\langle n|\bar{p}|j\rangle}{E_j - E_n}\right] - i\sum_n \langle i|\bar{r}_2|n\rangle\langle n|\Delta\bar{k}\cdot\bar{r}_2|j\rangle \,,$$

where $|n\rangle = |n0\rangle$.

The first term in (II.18) is null because the bands i and j have the same parity. Also the second term vanishes because $\bar{p}$ is the conjugate variable of $\bar{r}_2$ and

$$\frac{\hbar}{m}\frac{\langle i|\bar{p}|n\rangle}{E_i - E_n} = i\langle i|\bar{r}_2|n\rangle$$

Then, one could write (II.14) as

$$-\langle\phi^i|\frac{1}{|\bar{r}_e - \bar{r}_n|}|\phi^j\rangle = \frac{1}{N}\sum_{\bar{k},\bar{k}'} A^i(\bar{k}')B(\bar{k})\sum_{\bar{R}}\frac{e^{i\Delta\bar{k}\cdot\bar{R}}}{R^3}\sum_n \langle i|\bar{R}\cdot\bar{r}_2|n\rangle\langle n|i\Delta\bar{k}\cdot\bar{r}_2|j\rangle \qquad \text{(II.19)}$$

The summation over $\bar{R}$ could be approximated by an integral. The final result is

$$-\langle \phi^i | \frac{1}{|\bar{r}_e - \bar{r}_h|} | \phi^j \rangle = \sum_{\bar{k},\bar{k}'} A^i(\bar{k}') B^j(\bar{k}) \langle i | \frac{(\Delta\bar{k}\cdot\bar{r}_2)^2}{|\Delta k|^2} | j \rangle = 0 . \qquad \text{(II.20)}$$

The last step follows because the operator $\left| \frac{\Delta\bar{k}\cdot\bar{r}_2}{\Delta k} \right|^2$, when averaged over all Δk, transforms like the identical representation (Γ_1) and the product $\Gamma_7 \times \Gamma_8 = \Gamma_{12} + \Gamma_{15} + \Gamma_{25}$ does not contain the identity.

We have demonstrated that the Coulomb interaction <u>does not</u> mix the excitons formed independently from the split-off valence bands, even when linear variations with $\bar{k}$ are allowed. It is very unlikely that higher order terms are responsible for the large shifts observed, therefore we must consider other possible causes.

C H A P T E R I I I

SPHERICAL APPROXIMATION

1.- THEORY

The negative results found in the former chapter lead one to think that the details of the valence band must be taken into account before trying to build the exciton states. This can be done by using the theory by Luttinger (1956), where the general motion of an electron or hole in a cubic semiconductor is considered carefully, within the effective mass approximation. It is shown that the most general Hamiltonian describing this problem is

$$H = A\frac{P^2}{2m_0} - \frac{1}{m_0}\left\{B\left(P_x^2 J_x^2 + P_y^2 J_y^2 + P_z^2 J_z^2\right) - C\left[\{P_x P_y\}\{J_x J_y\} + \{P_y P_z\}\{J_y J_z\} + \{P_z P_x\}\{J_z J_x\}\right]\right\}, \quad \text{(III.1)}$$

where $\{ab\} = (ab+ba)/2$, $\bar{p}$ is the momentum operator and $\vec{J}$ is the total angular momentum operator. m_0 is the particle rest mass and A,B,C are constants that could be related to measurable band parameters.

The basic form of (III.1) does not change when spin-orbit coupling is considered. In the case of negligible spin-orbit interaction the matrices J_i correspond to spin unity, and in the opposite limit $\vec{J}$ is the operator corresponding to spin 3/2 or 1/2.

This Hamiltonian has been applied to the acceptor problem by Baldereschi & Lipari(1973) (BL from now on) by adding a screened Coulomb potential ($-e^2/\varepsilon r$) to (III.1). The analogy between this problem and the atomic systems is evident and therefore, one can make use of the techniques developed there, particularly those concerning the angular momentum, in order to solve (III.1). Introducing the second-rank tensors

$$P_{ij} = 3P_i P_j - \delta_{ij} P^2$$
$$J_{ij} = \frac{3}{2}\left(J_i J_j + J_j J_i\right) - \delta_{ij} J^2 \quad \text{(III.2)}$$

one can separate terms with pure cubic symmetry from those that are also spherical invariant. The spherical model consists of neglecting completely the cubic terms, which are usually very small. Cubic contributions may be treated as a perturbation afterwards (BL(1974)).

In the spherical approximation, the problem is reduced to solve a finite set of coupled differential equations. In this scheme, the admixture of different angular momenta in the acceptor wave functions make the effect of interband coupling. In the limit of strong spin-orbit coupling the spherical Hamiltonian is

$$H_{sph} = \frac{1}{\hbar^2} P^2 - \frac{2}{r} - \frac{1}{9\hbar^2} \mu \left(P^{(2)} \cdot J^{(2)} \right) , \qquad \text{(III.3)}$$

where there is a scalar product of the second-rank irreducible spherical tensors derived from (III.2) and

$$\mu = \left(6\gamma_3 + 4\gamma_2 \right) / 5\gamma_1 , \qquad \text{(III.4)}$$

where $\gamma_1, \gamma_2, \gamma_3$ are the Luttinger parameters (Luttinger (1956)). The effective Rydberg

$$R_0 = e^4 m_0 / 2\hbar^2 \varepsilon^2 \gamma_1 , \qquad \text{(III.5)}$$

and the effective Bohr radius

$$a_0 = \hbar^2 \varepsilon \gamma_1 / e^2 m_0 , \qquad \text{(III.6)}$$

were used in (III.3) as units of energy and length, respectively. The exciton Hamiltonian could be written as

$$H_{ex} = H_{sph} + P^2 / 2 m_e , \qquad \text{(III.7)}$$

where m_e is the electron effective mass. In fact, H_{ex} could be written exactly as (III.3) if one replaces γ_1 by $\gamma_1 + m_0/m_e$, except that μ is now multiplied by a factor $\alpha = \gamma_1 / (\gamma_1 + m_0/m_e)$, whose value is usually very small.

Therefore, the third term in (III.3) could be treated as a perturbation. BL(1970),(1971) made this perturbative calculation for arbitrary value of the spin-orbit splitting (Λ), provided that Λ is such as to allow the use of zero order functions belonging to $\Gamma_8(J=3/2)$ and $\Gamma_7(J=1/2)$ separately. Expressions for these functions are found in Elliott(1954) and Dresselhaus et al.(1955). A neater way of including the effects of the split -off valence band is described by BL(1978).

Although in Cu_2O the spin-orbit splitting is of the same order of the exciton binding energy, one could use the expressions in BL(1971) to estimate the energy shifts of the lowest levels, because these do not vary much with the magnitude of Λ. In that paper the deviations from the hydrogenic positions of the lowest levels of both series of excitons are calculated, up to second order, and are shown to be

$$\begin{aligned}
\Delta E(1S_g) &= \tfrac{-4}{5}\,\Phi\,[S_1(0)+S_1(\Lambda)] \\
\Delta E(2S_g) &= \tfrac{-1}{10}\,\Phi\,[S_2(0)+S_2(\Lambda)] \\
\Delta E(1S_y) &= \tfrac{-8}{5}\,\Phi\,T_1(\Lambda) \\
\Delta E(2S_y) &= \tfrac{-1}{5}\,\Phi\,T_2(\Lambda)\quad ,
\end{aligned} \tag{III.8}$$

where S_1, S_2, T_1 and T_2 are functions of the spin-orbit splitting Λ and are tabulated in BL(1971). The function Φ depends on the parameters

$$\text{a)}\quad \mu_0 = \left(\frac{1}{m_e} + \frac{\gamma_1}{m_0}\right)^{-1}$$

$$\text{b)}\quad \mu_1 = \frac{m_0}{\gamma_2} \tag{III.9}$$

$$\text{c)}\quad \mu_2 = \frac{m_0}{2\sqrt{3}\,\gamma_3}\quad ,$$

and it is

$$\Phi = 8\left(\frac{\mu_0}{\mu_1}\right)^2 + \left(\frac{\mu_0}{\mu_2}\right)^2 \quad . \tag{III.10}$$

2.- ESTIMATE OF THE SHIFTS

Let us now investigate the values of the parameters γ_1, γ_2 and γ_3 which, to our knowledge, have not been measured directly. Equations(III.8) are very sensitive to the values of these parameters, therefore an accurate determination of the band effective masses must be done. Hodby et al.(1976) have determined the mass of the electron in the conduction band (m_e) and the mass of the hole in the Γ_7 valence band (m_7) by cyclotron resonance; the masses of the light (m_ℓ) and heavy (m_h) holes in the degenerate Γ_8 band are ambiguous and the values calculated there are not really meaningful.

Trevin et al.(1981) have fitted some quantities with the exciton data and, from them, they have calculated some of the band parameters in (III.9) and (III.10). The results are given in Table III.1 .

Table III.1

Valence Band Parameters of Cu_2O from exciton data

Datum	parameter	relation to the data	calc. value
R_0=	μ_0	$\varepsilon^2(R_0/R_H)m_0$	.40 m_0
.107eV	γ_1	eq.(III.9a)	1.50
R_H=	m_7	m_0/γ_1	.66 m_0
13.6eV	m_ℓ	$m_0/(\gamma_1(1+\mu))$	.47 m_0
ε=7.11	m_h	$m_0/(\gamma_1(1-\mu))$	1.11m_0
m_e=	γ_2	eqs,(III.4),(III.11)	.30
.99m_0	μ_1	eq.(III.9b)	3.33m_0
μ=.4	μ_2	eqs,(III.9c),(III.11)	.96 m_0
	α	$\gamma_1/(\gamma_1+m_0/m_e)$	.60
	Φ	eq.(III.10)	.29

In order to verify these values. we used the band effective masses derived from the band calculation by Kleinman & Mednick(1980), obtained from the band energies

around several points near Γ given by Kleinman (private communication) and the results are shown in Table III.2.

In order to calculate γ_2 and μ_2 we have made the approximation

$$\gamma_3 \simeq \gamma_2 \qquad \text{(III.11)}$$

because we are neglecting the cubic contributions to the Hamiltonian from the very begining, these are proportional to $\delta \simeq (\gamma_3-\gamma_2)/\gamma_1$.

Table III.2

Valence Band Parameters of Cu_2O from Band Calculation

Datum	parameter	relation to the data	calc. value
$m_7=m_\ell=$	γ_1	m_0/m_7	1.56
$.64m_0$	μ_0	eq.(III.9a)	$.39m_0$
$m_h=4m_0$	μ	$m_0(1/m_e-1/m_h)/2\gamma_1$	.42
$m_e=.99m_0$	γ_2	eqs.(III.4),(III.11)	.33
	μ_1	eq.(III.9b)	$3.05m_0$
	μ_2	eqs(III.9c),(III.11)	$.88m_0$
	α	$\gamma_1/(\gamma_1+m_0/m_e)$	.61
	Φ	eq.(III.10)	.33

Knowing that $\Lambda \sim 1.2$, with Table 1 in BL(1971) we obtain:

$$\begin{aligned} S_1(0) &= 0.2246 \\ S_2(0) &= 0.7029 \\ S_1(\Lambda) &= 0.1523 \\ S_2(\Lambda) &= 0.3226 \\ T_1(\Lambda) &= 0.3997 \\ T_2(\Lambda) &= 0.0611 \end{aligned} \qquad \text{(III.12)}$$

With (III.12) and (III.8) we construct Table III.3 .

Table III.3

Energy shifts of the lowest exciton states by second-order perturbation theory, in cm^{-1}.

Level	ΔE from T(III.1)	ΔE form T(III.2)	ΔE exp.
1Sg	-74.4	-121.82	-191
2Sg	-25.3	-41.43	?
1Sy	-157.9	-164.76	-333
2Sy	-3.0	-3.1	not found

3.- DISCUSSION

As it is seen from Table III.3, the results are very sensitive to the choice of the effective Rydberg (the experimental values were chosen to form the third column of the table) but, even with these large fluctuations, it is difficult to agree with the experiment. The shifts found are too small and the theory is unable to explain the situation for the 2Sy exciton, because it predicts that the state should be found very near the expected value and this is not so.

One could doubt about the validity of the use of perturbation theory in this case, because $\alpha \sim .6$, which gives an effective $\mu \sim .24$. This value is just in the limit where one could use perturbation theory safely. Nevertheless, we think that the exact solution of the spherical Hamiltonian will not give a much better result.

In any case, Table III.3 could encourage one to think that the deficit in the theoretical values is due to the neglect of central-cell corrections, which once they are incorporated into the treatment, could increase the shifts so as to fit with the experiment. This statement is reasonable and supports the idea that one should continue on the same lines, considering all these facts (and exchange effects).

C H A P T E R I V

EXCHANGE EFFECTS

In ChapterIII, while deriving the effective mass equation, the exchange integrals between the electron and the hole were neglected. The effects due to these terms are usually very small (Elliott(1963)), because this is a short range interaction that takes place between S-states only.

Nevertheless, there are some cases where the spin-spin interaction becomes important. Elliott(1961) showed that the exchange energy is proportional to the probability of finding the electron and hole on the same atom, therefore one could expect that in alkali-halides, where the excitons have very small radii (Frenkel excitons), the exchange should be important (Onodera & Toyozawa (1967)).

In Cu_2O there are two reasons to suspect that the exchange interaction becomes important: First of all, an estimate of the ortho-para splitting of the 1Sy exciton, made by Elliott(1961), gave $\sim$15 cm^{-1}, which is very small compared to the experimentally observed one of $\sim$100 cm^{-1} (Kuwabara et al.(1977)). Also, the proximity of the 1Sg and 2Sy excitons could give rise to a large interband exchange.

The exchange term was considered by Waters et al. (1980) in a conventional perturbative approach to the diagonalization of the effective mass Hamiltonian, neglecting the mixing of the series. They could not explain the behaviour of the lines under strain fields, particularly the reversed splitting of the levels (compared to the 1Sy one) and the extremely large splitting of the 3Sy level. Their treatment is equivalent to ours in Chapter III, but including the deformation Hamiltonian and the exchange terms as perturbations.

For these reasons it is clear that the interband exchange interaction becomes extremely important in Cu_2O

and one has to solve the problem including this term from the very beginning, that is, to take the Hamiltonian H_{ex} (III.7) and add a term

$$H_{exch} \sim J_0 \, |\phi(r=0)|^2 \, B \qquad \text{(IV.1)}$$

where J_0 is the atomic exchange energy, B is a constant to be determined and $\Phi(r=0)$ is the envelope function of the exciton when the electron and hole are in the same cell.

It is necessary to mention that at this point we abandoned the calculation because Frölich and his group in Dortmund were doing it at the same time as this work was in progress and they obtained very good results that were published very recently (Uihlein et al.(1981)). Hence, we will describe their work briefly for the sake of completeness.

They consider the following Hamiltonian:

$$H = H_s + H_{so} + H_d + H_{exch.} \qquad \text{(IV.2)}$$

where the first three terms are exactly H_{ex} in (III.7), except that they add a contact potential $-V_0\delta(\bar{r})$ in order to account for central-cell corrections. V_0 is determined by the 1Sy binding energy. H_{ex} is diagonal in the representation $|F,m_F>$, where $\bar{F}= \bar{L}+\bar{J}$ is the total angular momentum operator, formed by the coupling of the angular momentum $\bar{L}$ associated with the envelope function to the effective spin of the hole $\bar{J}$. The exchange term is

$$H_{exch} = J_0 \left(\frac{1}{4} - \bar{\sigma}_e \cdot \bar{\sigma}_h\right) \delta(\bar{r}) \qquad \text{(IV.3)}$$

where J_0 is a constant determined by fitting the value of the 1Sy ortho-para splitting (96 cm^{-1}), $\bar{\sigma}_e$ and $\bar{\sigma}_h$ are the spin operators of the electron and hole respectively

and $\delta(\bar{r})$ takes care of the fact that the electron and the hole must be in the same unit cell.

Neither $\bar{J}$ nor $\bar{F}$ conmute with H_{exch} when there is a S-like component present and thus the states must be classified with $\bar{F}_{tot} = \bar{F}+\sigma_e$. The only states that could be affected by the exchange interaction are those with $F=\frac{1}{2}$ (Γ_7^+) and $F=\frac{3}{2}$ (Γ_8^+). For all the others F remains a good quantum number. In Table IV.1 we list the states that could be mixed by the exchange, according to their symmetry. The notation adopted for the states is $^{2J+1}L_F$, therefore a superscript 2 (4) refers to a yellow (green) exciton. This notation is not good for distinguishing between the ortho and paraexcitons and is misleading for it does not represent the true nature of the excitons.

A variational method is used to diagonalize the Hamiltonian and the energy levels are calculated for the lowest even-parity excitons. In Table 1 of Frölich et al. (1979) these energies are listed and the agreement with the experiment is remarkably good: all the predicted energies are identical to the observed ones within the experimental resolution (.1meV).

Table IV.1

Excitons that could be mixed by the exchange interaction

F_{tot} → / F ↓	0	1	2
1/2	$^2S_{\frac{1}{2}}$ $^4D_{\frac{1}{2}}$	$^2S_{\frac{1}{2}}$ $^4D_{\frac{1}{2}}$	
3/2		$^4S_{\frac{3}{2}}$ $^4D_{\frac{3}{2}}$ $^2D_{\frac{3}{2}}$	$^4S_{\frac{3}{2}}$ $^4D_{\frac{3}{2}}$ $^2D_{\frac{3}{2}}$
symmetry	Γ_2^+	Γ_{25}^+	$\Gamma_{12}^+ + \Gamma_{15}^+$

Appart from explaining the non-hydrogenic nature of the even-parity excitons, this theory has succeeded in solving other puzzling features of the exciton spectrum of Cu_2O and has led to a new picture of the situation. We list these features below:

1) The old assignment of the lines (Agekyan et al.(1974) and Washington et al.(1977)) reproduced in Fig.III.1, places the 2Sy exciton below the 2Py level; this has to be revised. The first one that arouse doubts about this assignment was Agekyan(1975) who, based on studies on the splitting of the S-excitons under simultaneous electric and strain fields, suggested that the exciton labeled 3Sy should be called the 2Sy and therefore, the nSy had to be (n-1)Sy. This classification is rather surprising because it places the nS components above the nP ones. The theory explains these facts by the strong exchange interaction of the 2Sy and the 1Sg excitons: The d-like part of the Hamiltonian mixes these states a fair amount, but when the exchange interaction is switched on, the mixing becomes such that both excitons lose their green or yellow nature. In Table IV.2 we give the composition of these states.This explains the shift towards higher energies of the 2Sy level and the strong S-D mixing suggested by resonant Raman scattering experiments (Washington et al.(1977)) and by two-photon absorption (Frölich et al.(1979)). This is the reason that prevented the identification of the 2Sy exciton for more than twenty years.

2) The complete admixture of the green and yellow excitons is also responsible for the reversed strain splitting of the 2Sy exciton and for the smallness of the one exhibited by the 1Sg one. The confusion that arose from the results by Waters et al.(1980) was clarified by interpreting the same data on the light of the present theory (Trevin et al.(1981)).

Table IV.2

Mixing of the yellow and green excitons

component		1Sg orthoexciton		2Sy orthoexciton	
		H_{ex}	$H_{ex}+H_{exch}$	H_{ex}	$H_{ex}+H_{exch}$
$^2S_{\frac{1}{2}}$	yellow	0%	87%	98%	34%
$^2D_{\frac{3}{2}}$		18%	3%	0%	33%
$^4S_{\frac{3}{2}}$		80%	9%	0%	33%
$^4D_{\frac{1}{2}}$	green	0%	1%	2%	0%
$^4D_{\frac{3}{2}}$		2%	0%	0%	0%

3) The splitting of the lines under magnetic fields is correctly predicted by the theory.

4) The unnaturally large difference between the Rydbergs of the two series is explained in terms of the shift of the yellow spectrum due to exchange, and not only in terms of the valence band effective masses. A calculation of μ taking into account these facts and the measured binding energies for the P-states, gives a value of .47, in close agreement with our estimate from the band parameters.

5) This theory demonstrates that the cubic terms are not important in Cu_2O. This conclusion is supported by the splitting of the S-D pairs on high magnetic fields.

One could think that there is not an open field for research on this subject because everything is perfectly understood now. This is not so, on the contrary one has to take advantage of the fact that the problems on interpretation of the experimental data are solved and of the

beautiful characteristics of the spectrum in order to perform finer and more detailed experiments. There still remain some problems like the detection of several dipole forbidden components of the P-excitons that are predicted by the theory or the verification of the predicted behaviour of the lines under strains along the (111) direction.

APPENDIX

BASIS FUNCTIONS FOR THE IRREDUCIBLE REPRESENTATIONS

Copper 3d orbitals.-

In order to find the 20 symmetry-adapted basis functions that are needed, we will make use of the formula

$$\frac{l_i}{h} \sum_R R\{\Psi_\alpha^{i*}\Psi\} = \sum_j \Psi_j^{i*}\phi_j^i \qquad \text{A.1}$$

Let us explain the way this formula works: Suppose that we know all the partners (α) that form a basis (Ψ_α^i) of an IR (i), and we have a set of arbitrary functions Ψ that have the appropriate symmetry, then we can find a new set of basis functions by applying all the operations R of the group to the product of those functions and the old basis, sum them up and multiply the result by a factor which is the ratio between the dimensionality of the IR (l_i) and the number of operations in the group (h).

The new basis functions are found to be the coefficients ϕ_j^i of the functions used before. In the case of having a one-dimensional representation this formula reduces to the proyection operator ($\chi(1)=\Psi=1$).

In the present case the set Ψ_α^i for each IR will be

Representation	Basis
Γ_1^+	1
Γ_{12}^+	$\begin{cases} 3z^2-r^2 \\ x^2-y^2 \end{cases}$
Γ_{15}^+	$\begin{cases} xy\,(x^2-y^2) \\ yz\,(y^2-z^2) \\ zx\,(z^2-x^2) \end{cases}$
Γ_{25}^+	$\begin{cases} xy \\ zx \\ yz \end{cases}$

The set of functions Ψ will be properly symmetrized combinations of the 20 atomic 3d orbitals. In order to do so, let us consider a unit cell (Fig.A.1), where the copper atoms are labeled A,B,C,D in the directions $(\bar{1}\bar{1}\bar{1})$, $(11\bar{1})$, $(1\bar{1}1)$, $(\bar{1}11)$ respectively. Taking these directions as the quantization axes for each atom, the functions that will be considered have the following properties:

atomic d-functions	Angular dependence like $(Y_\ell^m(\theta_i,\phi_i))$	Transfoms like
$A^0\ B^0\ C^0\ D^0$	Y_2^0	$3z^2-r^2$
$A^{+1}\ B^{+1}\ C^{+1}\ D^{+1}$	$i\,(Y_2^{-1}+Y_2^{1})/\sqrt{2}$	$y_i z_i$
$A^{-1}\ B^{-1}\ C^{-1}\ D^{-1}$	$(Y_2^{-1}-Y_2^{1})/\sqrt{2}$	$z_i x_i$
$A^{-2}\ B^{+2}\ C^{+2}\ D^{+2}$	$(Y_2^{-2}+Y_2^{2})/\sqrt{2}$	$x_i^2-y_i^2$
$A^{-2}\ B^{-2}\ C^{-2}\ D^{-2}$	$i\,(Y_2^{-2}-Y_2^{2})/\sqrt{2}$	$x_i y_i$

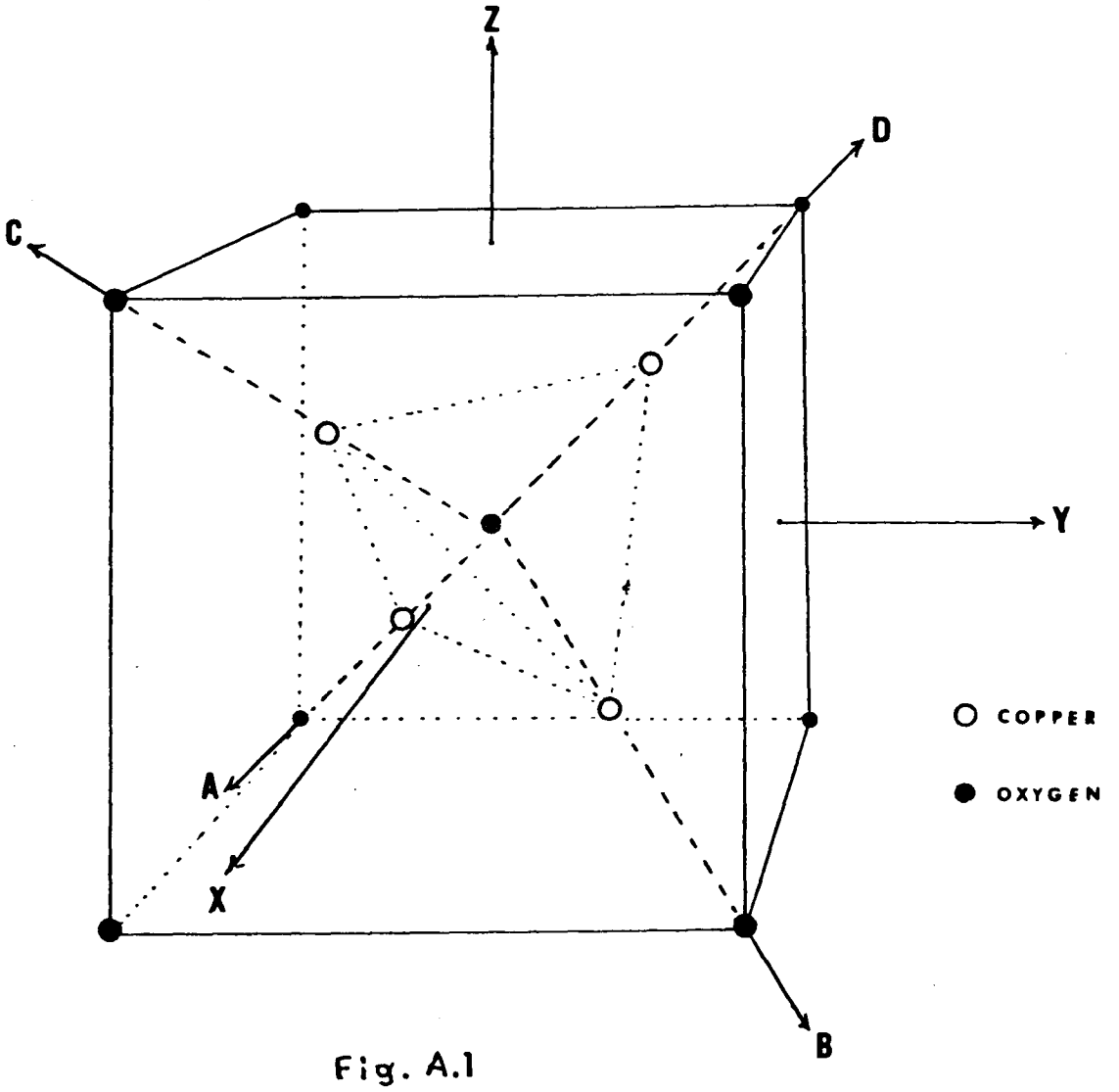

Fig. A.1

In order to apply formula A.1, one must know how the 48 operations of O_h transform the functions ψ_α^i and the 4 coordinate systems (x_i, y_i, z_i). This was done by using the tables given in Bradley & Cracknell (1972) p.37 . Then, for example, one obtains

$$\frac{1}{12}\sum_R R\,(xy\,(A^\circ+B^\circ+C^\circ+D^\circ)) = (A^\circ+B^\circ-C^\circ-D^\circ)xy + (A^\circ-B^\circ+C^\circ-D^\circ)xz + (A^\circ-B^\circ-C^\circ+D^\circ)yz$$

The results are:

Repr.	Basis Function	transf. like	name:
$\Gamma_1^+(0)$	$\frac{1}{2}(A^\circ + B^\circ + C^\circ + D^\circ)$	1	
$\Gamma_{12}^+(\pm1)$	$\frac{1}{2}(-A^{-1} - B^{-1} + C^{-1} + D^{-1})$	$3z^2-r^2$	
	$\frac{1}{2}(-A^{+1} - B^{+1} + C^{+1} + D^{+1})$	x^2-y^2	
$\Gamma_{12}^+(\pm2)$	$\frac{1}{2}(A^{+2} + B^{+2} + C^{+2} + D^{+2})$	$3z^2-r^2$	
	$\frac{1}{2}(A^{-2} + B^{-2} + C^{-2} + D^{-2})$	x^2-y^2	
$\Gamma_{15}^+(\pm1)$	$\frac{1}{2}(A^{+1} + B^{+1} + C^{+1} + D^{+1})$	$xy\,(x^2-y^2)$	
	$\frac{1}{4}(A^{+1} - B^{+1} + C^{+1} - D^{+1}) + \frac{\sqrt{3}}{4}(A^{-1} - B^{-1} + C^{-1} - D^{-1})$	$yz\,(y^2-z^2)$	
	$\frac{1}{4}(A^{+1} - B^{+1} - C^{+1} + D^{+1}) + \frac{\sqrt{3}}{4}(A^{-1} - B^{-1} - C^{-1} + D^{-1})$	$zx\,(z^2-x^2)$	
$\Gamma_{15}^+(\pm2)$	$\frac{1}{2}(-A^{-2} - B^{-2} + C^{-2} + D^{-2})$	$xy\,(x^2-y^2)$	
	$\frac{1}{4}(A^{-2} - B^{-2} - C^{-2} + D^{-2}) + \frac{\sqrt{3}}{4}(A^{+2} - B^{+2} - C^{+2} + D^{+2})$	$yz\,(y^2-z^2)$	
	$\frac{1}{4}(A^{-2} - B^{-2} + C^{-2} - D^{-2}) + \frac{\sqrt{3}}{4}(A^{+2} - B^{+2} + C^{+2} - D^{+2})$		
$\Gamma_{25}^+(0)$	$\frac{1}{2}(A^\circ + B^\circ - C^\circ - D^\circ)$	xy	d_0'
	$\frac{1}{2}(A^\circ - B^\circ + C^\circ - D^\circ)$	zx	d_0^2
	$\frac{1}{2}(A^\circ - B^\circ - C^\circ + D^\circ)$	yz	d_0^3
$\Gamma_{25}^+(\pm1)$	$\frac{1}{2}(A^{-1} + B^{-1} + C^{-1} + D^{-1})$	xy	d_1'
	$-\frac{1}{4}(A^{-1} - B^{-1} - C^{-1} + D^{-1}) + \frac{\sqrt{3}}{4}(A^{+1} - B^{+1} - C^{+1} + D^{+1})$	zx	d_1^2
	$-\frac{1}{4}(A^{-1} - B^{-1} + C^{-1} - D^{-1}) - \frac{\sqrt{3}}{4}(A^{+1} - B^{+1} + C^{+1} - D^{+1})$	yz	d_1^3 ...
$\Gamma_{25}^+(\pm2)$	$\frac{1}{2}(-A^{+2} - B^{+2} + C^{+2} + D^{+2})$	xy	d_2'
	$\frac{1}{4}(A^{+2} - B^{+2} + C^{+2} - D^{+2}) - \frac{\sqrt{3}}{4}(A^{-2} - B^{-2} + C^{-2} - D^{-2})$	zx	d_2^2
	$\frac{1}{4}(A^{+2} - B^{+2} - C^{+2} + D^{+2}) + \frac{\sqrt{3}}{4}(A^{-2} - B^{-2} - C^{-2} + D^{-2})$	yz	d_2^3

For the oxygen atoms the quantization axis was chosen to be the z-direction in Fig.A.1; the atom at the origin is labeled b and the one at (111) is c. Then the functions are

atomic p-functions	Angular dependence $(Y_\ell^m(\theta_i,\phi_i))$	transfoms like
ϕ_c^x , ϕ_b^x	$\frac{1}{\sqrt{2}}(y_1^{-1} - y_1^{1})$	x_i
ϕ_c^y , ϕ_b^y	$-\frac{i}{\sqrt{2}}(y_1^{-1} + y_1^{1})$	y_i
ϕ_c^z , ϕ_b^z	y_1^0	z_i

Then, the symmetrized functions are

Repr.	Basis Function	transf. like	Name
Γ_{15}^-	$\frac{1}{2}(\phi_c^x + \phi_b^x)$	x	
	$\frac{1}{2}(\phi_c^y + \phi_b^y)$	y	
	$\frac{1}{2}(\phi_c^z + \phi_b^z)$	z	
Γ_{25}^+	$\frac{1}{2}(\phi_c^z - \phi_b^z)$	xy	p'
	$\frac{1}{2}(\phi_c^y - \phi_b^y)$	zx	p^2
	$\frac{1}{2}(\phi_c^x - \phi_b^x)$	yz	p^3

The atomic functions are assumed to be normalized throughout this appendix, therefore the factors shown take care of the normalization of the basis functions.

REFERENCES

Agekyan V.T., Monozon B.S. & Shiryapov I.P., Phys. Status Solidi (b) 66,359(1974)

Agekyan V.T. & Stepanov Yu.A., Fiz. Tverd. Tela 17, 1592 (1975) (engl. transl. Sov. Phys. Solid State 17, 1041 (1975))

Agekyan V.T., Phys. Status Solidi A43,11(1977)

Agrawal B.K., Phys. Rev. Lett. 46,774(1981a)

Agrawal B.K., Solid State Commun. 37,271(1981b)

Axe J., Thorpe M.F. & Barrio R.A. (to be published)

Baldereschi A. & Lipari N.O., Phys. Rev. Lett. 25,373(1970)

Baldereschi A. & Lipari N.O., Phys. Rev. B3,439(1971)

Baldereschi A. & Lipari N.O., Phys. Rev. B8,2697(1973)

Baldereschi A. & Lipari N.O., Phys. Rev. B9,1525(1974)

Baldereschi A. & Lipari N.O., Solid State Commun.25,665(1978)

Barrio R.A. & Thorpe M.F. (to be published)

Bates J.B., Hendrick R.W. & Shaffer L.B., J. Chem. Phys. 61, 4163(1974)

Bell R.J., Bird N.F. & Dean P.,J. Phys. C 1.299(1968)

Bell R.J. & Dean P. Disc. Faraday Soc. 50,55(1970)

Bell R.J., Dean P., Hibbins-Butler D.C., J. Phys. C 3,2111 (1970)

Bethe H.A., Proc. Roy. Soc. A216,45(1935)

Bloch P.D. & Schwab C., Phys Rev. Lett. 41,514(1978)

Born M., Ann. Phys. (Leipz) 44,605(1914)

Bourret A. & Chenevas-Paule A., 9th Int. Conf. of Amorphous and Liquid Semicond., Grenoble (1981)

Bradley C.I. & Cracknell A.D. "The Mathematical Theory of Symmetry in Solids" Oxford, Clarendon Press (1972)

Brahms S., Nikitine S. & Dahl J.P., Phys. Lett. 22,31(1966)

Brink D.M. & Satchler G.R. "Angular Momentum", 2nd ed. Clarendon Press, Oxford (1971)

Brodsky M.H., Cardona M. & Cuomo J.J., Phys. Rev B16,3556. (1977)

Cochran W., "Phonons in Perfect Lattices and in Lattices

with Point Imperfections" ed. R.W.H. Stevenson (New York, Plenum)p.53 (1966)

Condon E.U. & Shortley G.H., "The Theory of Atomic Spectra" Cambridge Univ. Press(1953)

Cowley R.A., Proc. Phys. Soc. 84,281(1964)

Dahl J.P. & Switendick A.C. J. Phys. Chem. Solids 27,931 (1966)

Dawber P.G. & Elliott R.J., Proc. R. Soc. Lond. 88 ,217 (1963)

Dean P. Rev. Mod. Phys., 44,127(1972)

Domb C., Adv. Phys. 9.145(1960)

Dresselhauss G., Kip A.F. & Kittel C., Phys. Rev. 98,368 (1955)

E-Ni Foo, Thorpe M.F. & Weaire D. Surface Sci. 57,(1976)

Elliott R.J., Phys. Rev. 96,266(1954)

Elliott R.J., Phys. Rev. 124,340,(1961)

Elliott R.J., Theory of Excitons I in "Polarons and Excitons" (C.G. Kuper & G.D. Whitfield, eds.)p.269, Plenum Press, N.Y.(1963)

Elliott R.J., Krumhansl J.A. & Leath P.L., Rev. Mod. Phys. 46,465(1974)

Elliott R.J. & Leath P.L. in "Dynamical Properties of Solids" V.2 (G.K. Horton & A.A. Maradudin, eds.) North Holland, Amsterdam, Oxford, P.391 (1975)

Falicov L.M. & Yndurain F., Phys. Rev. B12,5664(1975)

Feldman D.W., Ashkin M. & Parker J.R.Jr., Phys. Rev. Lett. 26,642(1971)

Frölich D., Kenklies R., Uihlein Ch. & Schwab C., Phys. Rev. Lett. 43,1260(1979)

Galeener F.L., Phys Rev. B19,4292(1979)

Galeener F.L., J. Non-Crystalline Solids 40,527(1980)

Galeener F.L. & Lucovsky G., Phys. Rev. Lett. 37,1474 (1976)

Galeener F.L. & Sen P.N., Phys. Rev. B17,1928(1978)

Galeener F.L., Lucovsky G. & Mikkelsen J.C.Jr., Phys. Rev. B22, 3983(1980)

Gross E.F. & Kaplyanskii A.A., Fiz. Tverd. Tela 2,379 (1960) (engl. tranl. Soviet Phys. Solid State 2, 353(1960))a

Gross E.F. & Kaplyanskii A.A., Fiz. Tverd. Tela 2,1676 (1960) (engl. transl. Soviet Phys. Solid State 2, 1518(1960))b

Gross E.F. & Kaplyanskii A.A., Fiz. Tverd. Tela 2,2968, (1960) (engl. transl. Soviet Phys. Solid State 2, 2637(1961))

Gross E.F., Kaplyanskii A.A. & Agekyan V.T., Fiz. Tverd. Tela 4,1009(1962) (engl. transl. Soviet Phys. Solid State 4,744(1962))a

Gross E.F., KaplyanskiiA.A., Agekyan V.T. & Bulyanitsa D.S., Fiz. Tverd. Tela 4,1660(1962) (engl. transl. Soviet Phys. Solid State 4,1219 (1962))b

Haken H. Theory of Excitons II in "Polarons and Excitons" (C.G.Kuper & G.D. Whitfield eds.) p.295 Plenum Press N.Y.(1963)

Hodby J.W., Jenkins T.E., Schwab C., Tamura H. & Trivich D., J. Phys C 9,1429(1976)

Joannopoulos J.D. & Yndurain F., Phys. Rev. B10,5164(1974)

Keating D.T., Phys.Rev. 145,637(1966)

Kleinman L. & Mednick K., Phys. Rev. B21,1549(1980)

Knights J.C. AIP. Conf. Proc. 31,296(1976)

Knox R.S. Solid State Phys. Suppl. 5 sec.2 (1963)

Kuwabara G., Tanaka M. & Fukutani H., Solid State Commun. 21,599(1977)

Lannin S.J., in "Amorphous and Liquid Semiconductors" (J. Stuke & W. Breing, eds.) Taylor&Francis, London (1974)

Laughlin R.B. & Joannopoulos J.D., Phys. Rev. B16,2942 (1977)

Laughlin R.B., Joannopoulos J.D., Murray C.A., Hartnett K.J. & Greytak T.J., Phys.Rev. Lett. 40,461(1978)

Leadbetter A.J. & Stringfellow M.W. Neutron Inelastic

Scattering (International Atomic Energy Agency, Vienna)p.501 (1972)

Lipari N.O. & Baldereschi A., Solid State Commun. 25, 665(1978)

Lucovsky G., Phil. Mag. B39,513(1979)

Luttinger J.M., Phys. Rev. 102,1030(1956)

Merle J.C., Wecker C., Daunois A., Deiss J.L. & Nikitine S., Surface Sci. 37.347(1973)

Mikkelsen J.C.Jr. & Galeener F.L. J. Non-Crystalline Solids 37,71(1980)

Nagle J.F., Bonner J.C. & Thorpe M.F., Phys. Rev. B4,2233 (1972)

Nikitine S.,Grun J.B. & Sieskind M. J. Phys. Chem. Solids 17,292(1961)

Nikitine S. in "Optical Properties of Solids" (S. Nudelman & S.S. Mitra, eds.) Plenum N.Y.(1969)

Onodera Y. & Toyozawa Y., J. Phys. Soc. Japan 22,833(1967)

Peierls R.E., Proc. Camb. Phil. Soc. 32,477(1936)

Petroff Y., Yu P.Y. & Shen Y.R.,Phys. Rev. B12,2488(1975)

Sasaki H. & Kuwabara G., J. Phys. Soc. Japan 34,95(1973)

Sawai T., Ueno Sh. & Matsubara T., Suppl. Prog. Theor. Phys. 53,222(1973)

Sen P.N. & Thorpe M.F., Phys. Rev. B15,4030(1977)

Shen S.C., Fang C.J., Cardona M. & Genzel L., Phys. Rev. B 22, 2913(1980)

Shuker R. & Gammon R.W., Phys. Rev. Lett. 25,222(1970)

Springer T. in "Springer Tracts in Modern Physics" Vol.64 p.28, Springer-Verlag, Berlin (1972)

Stolen R.H., Krause J.T. & Kurljian C.R., Disc. Faraday Soc. 50,103(1970)

Stolen R.H. & Walrafen G.E., J. Chem. Phys. 64,2623(1976)

Straley J.P., Phys. Rev. B6,4086(1972)

Taylor D.W., Phys. Rev. 156,1017(1967)

Taylor D.W. in "Dynamical Properties of Solids" (G.K. Horton & A.A. Maradudin, eds.)p.302 North Holland Amsterdam, Oxford(1975)

Thorpe M.F., Phys. Rev. B8,5352(1973)

Thorpe M.F., J. Phys. C 7,4037(1974a)

Thorpe M.F., Proc. of the AIP conf. on Tetrahedrically Bonded Amorphous Semiconductors, Yorktown Heights (1974b)

Thorpe M.F. in "Physics of Structurally Disordered Solids" (S.S. Mitra, ed.)p.623 Plenum, N.Y.(1976)

Thorpe M.F. & Weaire D., Phys. Rev. B4,3518(1971)

Thorpe M.F., Weaire D. & Alben R., Phys. Rev. B7,3777(1973)

Thorpe M.F. & Galeener F.L., Phys. Rev. B22,3078(1980)

Trevin H.R., Cummins H.Z. & Birman J.L., Phys. Rev. B23,597(1981)

Uihlein Ch., Frolich D. & Kenklies R., Phys. Rev. B23,2731(1981)

Velický B., Kirkpatrick S. & Ehrenreich H., Phys. Rev 175, 747(1968)

Wannier G., Phys. Rev. 52,191(1937)

Washington M.A., Genack A.Z., Cummins H.Z., Bruce R.H., Compaan A. & Forman R.A., Phys. Rev. B15,2145(1977)

Waters R.G., Pollak F.H., Bruce R.H. & Cummins H.Z., Phys. Rev. B 21, 1665(1980)

Weaire D. & Alben R., Phys. Rev. Lett. 29,1505(1972)

Weaire D. & Thorpe M.F., Phys. Rev. B4.2508(1971)

Weaire D. & Thorpe M.F. in IBM Conf. "Computational Methods for Large Molecules and Localized States in Solids" (F. Herman, A.D. McLean & R.K. Nesbet, eds.)p.295 Plenum, N.Y.(1973)

Weber W. & Thorpe M.F., J. Phys. Chem. Solids 36,967(1975)

Yndurain F., Phys. Rev. Lett. 37,1062(1976)

Yndurain F., Phys. Rev. B18,2876(1978)

Yndurain F. & Sen P.N., Phys Rev. B14,531(1976)

Yonezawa F. & Morigaki K., Suppl. Prog. Theor. Phys. 53, 1(1973)

Zachariasen W.H., J. Am. Chem. Soc. 54,3841(1932)

Zeiger H.J. & Pratt G.W. "Magnetic Interactions in Solids" Clarendon Press, Oxford(1973)

Ziman J.M. "Models of Disorder" Cambridge Univ. Press(1979)

Zubarev D.N., Ups. Fiz. Nauk 71,71(1960) (engl. transl. Sov. Phys.-Ups. 3,320(1960)